Maximum Efficiency Control of a Step Skewed Ferrite-Assisted Synchronous Reluctance Machine Accomplished by Quadratic Interpolation

Master's Thesis

Power Electronics and Drives

AALBORG UNIVERSITY
STUDENT REPORT

Written By:
Kristian Buchwald Pedersen
Frederik Brath Severinsen

Group PED4-1041
Department of Energy
Aalborg University

AALBORG UNIVERSITY
STUDENT REPORT

School of Engineering and Science (SES)
Energy Engineering
Pontoppidanstræde 111
9220 Aalborg Ø, Denmark
http://www.ses.aau.dk/

Title:
Maximum Efficiency Control of a Step Skewed Ferrite-Assisted Synchronous Reluctance Machine Accomplished by Quadratic Interpolation

Theme:
Master's Thesis in Power Electronics and Drives

Project period:
February 2022 - June 2022

Project group:
PED4-1041

Participants:

Kristian Buchwald Pedersen

Frederik Brath Severinsen

Supervisor:
Kaiyuan Lu

Abstract:

This thesis is a continuation of the work done in [1][2] in collaboration with Grundfos and aims to develop a control strategy to maximize the efficiency of a step skewed Ferrite Assisted Synchronous Reluctance Machine (FASynRM). As the machine is to be used in a pump application, the performance of the FASynRM will be evaluated with regards to the Energy-Efficiency-Index (EEI) designed for pump applications. It will be investigated how the losses in the machine will influence the maximum efficiency (ME) control of the FASynRM, and how it might be different from conventional control strategies, such as Maximum Torque Per Ampere (MTPA). Likewise, the challenges regarding control of a FASynRM will be presented, such as demagnetization current limitations and rotor d-axis localization. The Maximum Efficiency Algorithm (MEA) is also presented, which uses quadratic interpolation to minimize either the input power or power losses in the FASynRM. In the experimental work it was found that the active power equation did not calculate the input power correctly and therefore input power LUTs were used to validate the MEA. A power loss estimation profile was comprised based on the core losses, which also enabled the MEA to locate the ME angle for the EEI operating conditions. In the end it was found that the EEI value was negligibly different between ME, MTPA or Constant Angle (CA) control. It was therefore left to the user to decide which control method to use, based on the number of operating conditions and implementation effort.

Circulation: Uploaded digitally
Page count: 61
Appendix count: 1
Appendix pages: 4
Finished: 30/05/2022

By signing this document, each member of the group confirms participation on equal terms in the process of writing the project. Thus, each member of the group is responsible for the all contents in the project.

Summary

This thesis is done in collaboration with Grundfos to investigate how maximum efficiency control can be obtained for a step skewed Ferrite-Assisted Synchronous Reluctance Machine (FASynRM). It builds on the work carried out in two previous reports [1][2], which also were made in collaboration with Grundfos. The outcome of the two previous reports, that investigated the rotor design with regards to torque performance and torque ripple, is a step skewed FASynRM that will be the main control target for this thesis. The main incentive for this machine topology is the robustness of the Synchronous Reluctance Machine (SynRM) combined with the inexpensive ferrite magnets to enhance its torque density and power factor performance. Since the FASynRM is to be used in a pump application, the Energy-Efficiency-Index (EEI) operating conditions specifically designed for pumps are used as a way to evaluate the performance of the FASynRM.

To investigate how maximum efficiency can be obtained, the losses present in an electrical machine are examined alongside the conventional control strategy for various types of electrical machines. Usually, only the copper losses are considered, which can be minimized by Maximum Torque Per Ampere (MTPA) but the core losses also contribute to the overall efficiency of the FASynRM and Maximum Efficiency (ME) control aims to minimize the sum of all the losses in the electrical machine.

After having established the motivation for the thesis both with regards to the promising performance of FASynRMs as well as the shortcomings of the conventional MTPA control, the FASynRM provided by Grundfos was examined in more detail. Measurements were performed to determine the stator phase resistance, the PM flux linkage and the d- and q-axis inductances of the machine. The results for the d-axis inductance were found to match well with the previous work done in [1], however the q-axis inductance saturated faster than expected, suspected to be because of misalignment when locking the rotor. The Field-Oriented Control (FOC) scheme used to control the FASynRM was presented, where the amplitude of the current vector was controlled by the speed loop, and the angle of the current vector was determined by the Maximum Efficiency Algorithm (MEA). To avoid demagnetizing the ferrite magnets in the FASynRM, the maximum allowable negative d-axis current was investigated with regards to the step skewed rotor. Lastly, it was examined how the initial rotor position could be found, as it was required by the incremental encoder used in the FOC shceme. By using the torque equation for the FASynRM it was found that two stable parking positions were possible, however both of these were displaced from the rotor d-axis. To compensate for this displacement, the BEMF of the FASynRM would have to be measured to detect the true rotor d-axis.

Afterwards, the control technique to maximize the efficiency, was investigated. This was done by looking at the efficiency equation for the FASynRM, both in relation to the active power equation and the copper and core losses. The MEA was then presented, which relied on quadratic interpolation to locate the optimum current vector angle through a series of power evaluations at different current vector angles.

The preceding findings from the other chapters were then used to test the FASynRM in multiple experiments. Firstly, it was verified that the true rotor d-axis could be located, which meant that the ME angle of the FASynRM could be found for the EEI operating conditions afterwards. The power measurements to locate the ME angle were done manually, and the results were comprised into a table, which were used as a comparison for the following experiments. It was found that the active power equation was incapable of determining the correct input power, so the MEA was tested online with the help of power Look-Up Tables (LUTs) developed from the power measurement tables. To avoid developing LUTs for various different operating conditions it was investigated if a power loss estimation profile could be determined, to estimate the power losses in the FASynRM based on only a few sets of experiments. A linear relation was found between the q-axis current and the core losses for 2000, 2500 and 3000 rpm. Likewise, a linear relation for the three speeds combined was also determined. All four linear functions were individually combined with the copper losses to provide four functions to online determine the power losses in the FASynRM. During testing of the MEA, it was found that all functions were capable of finding the ME angle, provided that a correct initial angle interval was used in the MEA.

The three different ways to maximize the efficiency of the FASynRM each had its advantages and disadvantages. The active power equation should in theory be able to estimate the input power in real-time but required a set of offline experiments to determine a voltage error compensation LUT. However, in the end it was not capable of estimating the input power correctly. The input power LUT approach was capable of finding the ME angle for all operating conditions and tests, but required a set of experiments for each operating condition. The power loss estimation profile was also capable of finding the ME angle and only required a set of experiments for one speed and various load torques. Having found a reliable way of estimating the power losses in the FASynRM and thereby enabling ME control of the machine, the gains in the ME control strategy was compared to MTPA and Constant Angle (CA) control. It was found that the EEI value and annual energy consumption between the different control strategies was negligible and therefore left to the user to determine which of the three control strategies was the most suitable based on the implementation effort and number of operating conditions.

Preface

This Master's Thesis in Power Electronics and Drives is written by group *PED4 - 1041* at the Department of Energy Technology at Aalborg University. The following software has been used to:

- **Overleaf** - Write the report.
- **MATLAB & Simulink** - Model and simulate the system, and generate C-code for the experimental setup.
- **Inkscape** - Edit figures.
- **dSpace** - Control the experimental setup in real time.
- **Mathcha** - Graphic design.

Reader's Guide:

On page vi, a table of contents is given. When viewing this report as a PDF, hyperlinks in the table of contents will allow fast navigation to the desired sections.
Page viii displays a nomenclature listing the abbreviations, as well as the variables and their respective units used in this report. The indices will also be presented here.

The bibliography on page 57 presents the literature used in this report. The references are given in the following format:

[Author][Title](Institution)(ISBN)[Year](URL)(Date Accessed)

Where fields in square brackets are mandatory, while regular brackets are only relevant for certain formats, i.e books or web pages. The bibliography entries are sorted after their appearance in the text. Sources will be cited with the Vancouver method [number] where the number represents the number in the bibliography.

Equations will be referenced according to their appearance in the report. As such, equation number 4 in chapter 2 will be referred to as Equation (2.4).

The reference used for figures and tables follow the same logic as for the equations, however without the parentheses.

Table of Contents

Nomenclature

Abbreviations

a	Phase a
AC	Alternating Current
b	Phase b
BEMF	Back Electromotive Force
c	Phase c
CA	Constant Angle
d	Direct
DC	Direct Current
Diff	Difference
EEI	Energy-Efficiency-Index
FASynRM	Ferrite Assisted Synchronous Reluctance Machine
FE	Finite Element
FEM	Finite Element Method
FOC	Field Oriented Control
IE	International Efficiency
IM	Induction Machine
LUT	Look-Up Table
ME	Maximum Efficiency
MEA	Maximum Efficiency Algorithm
MEI	Minimum-Efficiency-Index
Min	Minimum
MMF	Magnetomotive Force
MTPA	Maximum Torque Per Ampere
PI	Proportional Integral
PM	Permanent Magnet
PMSM	Permanent Magnet Synchronous Machine
PWM	Pulse Width Modulation
q	Quadrature
RMS	Root Mean Square
SMPMSM	Surface Mounted Permanent Magnet Synchronous Machine
SVM	Space Vector Modulation
SynRM	Synchronous Reluctance Machine

Variables

Symbol	**Description**	**Unit**
δ	Stop criterion for MEA	[W]
η	Efficiency	(%)
γ	Core Loss Coefficient	[-]
λ	Flux Linkage	(Wb-t)
$\mathcal{R}$	Reluctance	[H^{-1}]
μ	Permeability	[H/m]
μ_0	Permeability of air	[H/m]
ω	Angular Frequency	(rad/s)
ϕ	Current Vector Angle	[°]
θ	Rotor position	(° || rad)

α	Alpha	(-)
β	Beta	(-)
$\vec{}$	Vector	(-)
*	Reference	(-)
A	Area	[m^2]
a	Slope of linear function	(-)
a_0, a_1 and a_2	Quadratic function coefficients	(-)
B	Flux Density	[Wb/m^2]
b	Intersection with y-axis	(-)
d	Thickness	[m]
f	Frequency	(Hz)
f	Function	(-)
H	Field Intensity	[A·turns/m]
H	Head	[m]
I	Current Amplitude	[A]
i	Current	(A)
K	Gain	(-)
L	Inductance	(H)
l	Length	[m]
N	Number	(-)
n	Rotational Speed	(rpm)
P	Active Power	(W)
Q	Flow Rate	[m^3/h]
q	Estimated function	(-)
R	Ohmic Resistance	(Ω)
T	Temperature	(°C)
T	Torque	(Nm)
t	Time	(s)
V	Voltage Amplitude	[V]
v	Voltage	(V)
x	Arbitrary number	(-)

Indices

α	Alpha
β	Beta
a	Phase a
ab	Between Phase a and Phase b
avg	Average
b	Phase b
c	Phase c
cmd	Command
co	Coercive
comp	Compensation
core	Core
cu	Copper
d	Direct
diff	Difference
dS	dSpace
e	Eddy
EEI	Energy-Efficiency-Index

em	Electromagnetic
err	Error
est	Estimated
fric	Friction
h	Hysteresis
i	Inner
in	Input
l	Lower
loss	Loss
m	Mechanical
max	Maximum
meas	Measured
min	Minimum
mpm	Maximum Permanent Magnet
new	New Measurement
norm	Normalized
old	Previous Measurement
opt	Optimum
out	Output
pk	Peak
pm	Permanent Magnet
pos	Position
pp	Pole-Pairs
q	Quadrature
r	Rotor
re	Rotor Electrical
ref	Reference
rel	Reluctance
rem	Remanence
rms	Root Mean Square
s	Stator
str	Stray
tot	Total
u	Upper
yoko	Yokogawa Power Analyzer

Chapter 1

Introduction

Electric machines are being used more and more because of the desire to reduce the use of fossil fuels. There are three main types of machines which are Permanent Magnet Synchronous Machines (PMSMs), Induction Machines (IMs) and Synchronous Reluctance Machines (SynRMs). PMSMs have high torque density and high efficiency. However, because of the use of magnets made of rare earth materials the price of this type of machine can be high. There is also a risk of demagnetizing the magnets and displacement of the magnets inside the machine, thus reducing the robustness of PMSMs.[3] Furthermore, the PMSMs have poor high speed performance as the BEMF at high speed becomes too large, hence flux weakening is needed. For IMs the price is lower than PMSMs, however the copper losses are larger compared to the other types of machines because current is generated in the rotor which leads to lower efficiency. Furthermore, the copper losses in the rotor could lead to increased temperature of the rotor thus requiring thermal cooling of the rotor, which is usually more difficult to obtain compared to cooling of the stator. SynRMs have a torque density and efficiency between that of PMSMs and IMs and the robustness is high. However, the kVA rating of the inverter is larger for SynRMs because of a low power factor.[4] SynRMs have shown to be a good competitor to the PMSM, however the power factor and torque density are lower for the SynRM. To improve the power factor and torque density, magnets can be put into the flux barriers of the SynRM. This way the power factor is improved and PM torque is added to the torque equation resulting in a larger torque density. By using NdFeB as Permanent Magnets (PMs) more torque can be produced by the magnets compared to ferrite magnets. However, using NdFeB magnets is expensive and to reduce the price, ferrite magnets are usually preferred.[5]

In [1] a moulding technique to insert ferrite magnets into the flux barriers of the SynRM was suggested. This makes it possible to avoid inserting the magnets manually, avoiding glue, displacement of the magnets and unwanted airgaps. This type of machine is called a ferrite assisted SynRM (FASynRM) and this type of machine will be investigated in this report. The work in [1] was done in cooperation with Grundfos to replace an existing commercially used IM. The work showed compelling results, outperforming the target IM, however several design aspects of the FASynRM were still to be addressed. In continuation of this, a secondary report was made, also in cooperation with Grundfos, investigating the effect of step-skewing the rotor to reduce the torque ripple [2]. The optimal skewing angle of either 5 or 15 electrical degrees was found to be a compromise between reduction in average torque production and reduction in torque ripple. This thesis builds on the two previous reports made together with Grundfos. For this project Grundfos has provided a FASynRM resultant of the work done in [1][2]. Grundfos is a pump manufacturer and the FASynRM is therefore intended to be applied to their TPE 65-250/2 A-F-A-BAQE-KDB 4 kW pump unit (Shortened to TPE Pump). Grundfos is interested in operating their pump application with the highest efficiency possible. To asses and compare the efficiency of different types of pumps a standardized way of determining the efficiency has been made and will be described in the following section.

1.1 Standardized Efficiencies for Pump Applications

As a way to combat climate change, the European Commission has in collaboration with the association of European pump manufacturers (EUROPUMP) introduced regulations specifically for rotodynamic clean water pumps to increase their energy efficiency[6]. These regulations were enforced from the 1st of January 2013 and define a required Minimum-Efficiency-Index (MEI) in order for the pumps to be allowed on the European market. The MEI is an index defining the minimum allowable pump efficiency at specific flow rates. Similarly, a classification of AC motors has also been introduced by the IEC standard, which divides the motors in International Efficiency (IE) classes, based on their efficiency at rated load. The regulations regarding the MEI for rotodynamic clean water pumps and the IE classification for AC motors only take the efficiency of the product into account and does not account for the application type the products are used in. As such, a new classification system known as the Energy-Efficiency-Index (EEI) has been developed, which takes both the product efficiencies and application types into consideration. This classification system is already mandatory for circulatory pumps as of 2013 but has yet to be applied to the field of rotodynamic clean water pump applications. As a customer it would be cumbersome to determine which motor and pump to choose for a specific application, as the customer would have to relate the pump and motor efficiency for all the products on the market at different load conditions corresponding to the specific load profile. Therefore, a standardized load profile has been developed by the EUROPUMP group, which is meant to generalize most applications into a standardized load profile and thus enable a comparison of the EEI for various pump units. The load profile can be seen in Table 1.1 [6].

Use Case #	Flow Rate $\frac{Q_i}{Q_{Rated}}$ [%]	Load Time $\frac{t_i}{t_{tot}}$ [%]
1	100	6
2	75	15
3	50	33
4	25	44

Table 1.1. The standardized load profile shows the yearly operating times in percentage relative to the pump flow rate[6]. Q_i is the flow rate for use case i, Q_{Rated} is the rated flow rate, t_i is the operating time of use case i and t_{tot} is the total operating time of the pump.

From Table 1.1 it can be seen that for the EEI calculation, four different use cases are considered for the TPE Pump. Each use case constitute a different power consumption, which means that the total average power consumption of the TPE can be calculated as shown in Equation (1.1).

$$P_{avg} = \frac{t_1}{t_{tot}} \cdot P_{in,EEI,1} + \frac{t_2}{t_{tot}} \cdot P_{in,EEI,2} + \frac{t_3}{t_{tot}} \cdot P_{in,EEI,3} + \frac{t_4}{t_{tot}} \cdot P_{in,EEI,4} \tag{1.1}$$

where P_{in} is the input power for each EEI case. The average power consumption is compared to a reference input power for 4 kW pumps, P_{ref} = 4933.7 W. The EEI value is then given by Equation (1.2).

$$\text{EEI} = \frac{P_{avg}}{P_{ref}} \tag{1.2}$$

In order to optimize the EEI value for the pump unit both the pump itself and the motor will have to be made more efficient, especially at use case 3 & 4 as they weigh heavily in the EEI calculation due to the larger load times. This report will only consider the optimization of the motor part of the pump unit by finding the most optimal control strategy to minimize its power losses, thus leading to the following initial problem:

"What types of losses are associated with FASynRMs and how are these losses minimized to lower the EEI for the Grundfos TPE Pump?"

Chapter 2

Problem Analysis

In this chapter the different losses present in an electrical machine will be explained. Afterwards, the topology of a FASynRM will be presented and be related to other types of machines to examine how the control of a FASynRM might might be different from conventional motor control strategies. This will lead into an investigation of how the optimum current vector angle changes when the FASynRM is controlled with Maximum Torque Per Ampere (MTPA) vs. Maximum Efficiency (ME) control. Lastly, the operating conditions of the FASynRM will be outlined, which are based on the EEI TPE Pump requirements.

2.1 Machine losses

Losses in an electric machine can be divided into four different groups. These groups are the copper losses, core losses, friction losses and stray losses. The different types of losses will be explained in detail in the following subsections.

Copper Losses

Copper losses occur when current is flowing through the conductors in the stator. The copper losses are given by Equation (2.1).

$$P_{\text{cu}} = 3 \cdot I_{\text{s,rms}}^2 \cdot R_{\text{cu}} \tag{2.1}$$

where $I_{\text{s,rms}}$ is the rms phase currents in the stator and R_{cu} is the resistance of the copper wires in the stator. It is multiplied with 3 since there are three phases in the stator.

The resistance increases with temperature therefore it is advantageous to keep the temperature of the conductors in the stator as low as possible to reduce the copper losses. It is also advantageous to keep the amplitude of the current vector as low as possible. This can be done by using MTPA control. [7]

Another phenomenon is the skin effect which depends on the frequency. With higher frequency the current will concentrate on the edge of the conductor reducing the effective area the current passes through, hence increasing the resistance. [8]

Core losses

Core losses occur in the core part of the stator and rotor. The core losses can be divided into two types. Hysteresis losses and eddy current losses.

The stator and rotor is made of a ferromagnetic material which will be magnetized when it is subjected to a magnetic field. The material can be divided into small domains of small magnets. When there is no external field the small magnetic domains are oriented in random directions and the material is said to be unmagnetized. When an external field is applied the small domains will align and the material is said to be magnetized. Magnetization of a material can be illustrated by the hysteresis loop shown in Figure 2.1.

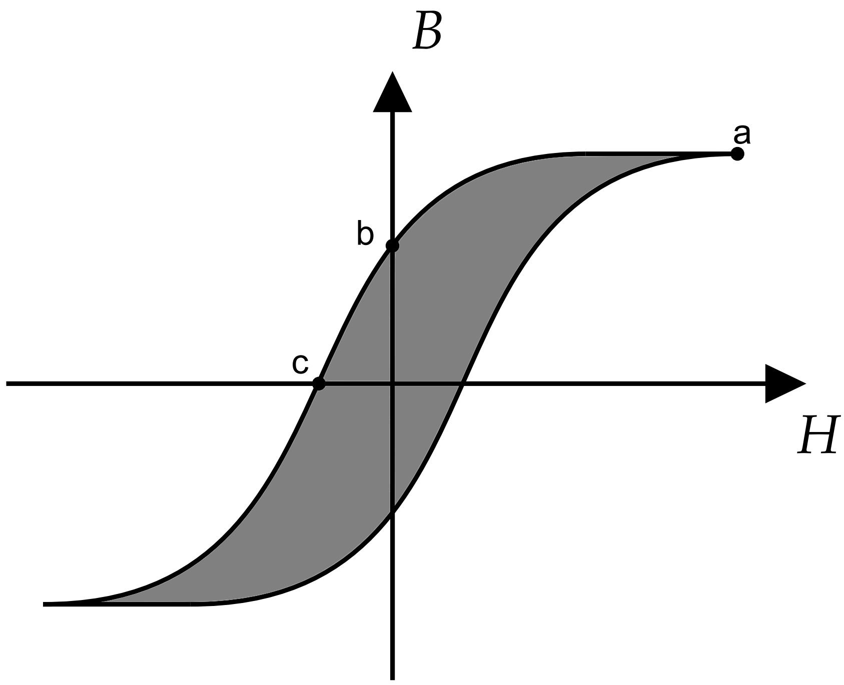

Figure 2.1. BH-curve for a magnetic material. Point a is where the material is saturated, point b is the remnant flux density and point c is the coercive force where the material stops being magnetic.

In Figure 2.1 the x-axis is the magnetic field intensity H [A·turns/m] and the y-axis is the flux density B [Wb/m^2]. Point a is where the magnetic material is saturated. Here an increase in the magnetic field intensity will only result in a small increase in the magnetic flux density. If the external field is removed the material will not be demagnetized completely. It will have a remnant flux density which is located at point b. If the magnetic field intensity is reversed i.e. in negative direction the magnetic material will be demagnetized. Complete demagnetization occurs at point c where the field intensity at this point is called the coercive force.

The stator is made of a magnetic material which will undergo a hysteresis loop when the current, i.e. field intensity, in the stator is varied like the one shown in Figure 2.1. The orientation of the magnetic domains inside the material will move around according to the magnetic field supplied to it. The energy required to do this corresponds to the hysteresis losses and this energy will be dissipated as heat in the material. The hysteresis losses can be expressed as seen in Equation (2.2).

$$P_\mathrm{h} = A_\mathrm{core} \cdot l_\mathrm{core} \cdot f \cdot \oint H_\mathrm{core}\ \mathrm{d}B_\mathrm{core} \tag{2.2}$$

where A_core is the area of the core, l_core is the length of the core and f is the frequency of the exciting current. It can be seen that the hysteresis losses are proportional to the volume of the core and the area of the hysteresis loop. The hysteresis losses are also proportional to the frequency of the applied field since it will undergo the hysteresis loop each cycle. To reduce the hysteresis losses a material with a slim hysteresis loop can be chosen. [9, pp. 22-25]

The second type of core losses is eddy current losses. These occur because of Lenz' law which states that if a conducting material is subjected to a changing magnetic field, a current will be induced in the material that counteracts the original change. The induced currents in the magnetic material due to the changing magnetic field from the stator are called eddy currents. These will circulate in the magnetic material and cause ohmic losses. Since the induced field counteracts the original field it results in demagnetization, hence the exciting field must increase which results in a wider dynamic hysteresis loop. The eddy currents induced in the core increase with frequency. To reduce the effect of eddy currents the core can be built with several sheets or lamination of material joined together and insulated from each other. This way the current loop of the induced eddy currents is reduced. This decreases the eddy current losses and the thinner the lamination the lower the losses. The eddy current losses under normal machine conditions can be approximated with Equation (2.3).

$$P_{\mathrm{e}} = K_{\mathrm{e}} \cdot (B_{\mathrm{max}} \cdot f \cdot d)^2 \tag{2.3}$$

where K_{e} is a proportionality factor which depends on the volume and resistivity of the core, d is the thickness of the lamination and B_{max} is the maximum flux density [9, p. 678]. It can be seen in Equation (2.3) that the eddy current losses depend on the square of the flux density, frequency and thickness of the laminations. [9, pp. 25-26]

According to [10] an emperical formula describing the total core losses can be determined. The formula can be seen in Equation (2.4).

$$P_{\mathrm{core}} = K_{\mathrm{core}} \cdot \omega_{\mathrm{re}}^{\gamma} \cdot (\lambda_{\mathrm{d}}^2 + \lambda_{\mathrm{q}}^2) \tag{2.4}$$

where ω_{re} is the electrical angular speed, $\gamma = 1.5 \sim 1.6$ and K_{core} is the core loss coefficient. λ_{d} and λ_{q} are the d- and q-axis flux linkages, respectively. It can be seen that the magnitude of the flux linkage squared is used in Equation (2.4). It has been written in terms of the d- and q-axis flux linkages separately so the core losses can be related to the d- and q-axis currents and inductances, since these are used in the dq-control of the machine.

Stray losses

The stray losses are due to a non-uniform current distribution in the conductors and distortion of the magnetic flux density. It is typically set to be 1 % of the rated output. [9, p. 678] They can be approximated by Equation (2.5).

$$P_{\mathrm{str}} = K_{\mathrm{str}} \cdot \omega_{\mathrm{re}}^2 \cdot (i_{\mathrm{d}}^2 + i_{\mathrm{q}}^2) \tag{2.5}$$

where K_{str} is the stray loss coefficient and i_{d} and i_{q} are the d- and q-axis currents, respectively. [10]

Friction losses

The friction losses, P_{fric}, are the losses related to the friction in the bearings and windage which is friction between the rotor and the air around it. The friction losses are not related to the current or flux in the machine and solely depend on the mechanical construction of the electrical machine. These power losses cannot be minimized by optimising the control strategy, but vary with the operating speed.

2.2 FASynRM Description

The electrical machine is controlled by varying the AC currents supplied from the inverter in order to vary the rotating Magnetomotive Force (MMF) that causes the rotor in the machine to rotate. To simplify the equations used in the modelling and control of the FASynRM the three-phase AC currents and voltages are projected into the synchronous rotating dq-reference frame as this reduces the number of equations from three to two and transforms the sine signals into DC-values. The motor voltage equations in the synchronous dq-reference frame are given by Equation (2.6).

$$
\begin{aligned}
v_\mathrm{d} &= R_\mathrm{s} \cdot i_\mathrm{d} + \frac{d\lambda_\mathrm{d}}{dt} - \omega_\mathrm{re} \cdot \lambda_\mathrm{q} \qquad & \lambda_\mathrm{d} &= L_\mathrm{d} \cdot i_\mathrm{d} + \lambda_\mathrm{mpm} \\
v_\mathrm{q} &= R_\mathrm{s} \cdot i_\mathrm{q} + \frac{d\lambda_\mathrm{q}}{dt} + \omega_\mathrm{re} \cdot \lambda_\mathrm{d} \qquad & \lambda_\mathrm{q} &= L_\mathrm{q} \cdot i_\mathrm{q}
\end{aligned} \tag{2.6}
$$

where the subscripts d and q describe the d- and q-axis component, respectively. v is the voltage and L is the inductance. R_s is the resistance in the stator windings and λ_mpm is the flux linkage caused by the permanent magnet.

A schematic of a 2 pole-pair FASynRM can be seen in Figure 2.2.

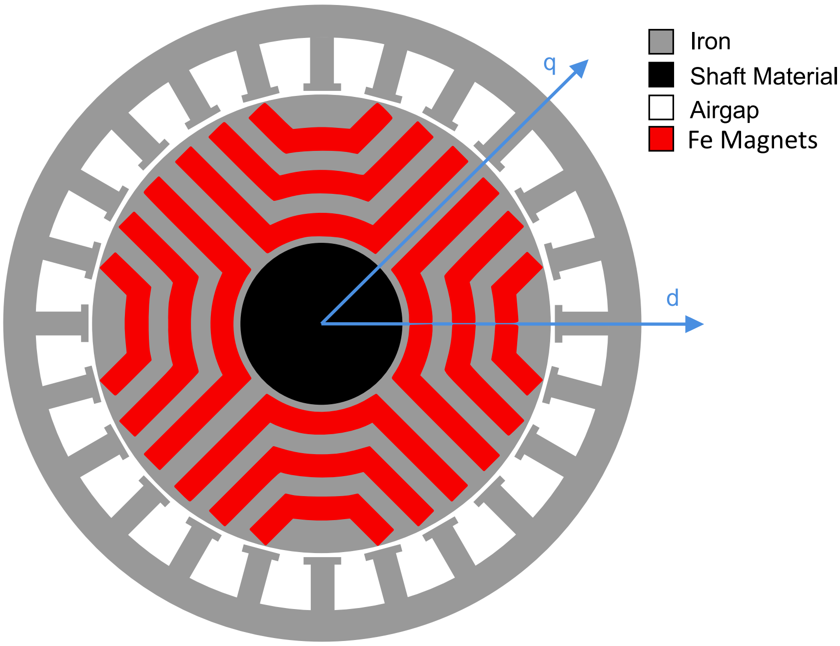

Figure 2.2. Cross-sectional area of a 2 pole-pair FASynRM showing both the stator and the rotor. The d-axis is defined to be aligned on the high reluctance path, i.e the permanent magnets.

Due to the fact that the q-axis is defined to lead the d-axis by 90 electrical degrees and the rotor in the FASynRM consists of two pole-pairs, the d- and q-axis are located 45 mechanical degrees apart as indicated in Figure 2.2. Furthermore, for this case the d-axis is defined to be aligned with the high-reluctance path in the rotor. This means that it is centered along the permanent magnets (PMs) as their permeability is similar to that of air, whereas the q-axis is aligned with the least reluctance path through the core of the rotor, which can be seen in the figure. Since the reluctance for the d- and q-axis are different, so are the inductances. The relation between the inductance and the reluctance can be seen in Equation (2.7).

$$
L = \frac{N^2}{\mathcal{R}} \qquad \mathcal{R} = \frac{l}{\mu \cdot A} \tag{2.7}
$$

where N is the number of turns in the winding, $\mathcal{R}$ is the reluctance, l is the length of the reluctance path, μ is the permeability of the material and A is the area where the flux is crossing. Since the permeability of the core material is larger than the permeability of both the magnet and air ($\mu_{\text{core}} > \mu_0$) the reluctance for the d-axis is larger than that for the q-axis. Hence, the inductance for the d-axis is smaller than that for the q-axis leading to a saliency ratio larger than one ($L_\text{q}/L_\text{d} > 1$) for both a SynRM and a FASynRM. The difference in the d- and q-axis inductances is what causes the torque production in SynRMs. For a FASynRM the PMs also produce torque, hence the torque equation for a FASynRM is given by Equation (2.8).

$$T_\text{em} = \frac{3}{2} \cdot N_\text{pp} \cdot (\lambda_\text{mpm} \cdot i_\text{q} + (L_\text{d} - L_\text{q}) \cdot i_\text{d} \cdot i_\text{q}) \tag{2.8}$$

where N_pp is the number of pole-pairs in the machine. The last term $(L_\text{d} - L_\text{q}) \cdot i_\text{d} \cdot i_\text{q}$ is known as the reluctance torque, T_rel, and is a result of the inductance difference on the d- and q-axis due to the different air gap lengths. With the definition of the d-axis as in Figure 2.2 a negative d-axis current will have to be supplied to produce a positive reluctance torque since $L_\text{d} < L_\text{q}$. The first term, $\lambda_\text{mpm} \cdot i_\text{q}$, is the torque contribution from the PMs, T_PM, in the rotor and is directly proportional to the q-axis current amplitude. For Surface mounted Permanent Magnet Synchronous Machines (SPMSMs) no reluctance torque can be generated as the d- and q-axis inductances are approximately equal and MTPA is achieved by aligning the current vector on the q-axis. For SynRMs there are no PMs and torque is solely dependent on the reluctance torque and MTPA is achieved at a current vector angle of 135° if L_d and L_q are considered to be constant. This can be realised from Equation (2.8) and the fact that $L_\text{d} < L_\text{q}$. i_d and i_q must be equal and i_d should be negative, hence the MTPA angle is 135°. However, for a real SynRM cross-saturation for the d- and q-axis inductances has an influence on the MTPA point. Hence, the inductance difference changes with the current, meaning that the MTPA angle differs from 135° [11]. However, this is not considered here. The MTPA current vector for three different machines is depicted in Figure 2.3.

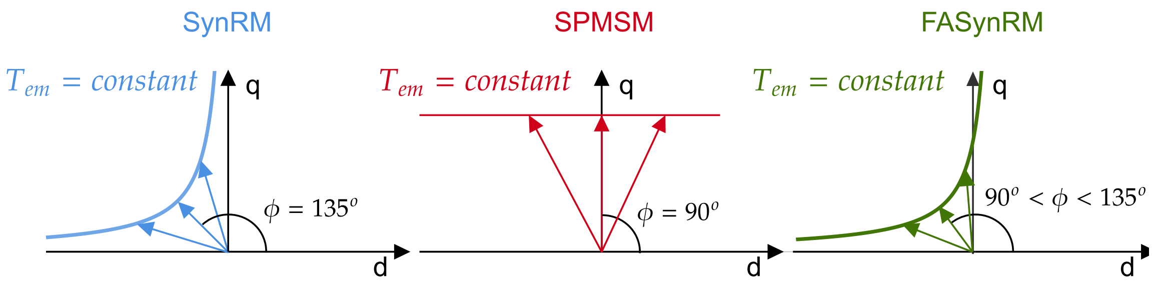

Figure 2.3. Illustration of the MTPA current vector angle, ϕ, for various types of electrical machines. This angle corresponds to the lowest current vector amplitude for a given torque command.

From Figure 2.3 it can be seen that the optimal current vector angle is dependent on the type of electrical machine, which is due to their different torque productions earlier explained in relation to Equation (2.8). As the FASynRM both produces reluctance torque and PM torque its optimal current vector angle is somewhere between 90° and 135° depending on the flux linkage from the PM and the d- and q-axis inductance difference. Another way to explain the MTPA current vector angle is by looking at the flux lines in the rotor during one rotation. This is illustrated for a SynRM in Figure 2.4

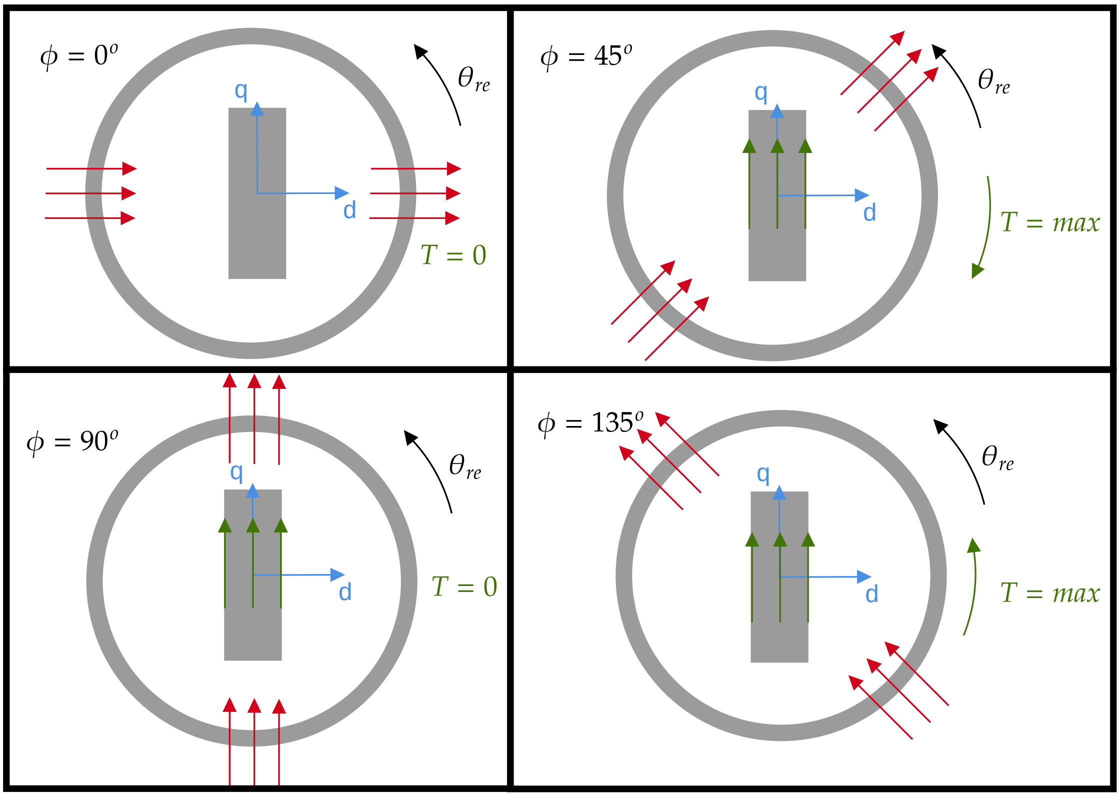

Figure 2.4. Figure showing the flux lines going through the rotor at different current vector positions. The rotor schematic has been simplified to a one pole-pair rectangle where the rotor d-axis is aligned with the high reluctance path, i.e. at the largest air gap. The rotor is fixed in the same position and the stator MMF is rotated in the counter-clockwise direction. The rotor position, θ_{re}, and electromagnetic torque is defined to be positive in the anti-clockwise direction.

From Figure 2.4 it can be seen that when the current vector angle is at 0° the machine is symmetrical relative to the stator field axis and thus no torque is experienced between the stator and rotor MMF. When the stator MMF is located at 45° relative to the rotor d-axis maximum reluctance torque occurs in the negative direction as the flux lines from the stator travel through the low reluctance path in the rotor core. The flux lines inside the rotor will tend to align to the stator MMF and torque is created in the negative direction. When the current vector angle is at 90° in the dq-reference frame, the rotor flux lines are perfectly aligned with the stator flux lines and no torque occurs. At 135° the flux lines in the rotor core will create maximum torque in the positive direction as the rotor flux lines will try to align with the stator MMF. At 180° the reluctance torque will again reach zero as the rotor flux lines are again symmetrical around the stator flux axis. For the two pole-pair FASynRM prototype this then gives a total torque production as shown in Figure 2.5.

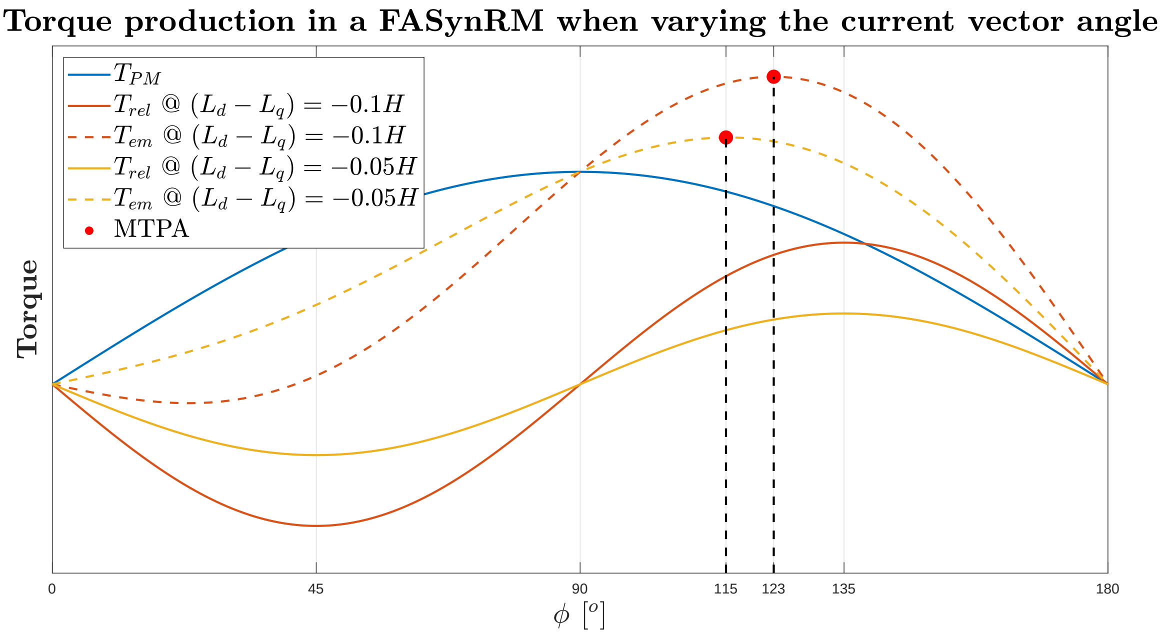

Figure 2.5. The different torque components as well as the total torque production in the FASynRM are shown for 180 electrical degrees. The electromagnetic torque is the sum of the PM torque and reluctance torque according to Equation (2.8). The d- and q-axis inductances are assumed constant.

From Figure 2.5 it can be seen that the reluctance torque has twice the frequency of the PM torque. The PM torque reaches its maximum value at an angle of 90 electrical degrees, whereas the reluctance torque reaches its positive peak at 135 electrical degrees equivalent to the description in Figure 2.3. The FASynRM is able to achieve a higher total torque as it is a combination of both the reluctance and PM torque. The MTPA angle depends on the relationship between the d- and q-axis inductance difference and the flux linkage of the PM. It can be seen from the figure that if the d- and q-axis inductance difference increases, the total torque production increases and the optimal current vector angle is moved towards 135 electrical degrees similar to the SynRM. However, in case the PM flux linkage increases the PM torque will contribute a greater portion to the total torque and the MTPA angle will move towards 90 electrical degrees similar to that of a SPMSM.

2.3 MTPA vs. ME Control

MTPA aims to generate the required torque with the minimum current vector amplitude as a way to minimize the copper losses for a fixed operating point. However, as earlier explained in Section 2.1 core losses also contribute to the overall losses in the FASynRM and therefore these also have to be considered to control the machine as efficiently as possible. From Equation (2.4) it can be seen that the core losses depend on the speed and the flux linkage. At a given speed the core losses vary with the d- and q-axis current, the d- and q-axis inductance and flux linkage of the magnet. To illustrate how the core and copper losses vary with the current vector angle and how the angle for the minimum copper and core losses influences the optimum angle for the sum of the two types of losses an example is given. An arbitrary torque of $T_{\mathrm{em}} = 10$ Nm and d- and q-axis inductance values of $L_{\mathrm{q}} = 50$ mH and $L_{\mathrm{d}} = 25$ mH have been chosen. The flux linkage of the PM and the resistance of the wires have been chosen to represent the parameters of the machine used in this project. From the d- and q-axis currents and d- and q-axis inductances the copper and core losses are calculated using Equation (2.1) and (2.4). Figure 2.6 shows how the copper and core losses vary with the current vector angle at an arbitrary speed and constant torque.

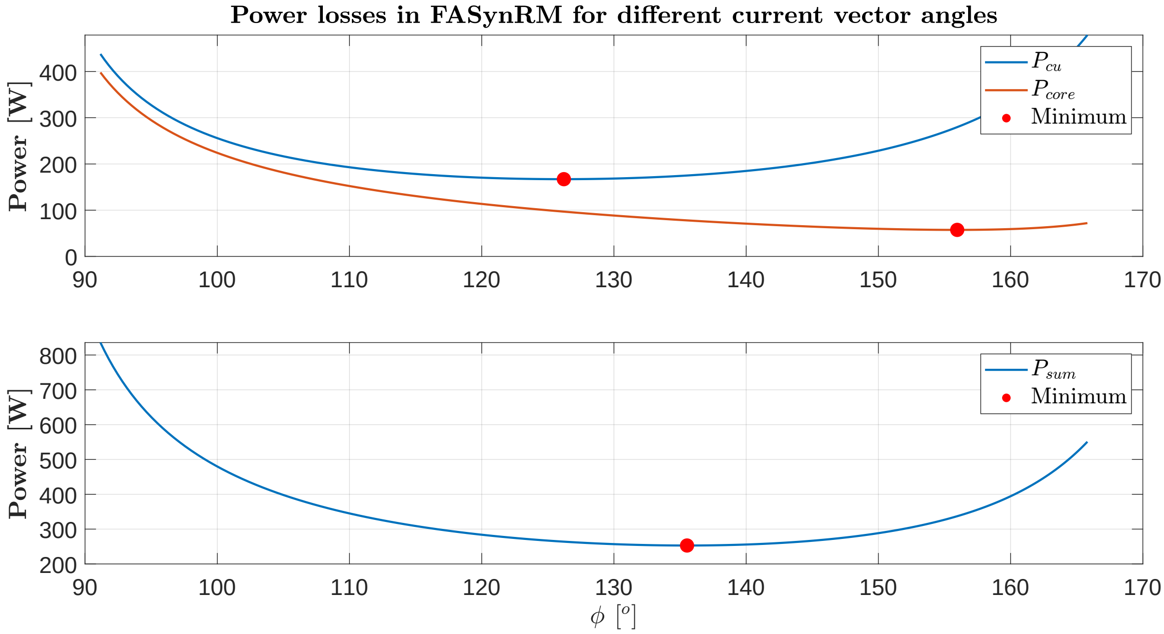

Figure 2.6. The variation of the copper and core losses with the current vector angle at an arbitrary speed and a constant torque. The L_d and L_q inductances are kept constant. The top figure shows the copper and core losses and the bottom figure shows the sum of the core and copper losses along with the minimum point for each curve.

From Figure 2.6 it can be seen that the copper and core losses vary with the angle of the current vector. It should be noted that the d- and q-axis inductances are kept constant in Figure 2.6, however in a real situation they vary with the amplitude of the d- and q-axis current. The figure is therefore only used as an illustration. From the figure it can be seen that the current vector angle for the minimum copper and core losses are different from each other. In the bottom plot of Figure 2.6 the sum of the copper and core losses can be seen. It can be seen that the MTPA angle occurs around 126° and the minimum core losses occur around 156°. However, when considering both the copper and core losses, the optimum angle for minimum power loss is found at 136°.

It is clear that the angle for the total minimum losses is different from the current vector angle that minimizes the copper losses. Hence the current vector angle to obtain MTPA can be different from the angle to obtain maximum efficiency. Depending on the operating conditions the current vector angle to obtain maximum efficiency will be skewed towards either the angle to obtain minimum copper losses or core losses. For low speed and high torque conditions the copper losses will be dominant resulting in the optimum angle being close to the angle for minimum copper losses and using the MTPA angle as the ME angle might suffice. However, for high speed and low torque conditions the ME point will be skewed towards the minimum core loss angle. As the FASynRM will be operated at rated speed in this project, the core losses cannot be considered negligible. Therefore, it might not be possible to obtain maximum efficiency by using MTPA, hence a different control strategy must be developed to obtain maximum efficiency control.

2.4 Operating Conditions based on EEI Standards

To calculate the flow rates for the Grundfos TPE pump, for the four different use cases used in the EEI calculations, the rated flow rate needs to be defined. To do so, the QH-curve for this pump is utilised and the head, H, is read as a function of flow rate, Q, when the motor is operating at 110% speed. The datapoints for the QH-curve for this pump unit are shown in Figure 2.7.

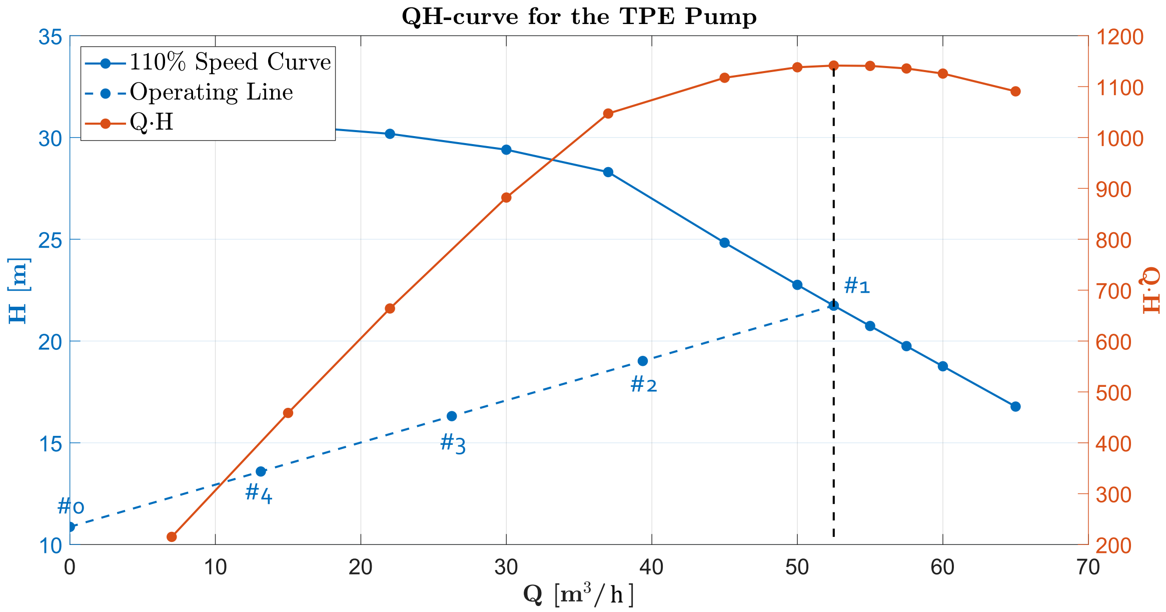

Figure 2.7. The QH-curve for the Grundfos TPE Pump. The blue solid line shows the head as a function of the flow rate at 110% operating speed. The blue dashed curve shows the operating line for the four different use cases of the TPE Pump as well as the point at #0, which has been used to draw the trend line of the QH-curve[12]. The orange line shows the product of the head and flow rate where the maximum value of this product defines the rated flow rate.

The rated flow rate is found where the product of the flow rate and head is the maximum, which in this case corresponds to a flow rate of 52.5 m^3/h read from point use case 1 in Figure 2.7. The head at this operating point is 21.74 m, where half of this value is used to define the head at a flow rate of 0 m^3/h, marked at point use case 0. The operating line of the TPE Pump is drawn between use case 0 and 1 and the head for use case 2-4 are read at 75%, 50% and 25% of the rated flow rate, respectively. Having specified the flow rate and head at the four use cases, both the shaft power and the operating speed of the pump can be read from the datasheet and are presented in Table 2.1.

Use Case #	Q [m^3/h]	H [m]	n [rpm]	P_{out} [W]	T_{em} [Nm]
1	52.5	21.74	3011	4000	12.7
2	39.375	19.02	2701	2682	9.5
3	26.25	16.31	2413	1673	6.6
4	13.125	13.59	2155	940	4.2

Table 2.1. The flow rate and head for the TPE Pump for the four different use cases used in the EEI calculation. The corresponding speed, output power and torque are also shown. The data is read from the product curves provided by Grundfos on their website[12].

Having specified the speed and output power of the electrical machine in the TPE Pump as shown in Table 2.1, the corresponding torque can be calculated. Thus, the operating conditions used in the EEI calculations for the FASynRM for the TPE Pump have been found and will be used as the operating conditions during testing of the FASynRM

In this chapter the four types of losses present in an electrical machine were presented. These included the copper, core, friction and stray losses. The friction losses only varied with the operating speed and could therefore not be minimized by the control strategy. The copper losses were minimized by MTPA where the optimal current angle depends on the type of electrical machine. For the FASynRM the control angle depended on the relationship between the PM flux linkage and the d- and q-axis inductance difference. To minimize the core losses, the optimal current vector angle was found to be different relative to the MTPA operating point, thus changing the control angle in case ME control was desired. Finally, the four operating conditions which the FASynRM will be subjected to were introduced. These were based on the EEI use cases for the TPE Pump.

Chapter 3

Problem Statement

Based on the introduction in Chapter 1 and the analysis carried out in Chapter 2, the following problem statement is proposed:

"How can online maximum efficiency control be achieved for a FASynRM and is the implementation of maximum efficiency control worthwhile compared to other control techniques when considering the EEI?"

Objectives
To answer the problem statement satisfactorily, the following objectives will be used to define the scope of this project.

- Conduct experiments to determine the motor parameters.
- Investigate the system prototype to find its limitations to ensure a robust control of the FASynRM.
- Design a search algorithm to determine the maximum efficiency current vector angle of the FASynRM at different operating conditions.
- Validate the implementation of the control scheme and search algorithm by performing experiments on the FASynRM prototype in the laboratory.
- Compare and asses if the potential increase in efficiency for the maximum efficiency control strategy outweighs its potentially more complex implementation, relative to a MTPA or constant current angle control strategy.

3.1 Delimitation

Due to the time constraint of this thesis the following delimitation are made:

- Cross-saturation of the d- and q-axis inductances will not be considered.
- The non-linearities of the inverter will not be considered but will be accounted for by implementing a voltage error Look-Up Table (LUT) from laboratory results.
- Sensorless control will not be considered and an encoder will be used to accurately determine the position and speed of the rotor.
- The location of the rotor d-axis is found by measuring the BEMF of the FASynRM.
- The stray and core losses are combined into a unified power loss profile, since they cannot be distinguished from each other. For simplicity the frictional losses are also included in this loss profile.
- The efficiency of the system only considers the FASynRM and does not take the power losses in the inverter into account.

Chapter 4

System Description

This chapter aims to describe the system used in this thesis by first presenting the FASynRM prototype supplied by Grundfos. Measurements are performed on the machine to determine the motor parameters, such as the resistance of the wires in the stator, the PM flux linkage and the d- and q-axis inductances. Afterwards, the voltage error caused by the inverter are accounted for. Next, the control scheme of the FASynRM is investigated, where both the limit of the d-axis current reference and the initial rotor position is needed. Therefore, the maximum allowable d-axis current reference is examined with regards to the demagnetization of the ferrite magnets in the rotor, and the initial rotor position is found with the help of the torque equation for the FASynRM.

4.1 Prototype Description

The prototype used in this thesis is the resultant work of two former reports. In the work carried out in [1] a rotor for the FASynRM was designed to match a 13 kW target IM, however due to practicalities the stack length of the rotor was reduced from 260 mm to 100 mm. This reduced the power output of the FASynRM to 5 kW, although it was found that rated operating conditions could not be obtained due to the limitations of the stator windings. In [2] the cogging torque of the FASynRM was investigated by step skewing the rotor. It was found that the optimal skewing angle was either 5 or 15 electrical degrees depending on whether the average torque or the torque ripple was considered most important. The rotor installed in the prototype used in this project has therefore been designed with a skewing angle of 7.5 mechanical degrees between the two rotor segments. Furthermore, due to the limitations of the stator windings present in [1] a new stator was produced with a lower number of turns to enable the FASynRM to operate at rated conditions. The rated condition of 5 kW are only attainable with water cooling, but the prototype designed by Grundfos is cooled by air, lowering the rated output power to around 4 kW. This corresponds well with the 4 kW output power required by the Grundfos TPE Pump to operate at rated flow rate. The specifications for the prototype are summarized in Table 4.1.

FASynRM Specifiations	
Rated power	4 kW
Rated speed	3000 rpm
Rated torque	12.7 Nm
Stator outer diameter	135 mm
Stator inner diameter	75 mm
Number of stator slots	24
Parallel wires	2
Parallel groups	2
Turns pr coil (New)	87
Turns pr coil (Old)	95
Air gap	0.8 mm
Rotor outer diameter	73.4 mm
Rotor inner diameter	17.5 mm
Number of pole pairs	2
Stack length	100 mm

Table 4.1. Specifications of the FASynRM.

4.2 Resistance Measurement

For measuring the resistance of the stator windings in the FASynRM, a Chroma programmable AC source is used as a DC source. Since it is not possible to access the neutral point in the provided motor, the line-to-line voltage is measured along with the phase current for one phase. The voltage and current is measured by a multimeter and the resistance is found by applying Ohms law. As the voltage is the line-to-line voltage between two phases, the two measured phases are connected in series and the phase resistance is therefore equal to half of the calculated resistance. This experiment is conducted between phase a and b at various currents and voltages and the stator phase resistance is found to be 0.75 Ω.

4.3 PM Flux Linkage Measurement

For this experiment the FASynRM is operated directly connected to a SPMSM, which will be operated at different speeds. In this case the FASynRM is operated as the load and the terminals are open-circuited meaning that no current can flow in the FASynRM. That way the machine voltage equations in Equation (2.6) reduce to $v_{\mathrm{q}} = \omega_{\mathrm{re}} \cdot \lambda_{\mathrm{mpm}}$. By measuring the RMS value of the line-to-line voltage on the open terminals for various speeds the PM flux linkage can then by found and the results from the tests are shown in Table 4.2.

Speed [rpm]	$V_{\mathrm{ab,rms}}$ [V]	V_{a} [V]	λ_{mpm} [Wb]
400	16.10	13.15	0.1570
800	32.17	26.27	0.1568
1200	48.27	39.41	0.1569
1600	64.37	52.56	0.1569
2000	80.46	65.70	0.1569

Table 4.2. PM flux linkage measurements for different operating speeds.

The average value of the PM flux linkage is found to be 0.1569 Wb. However, these measurements were made on 04.04.2022, but it has since been found that the PM in the rotor has been slightly demagnetized. This happened accidentally when an uncontrolled current spike occurred. The most recent measurements for the flux linkage were made on 18.05.2022 where the PM flux linkage was measured to be 0.140 Wb.

4.4 Measurement of the d- and q-axis Inductances

To measure the d- and q-axis inductances of the FASynRM, the rotor is physically locked to align both the rotor d- and q-axis with the stator α-axis. The d- and q-axis are located by operating the FASynRM as a load motor and then measure the BEMF of the FASynRM and marking both axes with a chalk mark on the shaft of the machine. This can be seen in Figure 4.1.

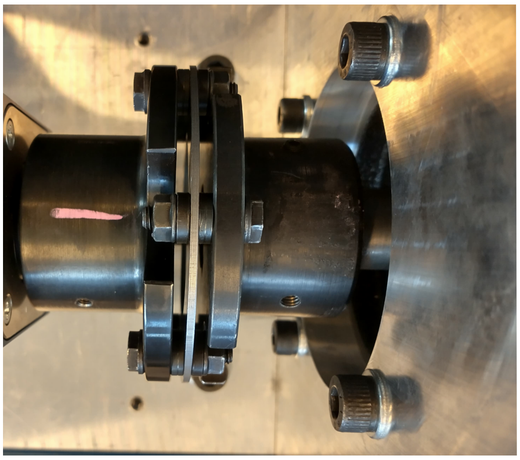

Figure 4.1. On the rotor it can be seen that a chalk mark was drawn, which was used to align the rotor.

The chalk mark used to indicate the location of the d-axis is shown in Figure 4.1. The rotor was locked in such a way that when the chalk mark was in a vertical position, a current vector on the stator α-axis would be aligned with the either the rotor d or q-axis. To supply an AC current on the stator α-axis, a single-phase transformer supplied by the grid is connected to the machine. Since the motor does not have a neutral connection, the positive terminal of the transformer is connected to phase a of the stator while the negative terminal is connected to phase b and c, which are shorted to create AC current on the stator α-axis. As the secondary side of the transformer is connected to the motor side, by varying the transformer ratio the voltage and current on the motor side can be changed. The inductance can then be calculated according to the motor voltage equations earlier presented in Equation (2.6) and the results for the d- and q-axis inductances can be seen in Figure 4.2.

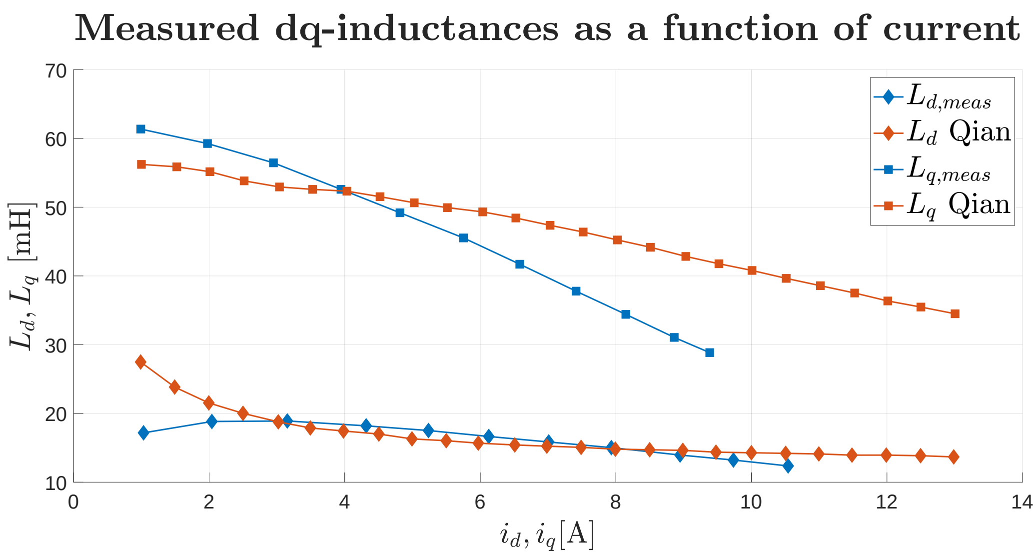

Figure 4.2. Measured d- and q-axis inductances for the FASynRM. The measured inductances from Qian's report[1] have been scaled with the ratio between the new and old number of turns according to Equation (2.7).

The measurements in Figure 4.2 are done by increasing the voltage on the secondary side of the transformer to create a peak current amplitude from 1 to 11 A, as the transformer is rated to 8 A RMS. Since some harmonics were present in the measurements, the inductances are calculated for the fundamental components. It can be seen from the figure that while the d-inductance matches well with the earlier work done in [1], the q-inductance deviates from the former results. The initial measured value is seen to be higher for lower current amplitudes but decreases faster, when the current amplitude increases. This means that the flux linkage from this experiment saturates faster, which could be caused by the way the rotor is locked. Since it is manually locked at the drawn chalk marks there is a possibility that it is not truly locked on the d- and q-axis. The width of the iron path along the q-axis is only 3.78 mm, which can be seen in Figure 4.3.

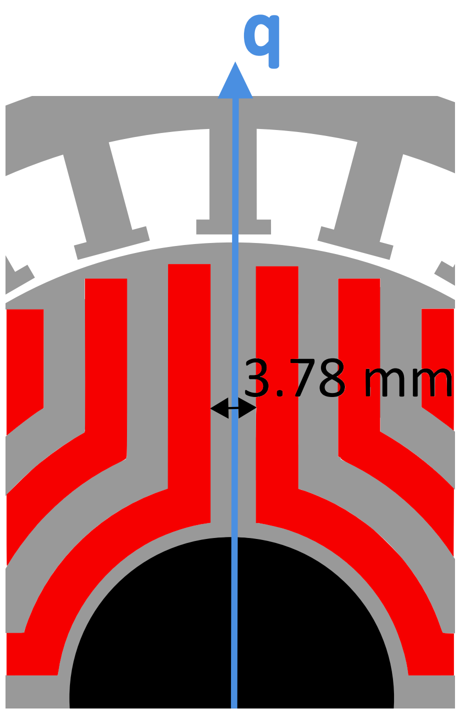

Figure 4.3. Zoomed view of Figure 2.2 of the q-axis along the low reluctance iron path in the FASynRM rotor.

As the iron path for the q-axis shown in Figure 4.3 is only 3.78 mm and with a rotor circumference of 230.6 mm, the iron path for the q-axis only accounts for 5.9 mechanical degrees of the rotor. In case the stator α-axis is misaligned with 1 mechanical degree, the effective area the flux lines can travel through has roughly been decreased by 1/6. This could be the cause for the faster saturation for the measured results of the q-inductance, which is seen in the figure. To test this theory, FEM analysis of the machine could be made for two cases to determine the q-axis inductance. One case where the rotor q-axis is aligned with the current vector and a second case where the rotor q-axis is displaced with 1 mechanical degree relative to the current vector. The calculated q-axis inductance for the two cases could then be compared to see the effect of the 1 degree displacement. However, this has not been done due to the time limitation of this project. As the d-inductance is not as sensitive to the exact position due to the large amount of air gaps in the rotor, it is seen to fit well with the former results.

4.5 Inverter Voltage Error

When controlling the FASynRM with an inverter, the command voltage sent to the inverter by Field-Oriented Control (FOC), later explained in Section 4.6, will be higher than the voltage required by the FASynRM. This is because voltage drops occur in the inverter transistors due to conduction losses as well as switching losses caused by dead-time and parasitics. The combined voltage drop across the transistor is difficult to calculate as it is non-linear and is therefore compensated for with a LUT. To generate the LUT a DC current vector is applied for various angles and fixed for a certain period to let the rotor settle at this position. As the rotor is at a stand-still the voltage equations for the machine in the $\alpha\beta$-frame are reduced to Equation (4.1).

$$\begin{aligned} v_\alpha &= R_s \cdot i_\alpha & \qquad v_\alpha &= v_{\alpha,cmd} - v_{\alpha,err} \\ v_\beta &= R_s \cdot i_\beta & \qquad v_\beta &= v_{\beta,cmd} - v_{\beta,err} \end{aligned} \tag{4.1}$$

where v_α and v_β are the $\alpha\beta$-voltages required by the machine and i_α and i_β are the corresponding $\alpha\beta$-currents. $v_{\alpha,cmd}$ and $v_{\beta,cmd}$ are the command $\alpha\beta$-voltages used in dSpace and $v_{\alpha,err}$ and $v_{\beta,err}$ are the $\alpha\beta$-voltage errors caused by the non-linearities in the inverter. Thus, by varying the current vector amplitude and angle, and by measuring the corresponding command voltages in dSpace, the inverter voltage errors can be found by (4.2).

$$\begin{aligned} v_{\alpha,err} &= v_{\alpha,cmd} - R_s \cdot i_\alpha \\ v_{\beta,err} &= v_{\beta,cmd} - R_s \cdot i_\beta \end{aligned} \tag{4.2}$$

The calculated values of the inverter voltage errors are stored in a LUT and used in the operation of the FASynRM by subtracting the inverter voltage errors from the dSpace command voltages to provide the required machine voltages according to Equation (4.1).

4.6 Control Strategy

For this project FOC is used to control the FaSynRM. An illustration of the control strategy can be seen in Figure 4.4.

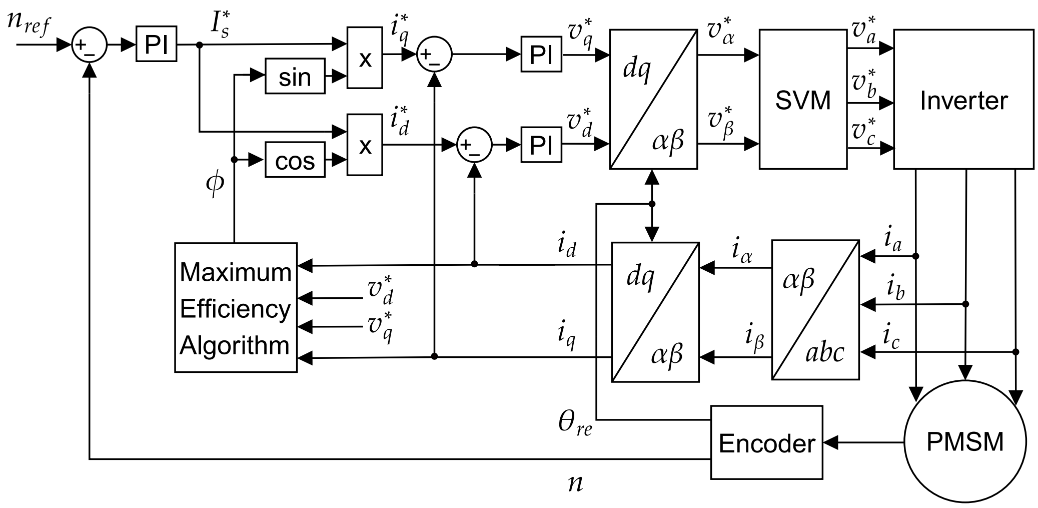

Figure 4.4. Block diagram of the FOC scheme for control of the FASynRM[13]. An incremental encoder is used to measure the position and speed and the Maximum Efficiency Algorithm (MEA) estimates the optimal current vector angle.

In Figure 4.4 it can be seen that there is a speed loop and a current loop with a PI controller for each loop. The speed reference is compared with the measured speed and the error is sent to a PI controller that gives a current vector amplitude reference. This amplitude reference is then multiplied with a cosine and sine function with an angle input. This way the d- and q-axis references are generated. The d- and q-axis references are compared with the measured d- and q-axis currents and the error is sent to the current loop PI controller. It can be seen that the angle input to the cosine and sine blocks is generated by the maximum efficiency algorithm (MEA), which will be described in Chapter 5.3. This algorithm determines where the current vector should be located relative to the rotor d-axis to provide the maximum efficiency at the given operating point. The current loop PI controller provides the necessary voltage command to obtain the needed current to provide the correct torque and maintain the reference speed. From the voltage commands, duty cycles are generated and sent to an inverter that supplies the machine. The position and speed of the rotor is determined by an encoder and this information is used for dq-transformations.

4.7 Demagnetization Current

As earlier mentioned in Section 4.1 the two segments of the rotor are skewed 7.5 mechanical degrees from each other. As the two rotor segments are skewed from each other this means that their high reluctance paths, i.e. their respective d-axes, are not aligned. The effective d-axis of both rotor segments is placed in between the two, which can be seen in Figure 4.5.

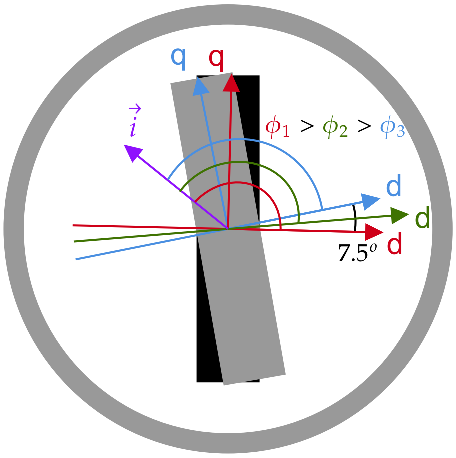

Figure 4.5. Cross sectional view of the step skewed FASynRM, simplified to one pole-pair. The angle between the two rotor segments is 7.5 mechanical degrees. The d-axis for the two rotor segments is placed on the high reluctance path and the effective d-axis of the rotor, shown by the green arrow, is in between the two d-axes for the different segments. The angle between the applied current vector and the three d-axes are different.

As one of the rotor segments is lagging the effective d-axis, the angle between the red d-axis and the current vector is larger than the angle between the effective green d-axis and the current vector. Therefore, when projecting the current vector onto the red d-axis it sees a numerically larger negative d-axis current which has to be taken into account when investigating the maximum allowable negative d-axis current. The maximum allowable negative d-axis current is limited based on the demagnetization of the rotor ferrite magnets. Ferrite magnets have a positive reversible temperature coefficient which means that it becomes less prone to demagnetization as the temperature of the magnets is increased[1]. This is shown in Figure 4.6.

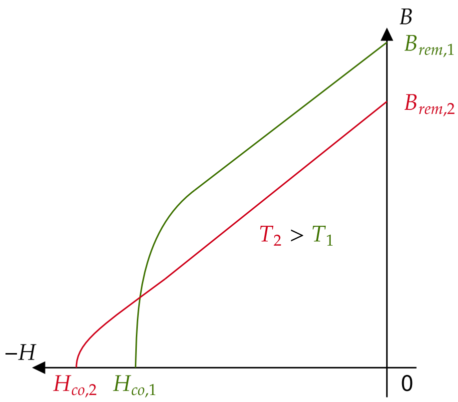

Figure 4.6. Second quadrant of the BH-curve for ferrite magnets. As the temperature of the magnets increase the remnant flux density decreases, while the absolute value of the coercive force increases[9].

Due to the fact that the ferrite magnets are more susceptible to demagnetization at lower temperatures, the maximum allowable d-axis current should be evaluated at lower temperatures, in this case down to 0°C. 2D FE modelling was carried out on the non-skewed rotor in [2] and a negative d-axis current of 10 A RMS was found to give a tolerable safety margin. To obtain the required MMF to demagnetize the rotor a larger current is needed since the number of turns have been reduced. However, the same current limit as in the previous report will be used for the experiments in this report even though the number of turns has been reduced to have an even larger safety margin. As the rotor used in this report is step skewed a second reference frame is used to take the rotor segment that sees a larger d-axis current into account. This is implemented by subtracting 7.5 electrical degrees from the position used in the FOC scheme and the d-axis current calculated from this reference frame is used as the protection limit in the software. The 7.5 electrical degrees stems from the angle between the effective d-axis and the red d-axis earlier shown in Figure 4.5.

4.8 Rotor Alignment

As the experimental setup uses an incremental encoder, an initial known rotor position is essential, in order to control the FASynRM with FOC, as this control scheme requires the knowledge of the rotor position. The rotor position is defined as the angle between stator α-axis and the effective rotor d-axis. Therefore, one way to specify the initial position is to apply a DC stator current vector on the α-axis. For a SPMSM where the d-axis is defined to be aligned with the PM north pole, this will align the rotor d-axis with the stator α-axis and the initial position can be set to 0 electrical degrees, assuming the torque production can overcome the friction. However, it was earlier presented in Section 2.2 that the total torque production of the FASynRM was the sum of both the reluctance torque and the PM torque. As a result, the combined torque production curve has three zero crossings within 180 electrical degrees. The two end points are fixed at 0 and 180 electrical degrees respectively, however the third zero crossing depends on the relationship between the d- and q-axis inductance difference and the PM flux linkage of the FASynRM. Furthermore, due to the fact that the reluctance torque is proportional to the square of the current amplitude whereas the PM torque only is proportional to the current amplitude as according to Equation (2.8), the zero crossing is also dependent on the applied current vector amplitude. Lastly, as it was shown in Section 4.4 the d- and q-axis inductances also vary with the applied current, thus changing the d- and q-axis inductance difference of the FASynRM. All this combined, results in a different torque zero crossing depending on the current amplitude, which can be seen in Figure 4.7.

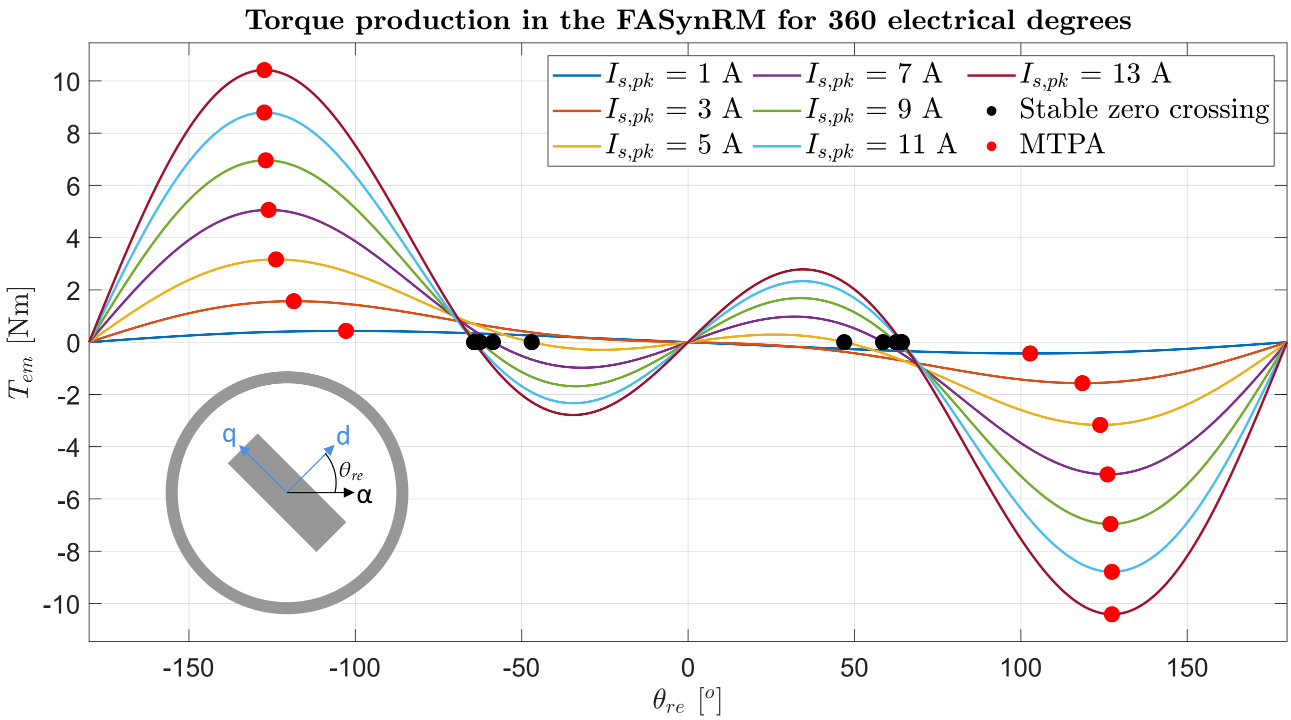

Figure 4.7. Total torque production of the FASynRM for various current vector amplitudes. The black dots indicate the zero stable crossing of the torque, whereas the red dots represent the MTPA points. A schematic of the machine is included where the positive direction of the rotor position is defined. The inductances used to create the figure are the ones from [1] shown in Figure 4.2 and the PM flux linkage is 0.140 Wb earlier found in Section 4.3.

As it can be seen from Figure 4.7 the black dots, which indicate the torque zero crossing, are moved depending on the current vector amplitude. In case a stator current vector is placed on the α-axis torque will be created between the stator and rotor MMF thereby rotating the rotor until the torque becomes zero. For current amplitudes above 3 A and at 0 electrical degrees, rotating the rotor in the positive direction will create a positive torque further moving the rotor in the positive direction. Likewise, in case the rotor is moved in the negative direction, more negative torque will be generated until it reaches the black dots at the zero crossing. This means that the zero crossing at 0 electrical degrees is unstable and the rotor is not able to stop at this location. The same occurs at the zero crossing at 180 electrical degrees. In fact, for the FASynRM there are only two stable zero crossings, which are marked by the black dots in both the positive and negative direction. At the zero crossings marked by the black dots in the positive position region, an increase in the rotor position will result in more negative torque, moving the rotor back to the stable zero crossing. If the rotor is moved in the negative direction, positive torque will be generated and move the rotor back to the same point. The same is valid for the stable zero crossings in the negative position region. This means that when aligning the rotor by applying a stator current vector on the α-axis there will be an offset with the rotor d-axis defined at $\theta_{\text{re}} = 0$, as the rotor will park at the black dots. As there is a stable zero crossing for each current vector amplitude in both the positive and negative direction, the rotor is able to park in two positions depending on the initial rotor position. It would be advantageous to use a current vector amplitude at 3 A or below as the torque curve here has a stable zero crossing at 0 electrical degrees. However, it was found through experiments that a current vector amplitude of this size resulted in insufficient torque production to overcome the friction and gave inconsistent results.

To overcome this offset with the initial rotor alignment, the FASynRM is rotated with the help of the load SPMSM motor. As the FASynRM is connected to the inverter, the BEMF will induce a voltage across the terminals of the FASynRM. The system can then be controlled with current control where the current is set to zero. Hence, the inverter will give a voltage that is equal but opposite to the BEMF from the machine meaning that no current will flow and the machine terminals are effectively open-circuited. By utilising the $\alpha\beta$-command voltages the true d-axis of the FASynRM can be found by Equation (4.3).

$$\theta_{\text{re}} = \tan^{-1}\left(\frac{-v_{\alpha,\text{cmd}}}{v_{\beta,\text{cmd}}}\right) \tag{4.3}$$

Having found the true position of the rotor d-axis by Equation (4.3), this position is then used in the FOC scheme to control the FASynRM.

In this chapter the specifications of the FASynRM, provided by Grundfos, were presented. Afterwards, the remaining motor parameters were found through experiments, where the stator phase resistance was found to be 0.75 Ω and the PM flux linkage was found to be 0.140 Wb. The d- and q-axis inductances were also measured where the d-axis inductance matched well with the work done in [1]. However the q-axis inductance was found to saturate faster than expected. This was deemed to be because of the imprecise alignment, when locking the rotor. Afterwards, the voltage error caused by the inverter was compensated for by a LUT. The maximum allowable d-axis current was determined to be 10 A rms, even with the new scaling of the stator windings. This limit was needed in the FOC scheme, which will be used to control the FASynRM. Lastly, the initial rotor position, that was also needed in the FOC scheme, was investigated. By the help of the torque equation it was found that the rotor had two stable parking positions which were displaced from the rotor d-axis. In order to compensate for this, the BEMF would have to be measured to locate the true rotor d-axis.

Chapter 5

Power Optimization

This chapter aims to describe a method to maximize the efficiency when operating the FASynRM. Two ways are investigated to determine the efficiency, where the first one uses the active power equation to determine the input power. The second method examines the losses present in the machine with the end goal of determining a function that describes the losses that can be minimized by varying the current vector. Lastly, the MEA will be presented which will be used to minimize both the input power and power loss function by using quadratic interpolation.

5.1 Online Power Measurement

To optimize the efficiency of the FASynRM, the input power to the machine has to be lowered as according to Equation (5.1).

$$\eta = \frac{P_{\mathrm{out}}}{P_{\mathrm{in}}} \tag{5.1}$$

where P_{out} is the output power of the FASynRM fixed at certain values corresponding to the four EEI points earlier presented in Table 2.1. P_{in} is the input power to the FASynRM from the inverter as the inverter efficiency is not considered as according to the delimitation in Section 3.1. In practice the output power is unknown to the controller as FOC only serves as speed control. This is because the current vector supplied by FOC, to balance the load torque and ensure the speed control, cannot be directly linked to the torque provided by the FASynRM. Even though it is possible to calculate the electromagnetic torque based on the d- and q-axis currents in the machine with the torque equation earlier presented in Equation (2.8), a correct torque estimation is difficult due to the cross-saturation of the d- and q-axis inductances. As such, it is difficult to estimate the output power of the machine but by assuming that FOC can operate the machine in steady-state, the output power, although unknown, should be constant. If the output power is constant, so is the torque produced by the FASynRM. It was shown earlier in the torque equation in Equation (2.8) that the torque varied with a combination of both the d- and q-axis current. Therefore, by varying the current vector angle in the FOC scheme earlier presented in Figure 4.4, the speed loop will change the amplitude of the current vector in order to produce the same torque. This means that there exists different combinations of the d- and q-axis currents to produce the same output torque. However, the d- and q-axis currents are also linked to the copper and core losses, which means that for the same output torque, i.e. output power, there exists a current vector angle that minimizes the input power and thus maximizes the efficiency.

The input power to the FASynRM can be calculated with the active power calculation for a three-phase system, which is given in Equation (5.2).

$$P_{\mathrm{in}} = \frac{3}{2} \cdot (v_{\alpha} \cdot i_{\alpha} + v_{\beta} \cdot i_{\beta}) \tag{5.2}$$

From Equation (5.2) it can be seen that both a current and voltage measurement is required in order to measure the input power to the FASynRM. The input current will be a smooth waveform due to the inductance in the machine, however the voltage supplied by the inverter is a PWM signal. Since the active power is only dependent on the fundamental of the voltage and current, the chopped voltage measurement cannot easily be used in an online power measurement. As the FOC scheme computes the command voltages required by the inverter, which are pure sinusoidal waveforms, these can be used to estimate the input power. However, the command voltages sent to the inverter are larger than the ones seen by the FASynRM, due to the inverter non-linearities as earlier explained in Section 4.5. Therefore, the calculated input power to the FASynRM becomes:

$$P_{\text{in}} = \frac{3}{2} \cdot \left((v_{\alpha,\text{cmd}} - v_{\alpha,\text{err}}) \cdot i_{\alpha} + (v_{\beta,\text{cmd}} - v_{\beta,\text{err}}) \cdot i_{\beta} \right) \tag{5.3}$$

5.2 Online Power Loss Estimation

A second way to determine the input power and increase the efficiency of the FASynRM can be achieved by rewriting the definition of the efficiency to the one stated in Equation (5.4).

$$\eta = \frac{P_{\text{out}}}{P_{\text{out}} + P_{\text{fric}} + P_{\text{cu}} + P_{\text{core}} + P_{\text{str}}} \tag{5.4}$$

where the terms different from P_{out} in the denominator represent the losses in the FASynRM earlier presented in Section 2.1. Similar to the explanation in Section 5.1 it is assumed that FOC is able to operate the FASynRM in steady-state, hence the output power is considered constant. The friction losses are dependent on the speed and cannot be optimized and the copper losses are calculated from Equation (2.1), only requiring current measurements. The stray and core losses are not straightforward to calculate, but can be evaluated experimentally. In case the input and output power along with the current can be measured, the core, stray and friction losses can be determined. This can be done by subtracting the output power, measured by a torque transducer, as well as the copper losses from the input power, which gives the sum of the core, stray and friction losses. The three individual losses are hard to separate from the calculated sum, but as the friction losses are only proportional to the speed, and thus cannot be optimized based on the current vector angle, and the stray losses only account for up to 1% of the total losses, they are both combined with the core losses. For the remainder of this report the friction, stray and core losses are therefore referred to as core losses. To maximize the efficiency, the copper and core losses are to be reduced. Since the core and copper losses are both dependent on the current it might be possible to determine a function for the total losses that depends on the current. The desired equation can be seen in Equation (5.5).

$$P_{\text{loss}}(I_{\text{s,pk}}(\phi)) = \frac{3}{2} \cdot R_{\text{s}} \cdot I_{\text{s,pk}}(\phi)^2 + P_{\text{core}}(I_{\text{s,pk}}(\phi)) \tag{5.5}$$

By minimizing Equation (5.5) maximum efficiency can be obtained.

5.3 Maximum Efficiency Algorithm

As described in Section 4.6 the amplitude of the current vector is found from the speed loop PI controller and the angle of the current is determined by the MEA. The MEA aims to minimize the input power and the input power can be written as Equation (5.6).

$$P_{\text{in}} = P_{\text{out}} + P_{\text{cu}} + P_{\text{core}} \tag{5.6}$$

From Equation (5.6) it can be seen that the input power is the sum of the output power, the copper and the core losses. Since the machine is operating in steady state the output power is constant, which means that the input power will vary in the same way as the copper and core losses. As earlier presented in Figure 2.6 it can be seen that the sum of the copper and core losses varies like a parabola, hence it is assumed that the input power varies in the same way. The idea of the MEA is to estimate the minimum point of the power in steady state by varying the current vector angle. To find this minimum current vector angle a line search method can be used. There exists several line search methods such as golden section, bisection and polynomial interpolation. The polynomial interpolation method has a very fast convergence and for this reason this method is chosen for the MEA. Specifically, quadratic curve fitting is used which requires a power measurement at three distinct angles to estimate the coefficients for the quadratic polynomial. Furthermore, an initial angle interval, known as the interval of uncertainty, needs to be determined where the minimum input power is located within that interval. An example can be seen in Figure 5.1.

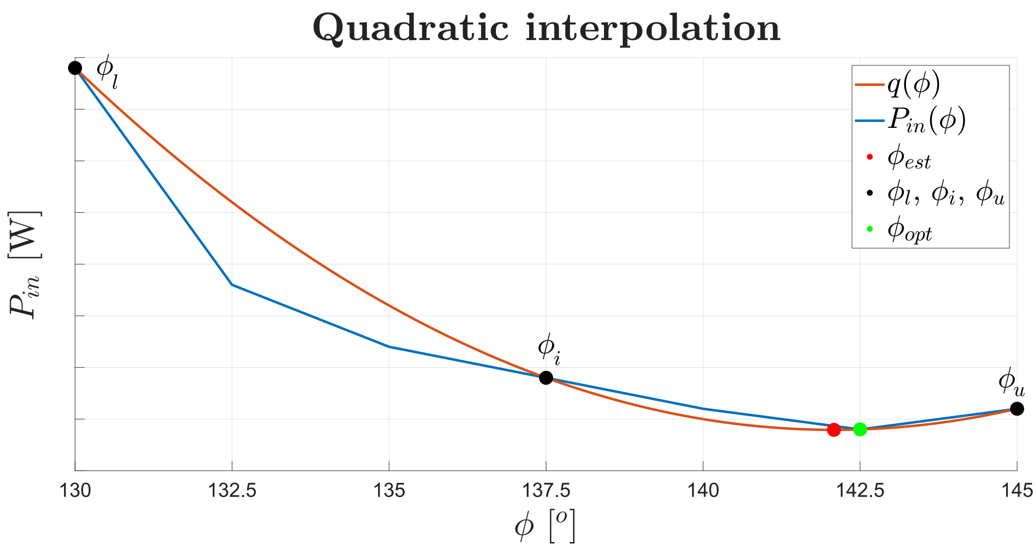

Figure 5.1. The Quadratic curve fitting of a function. The blue line is the function to be estimated and the red line is the estimated function. Three distinct angles and their corresponding function values are needed to estimate the function. The points in black represent the distinct angles, the red point represents the minimum of the estimated function and the green point represents the actual minimum of the original function.

Figure 5.1 has been made with real measurement values seen as the blue curve. The measurements are for EEI 1 operating conditions obtained later on in Figure 6.6 where the current vector angle has been varied. In the figure it can be seen that three different angles are to be used. These are the lower (ϕ_l) and upper (ϕ_u) angle of the interval where the minimum point is located within this interval. An inner angle (ϕ_i) is also needed to estimate the power function. For each of the three angles there should be a corresponding power measurement. From these three distinct angles an expression for the estimated function can be determined from Equation (5.7) to (5.10).

$$q(\phi) = a_0 + a_1 \cdot \phi + a_2 \cdot \phi^2 \tag{5.7}$$

$$a_2 = \frac{1}{(\phi_\mathrm{u} - \phi_\mathrm{i})} \cdot \left(\frac{P_\mathrm{in}(\phi_\mathrm{u}) - P_\mathrm{in}(\phi_\mathrm{l})}{(\phi_\mathrm{u} - \phi_\mathrm{l})} - \frac{P_\mathrm{in}(\phi_\mathrm{i}) - P_\mathrm{in}(\phi_\mathrm{l})}{(\phi_\mathrm{i} - \phi_\mathrm{l})} \right) \tag{5.8}$$

$$a_1 = \frac{P_\mathrm{in}(\phi_\mathrm{i}) - P_\mathrm{in}(\phi_\mathrm{l})}{(\phi_\mathrm{i} - \phi_\mathrm{l})} - a_2 \cdot (\phi_\mathrm{l} + \phi_\mathrm{i}) \tag{5.9}$$

$$a_0 = P_\mathrm{in}(\phi_\mathrm{l}) - a_1 \cdot \phi_\mathrm{l} - a_2 \cdot \phi_\mathrm{l}^2 \tag{5.10}$$

From Equation (5.7) to Equation (5.10) the estimated function and its coefficients a_2, a_1 and a_0 are determined. Assuming the curvature is positive, the optimum angle gives the minimum input power and this is found by differentiating the estimated function $q(\phi)$ and setting it equal to zero. The optimum angle can be found from Equation (5.11).

$$\phi_{\mathrm{min,est}} = -\frac{1}{2 \cdot a_2} \cdot a_1 \tag{5.11}$$

When the estimated optimum angle has been found a corresponding power at this angle must be measured. After measuring the power at the estimated optimum angle, the interval of uncertainty can be reduced. There are four possibilities for how the interval is reduced. An example will be given which corresponds to the situation in Figure 5.1.

The inner angle (ϕ_{i}) is compared to the estimated optimum angle ($\phi_{\mathrm{min,est}}$). If $\phi_{\mathrm{i}} < \phi_{\mathrm{min,est}}$ and $P(\phi_{\mathrm{i}}) > P(\phi_{\mathrm{min,est}})$ then the real optimum angle of the real power curve is between the inner and the upper angle of the interval ($\phi_{\mathrm{i}} \leq \phi_{\mathrm{min,real}} \leq \phi_{\mathrm{u}}$). The new limits can then be determined to be $\phi_{\mathrm{l,new}} = \phi_{\mathrm{i,old}}$, $\phi_{\mathrm{u,new}} = \phi_{\mathrm{u,old}}$ and $\phi_{\mathrm{i,new}} = \phi_{\mathrm{min,est}}$. After these new limits have been determined the coefficients for the function $q(\phi)$ can be calculated again from the new limits. A new estimated optimum can then be obtained and the power at this angle is measured and the current inner angle and the estimated optimum is compared along with the power measurement at these angles. It is then determined which of the four possibilities are true and then a new interval is determined. The Matlab script for the MEA can be seen in Appendix A along with how which of the four cases are chosen to determine the new interval. When the difference of the power at the previous estimated optimum angle and at the current estimated angle is within a certain limit, δ, the algorithm is stopped and the optimal angle is assumed to be at the current estimated angle. The algorithm then continues to output this angle and the machine is now running at this optimum angle where the efficiency is at its maximum. The MEA is displayed in a flowchart in Figure 5.2.

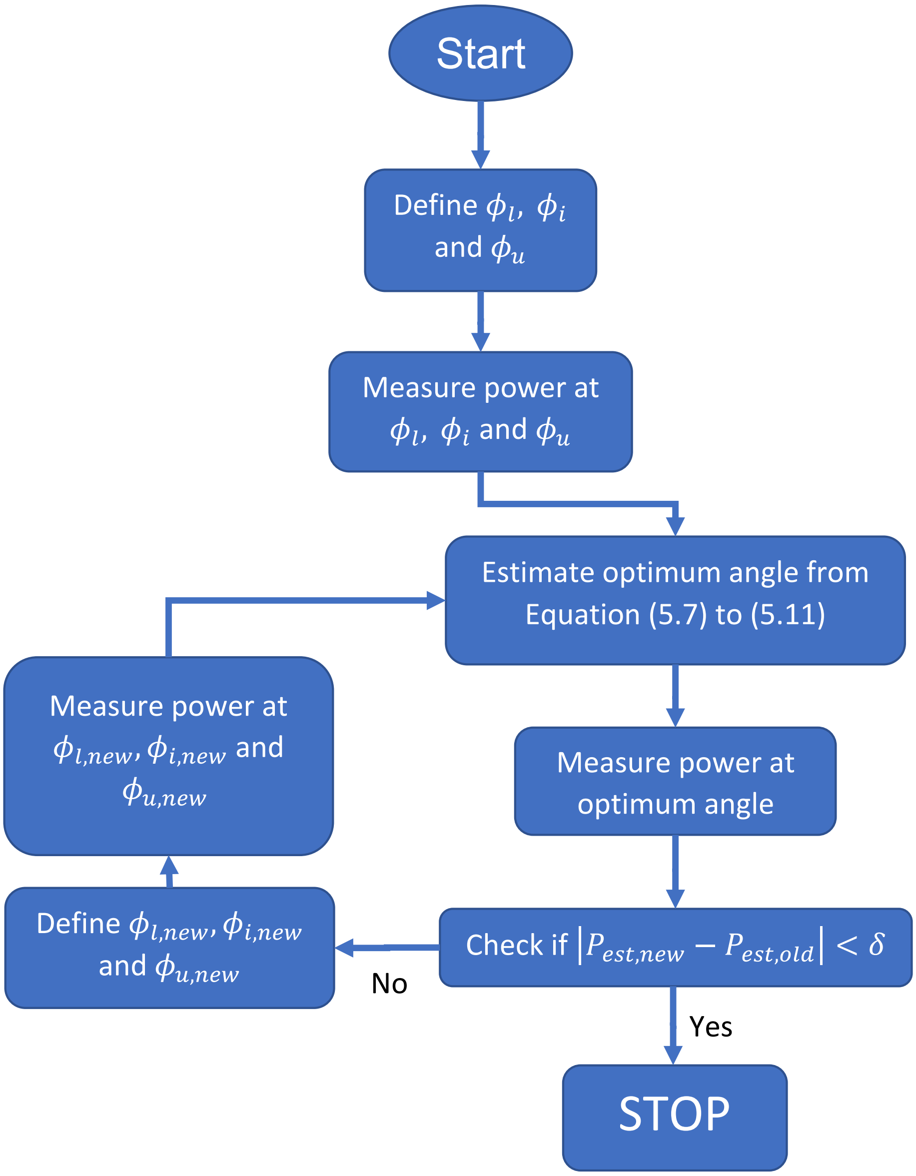

Figure 5.2. Flowchart of the MEA using quadratic interpolation. The script for the implementation in Matlab can be seen in Appendix A

The MEA presented in Figure 5.2 will then be used to find the ME angle for the EEI operating conditions when operating the FASynRM. This will be carried out in the experiments presented in the following chapter.

In this chapter it was found that the efficiency of the FASynRM could be maximized both by minimizing the input power by the help of the active power equation or by minimizing the power losses governed by the copper and core losses. The MEA consisted of a quadratic interpolation search method, which was capable of locating the minimum of the power functions through a series of power measurements at different current vector angles. A flowchart of the MEA was presented, which described steps necessary for the MEA in order to locate the ME angle of the FASynRM.

Chapter 6

Experimental Work

To give an overview of the structure of the experimental work chapter, a flowchart is given in Figure 6.1.

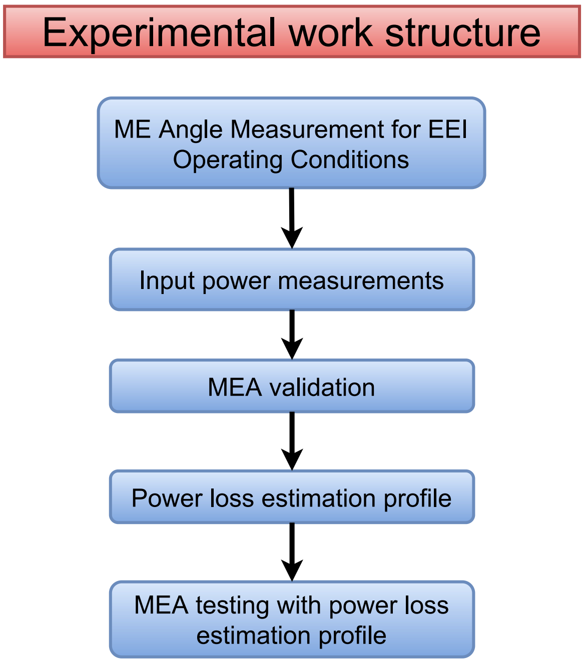

Figure 6.1. Structure of the experimental work chapter.

As it can be seen in Figure 6.1 the ME angles for each of the four EEI operating conditions will be determined first. This is done by measuring the input power to the FASynRM with a power analyzer and by sweeping the angle of the current vector manually. This way the ME current vector angles have been determined for each EEI operating condition and this can be used to check if the MEA finds the ME angle of the current vector during the experiments conducted later on. One way to maximize the efficiency of the FASynRM is to measure and minimize the input power online, which can be done by utilizing Equation (5.2). A way to minimize the input power is by using the MEA presented in Section 5.3. The MEA is validated by evaluating its ability to converge to the ME current vector angle during operation. After this validation a second option to obtain maximum efficiency is investigated. This is done because the online power measurement requires a voltage measurement, which is not always available. Therefore, it would be advantageous to develop a profile that can accurately estimate the power losses in the FASynRM based only on the current vector. By using the MEA on this power loss estimation profile it should be possible to reduce the power losses online by changing the current vector angle and test if the MEA is able to converge to the true ME angle.

6.1 Experimental Setup

The experimental setup consists of the FASynRM connected to a SPMSM via a common shaft containing a torque transducer as depicted in Figure 6.2.

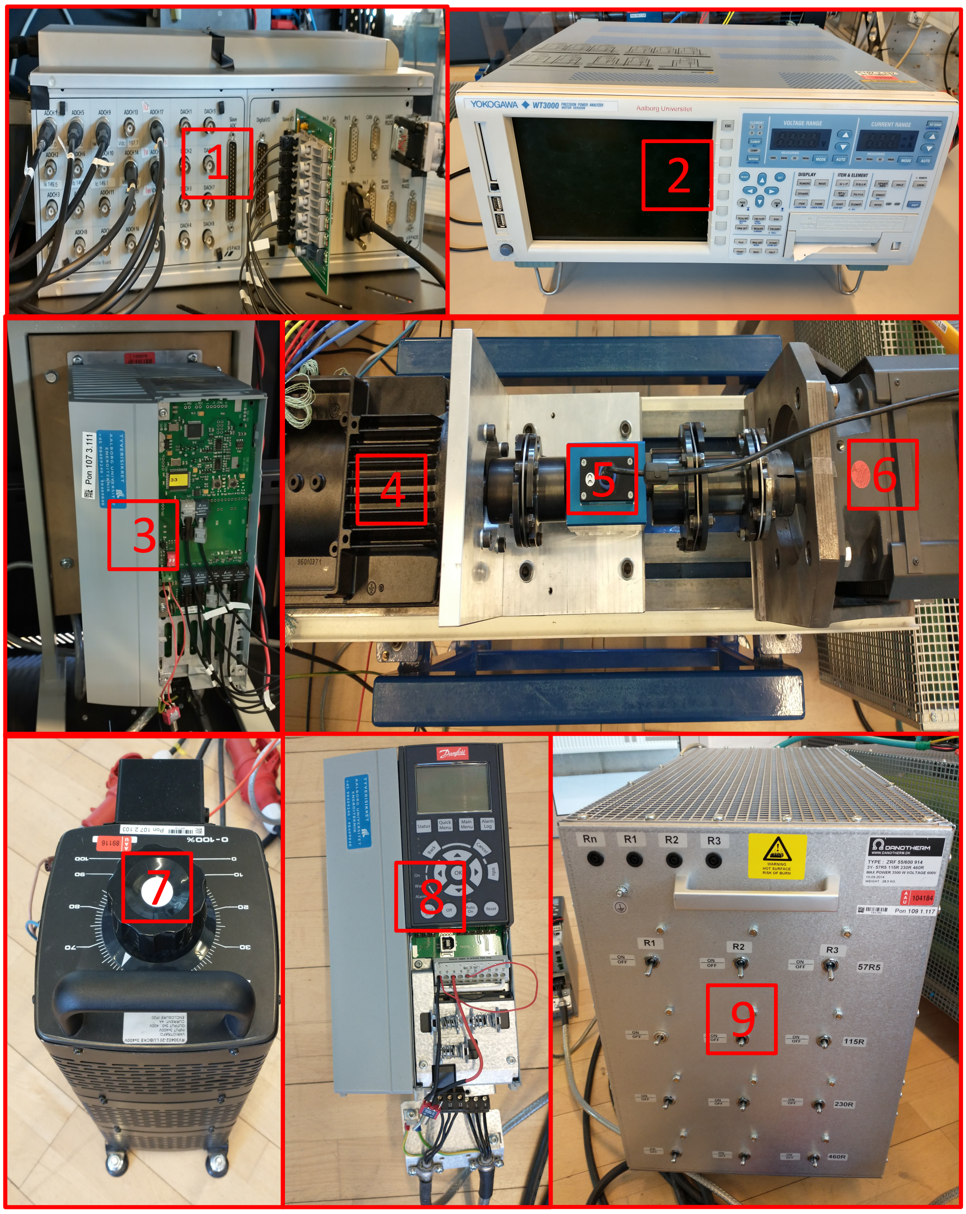

#	Description
1	dSpace Control Box
2	Yokogawa Power Analyzer
3	Danfoss Inverter for FASynRM
4	Grundfos Motor (FASynRM)
5	Torque Transducer
6	Load Motor (SPMSM)
7	3-Phase Transformer
8	Danfoss Inverter for SPMSM
9	Variable Resistor

Figure 6.2. The setup used in the laboratory.

The SPMSM is connected to a switch which allows for two operation modes. For one mode it is connected to a Danfoss VLT FC 302 inverter which enables speed control of the SPMSM. For the other mode it is connected to two transformers which each are connected in series with a variable resistor.

The variable resistors range from 460 Ω to 30.667 Ω. The reason for connecting two transformers and resistors is because each transformer can only handle 10 A RMS, which is already exceeded at EEI 2, as the SPMSM produces 10.46 A RMS at this operating point. Furthermore, each resistor can only tolerate 3.5 kW, therefore necessitating two resistors to operate the FASynRM at 4 kW at EEI 1. The SPMSM side is connected to the secondary side of the transformers and the primary side is connected to the variable resistors. When the FASynRM is operated as the motor it is controlled via FOC to obtain a constant speed. This means that the SPMSM which operates as the load is also operating at the same fixed speed. Due to the constant speed the BEMF of the SPMSM is also constant. By varying the transformer ratio, the voltage on the primary side changes which allows for a different output power as $P_{\text{out}} = V^2/R$. Thus, by varying the transformer ratios in the two transformers, the load torque seen by the FASynRM changes for a fixed operating speed.

The FASynRM is connected to a 2-level, 3-phase Danfoss FC-302 inverter supplied by a 550 V DC power supply from the grid. An incremental encoder is placed on the FASynRM to measure its speed and incremental position. The setup is connected to a dSpace control box which is connected to a PC where a Simulink model of the system is built and uploaded as C code to the dSpace control box. The system is controlled by varying the duty cycles sent to the inverter via space vector modulation. A Yokogawa WT3000 power analyzer is used to measure the input power sent to the FASynRM.

6.2 Rotor d-axis Alignment

As explained in Section 4.8 the torque production of the FASynRM is a combination of the PM torque and the reluctance torque resulting in a torque zero crossing offset from 0 electrical degrees. This means that when a DC current is applied on the stator α-axis two possible offsets are possible depending on the initial rotor position, which can be seen in Figure 6.3.

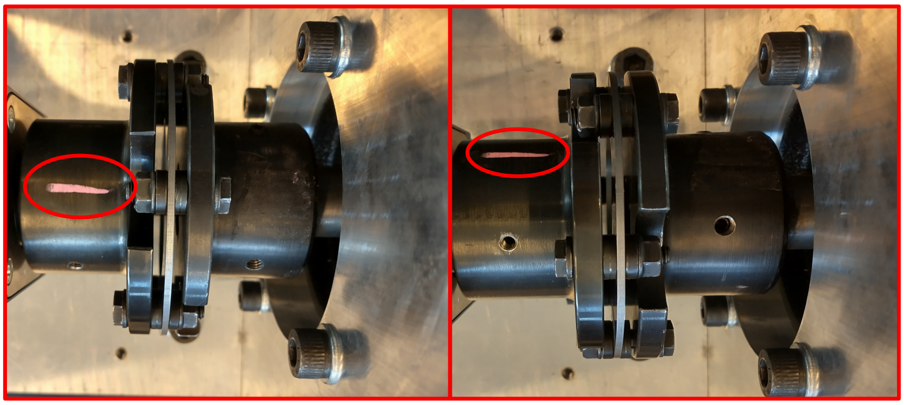

Figure 6.3. Two different rotor positions for the same stator current. A voltage vector of 13 V corresponding to a DC current of 5.1 A has been applied on the stator α-axis.

As it can be seen from Figure 6.3 there are two possible initial positions for the same applied stator current. According to the theory presented in Section 4.8 the true rotor d-axis is placed somewhere in between these two positions. In the control system it is necessary to determine the zero position of the encoder every time the control system is initialized. This is normally done by applying a DC current vector aligned with the phase a-axis. Since there is only PM torque in an SPMSM, applying a current on the a-axis will cause the rotor d-axis to align with the stator MMF and the initial encoder position can be set to zero. As described above there are two stable parking positions for the FASynRM, but they are both away from the d-axis. Hence, when the same method for determining the zero position for the encoder is used for the FASynRM the two parking positions that are away from the rotor d-axis will be defined as the zero position for the encoder. This means that there exists a position error between the encoder zero position and the real rotor d-aixs. If one of the two possible parking positions were used as the zero position for the encoder the control would not work properly, meaning that a way to compensate the position error is needed when using the DC-current alignment method.

To find the offset with the initial rotor alignment, the FASynRM is operated as the load where the current reference is set to 0 A to simulate open terminals. That way, the command voltages sent to the inverter are equal to the BEMF and the actual position of the rotor d-axis can be calculated according to Equation (4.3). Multiple experiments have been conducted where the angle difference between the real rotor d-axis and the defined zero position for the encoder has been measured. It was found that the position error varied even though the same current vector was applied. This means that every time the controller zero position is to be defined a way to compensate the controller zero position is needed. This is done by using the DC-current method and then running the FASynRM as load and finding the position error between the encoder zero position and the BEMF location and using this error to compensate so that the encoder zero position is in fact aligned with the rotor d-axis.

To verify that the true rotor d-axis has been found, the rotor is operated at different loads at a current vector angle of 90 electrical degrees in the defined reference frame. The results for this experiment are shown in Figure 6.4.

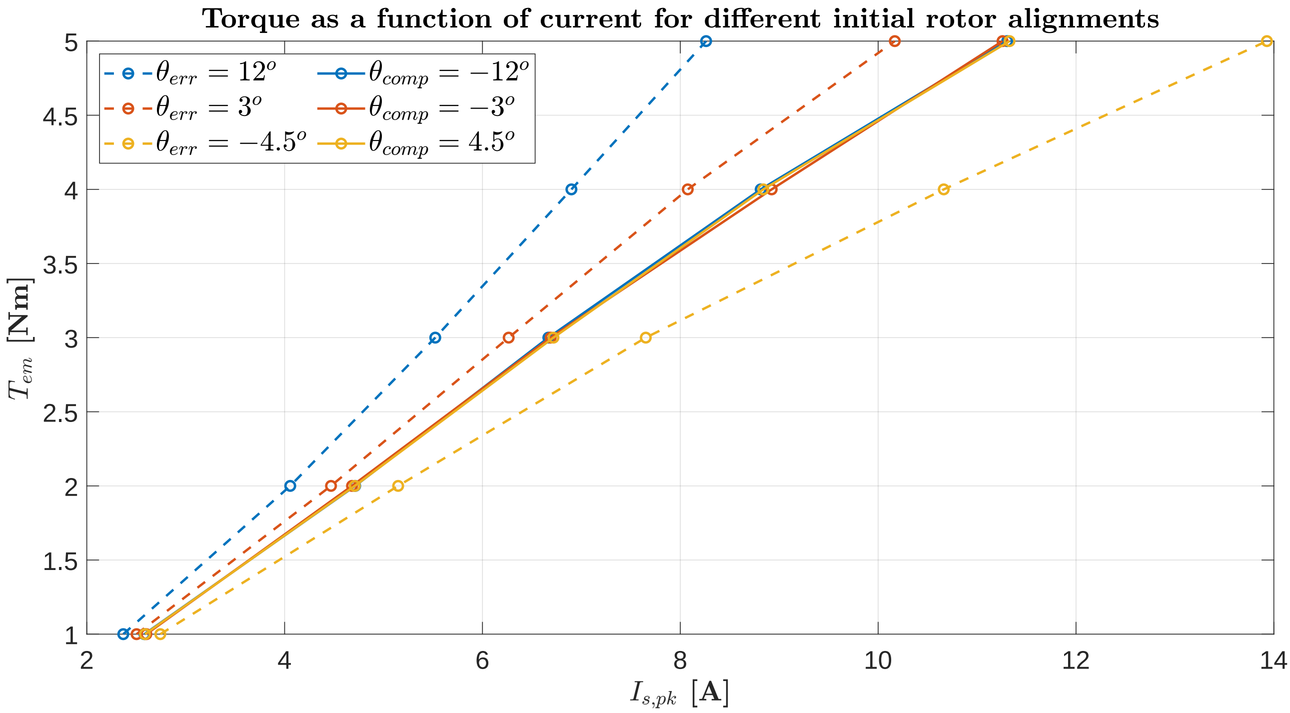

Figure 6.4. Torque production as a function of current. Three different position errors have been tested and also compensated for by adding a compensation angle to the position from the encoder.

From Figure 6.4 it can be seen that three different position errors have been tested. The position error in the blue curve was obtained with a current vector amplitude of 3.47 A, while the red and yellow curves were obtained by applying 2 A on the stator α-axis. Hence, it can be noted that different position errors were seen even though same current vector was applied. For a positive position error the true rotor d-axis is lagging the defined d-axis in the anti-clockwise direction. This means that when the current vector is located at 90 electrical degrees in the defined reference frame it is in fact located at 102 electrical degrees on the true rotor d-axis for the blue case. This matches well with the torque equation as in case the current vector angle is above 90 electrical degrees the reluctance torque, which is proportional to the square of the current starts to contribute to the total torque production. This is seen in the dashed blue line as it is seen to increase more than linearly. In case the position error is negative the current vector angle is placed in the first quadrant and the reluctance torque starts to counteract the PM torque. This is seen in the yellow dashed line, where an exponential trend is visible. By compensating for the various position errors the three different cases, represented by the full lines in the figure, are seen to lie on top of each other, which indicates that the true rotor d-axis has been found, as they are all directly proportional to the applied current vector amplitude, which in this case only consists of the q-component.

6.3 ME Angle Measurement for EEI Operating Conditions

The controllers for the FOC scheme have been tuned through an iterative process by investigating the speed step response and the speed oscillations during steady-state. It was found that the speed was oscillating during steady-state, which can be seen in Figure 6.5.

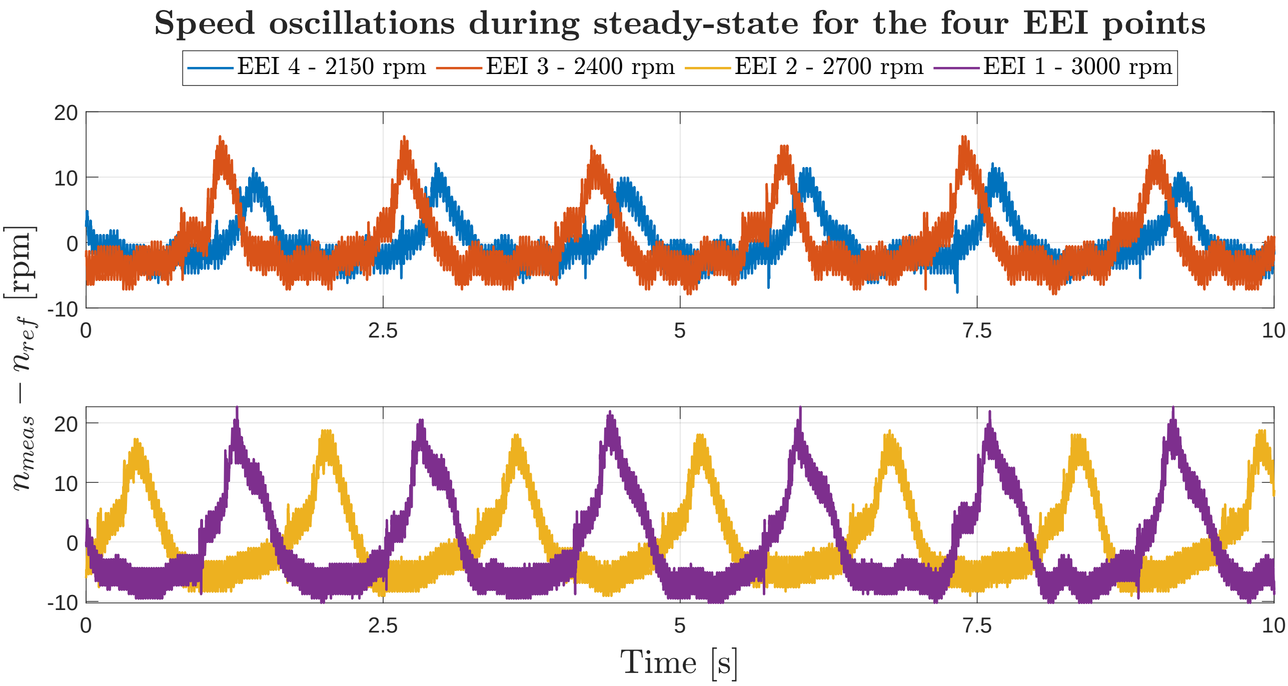

Figure 6.5. Speed oscillations during steady-state operation for the four different EEI cases. The reference speed has been subtracted from the measured value to more easily compare the results.

As it can be seen from Figure 6.5 the speed oscillates with a period of around 1.5 s, which is independent of the reference speed. As the reference speed increases the peak of the oscillation increases. The results shown in the figure are obtained with a proportional and integral gain of both 0.004 for the speed loop and a proportional and integral gain of 5 and 200, respectively, for the current loop. This controller provided a slow speed response but was deemed necessary to ensure a stable system, because of this oscillation. If faster controllers were used the system became unstable when the FASynRM was operating at high speeds. The origin of this oscillation has not been found, hence it could not be solved. However, it might be because of the fact that the control is carried out in dSpace which could be the source of the oscillation. Other setups in the laboratory that used dSpace experienced the same oscillations.

Four experiments have been conducted where the current vector angle has been varied for each EEI case. The input power along with the current vector amplitude has been recorded. The efficiency has been calculated from the output power measured by the torque transducer and the measured input power by the Yokogawa power analyzer. The output power of the motor has been fixed at the four different values for the EEI cases earlier shown in Table 2.1. The efficiency curves for the four EEI operating points can be seen in Figure 6.6.

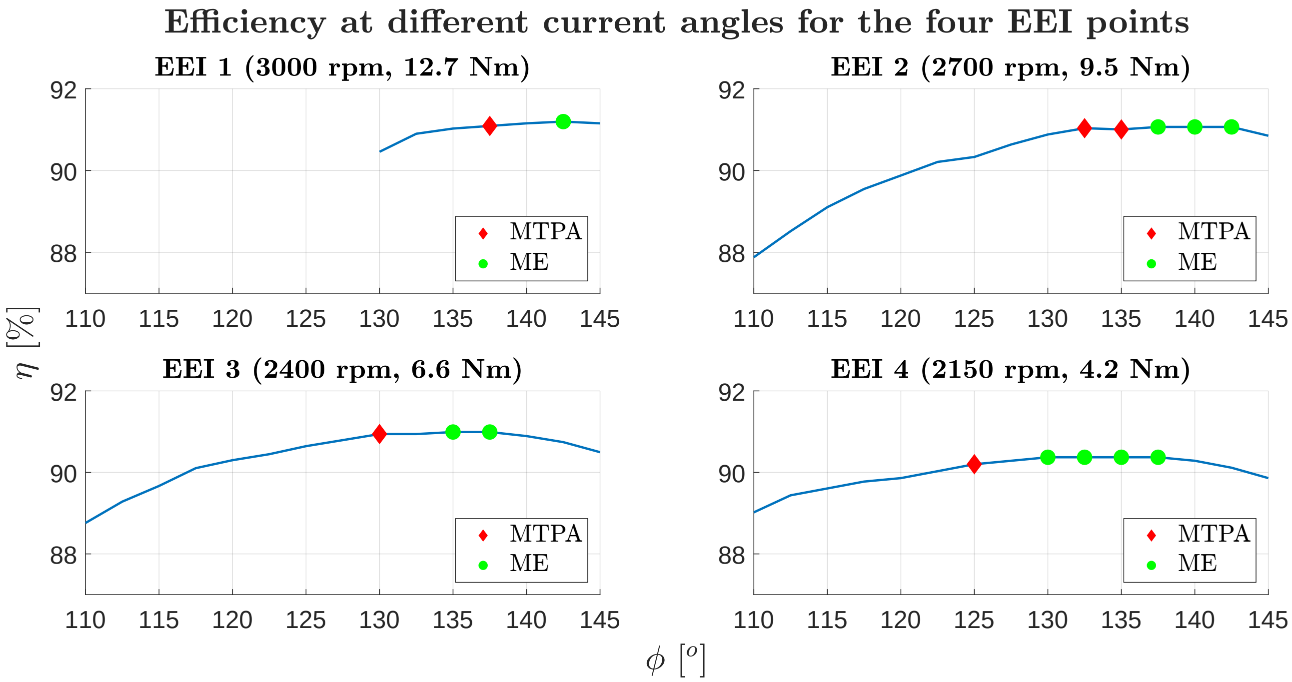

Figure 6.6. Efficiency as a function of the current vector angle for the four EEI operating points with a resolution of 2.5° and 1 W for the angle and power, respectively. The red diamonds indicate the efficiency at the MTPA operating angle and the green circles indicate the efficiency at the ME operating point. The load torque for EEI 1 was limited to 12.4 Nm due to the voltage limitation.

From Figure 6.6 it can be seen that the current vector angle has been swept from 110° to 145° for EEI 2 to 4. For EEI 1 the current vector angle has only been swept from 130° to 145°. This is due to the fact that the needed voltage to obtain the needed current vector could not be reached for lower angles as the DC-link voltage was fully used and the duty cycles for the inverter approached 1. Furthermore, even though the stator had been produced with fewer number of turns as according to [2], the FASynRM was not able to produce 12.7 Nm at 3000 rpm, due to the voltage limitation and was limited to 12.4 Nm. This could be caused by the fact that the rotor had been demagnetized to a new value of 0.140 Wb. In the figure the MTPA angles along with the ME angles have been marked. It can be seen that for EEI 2, 3 and 4 there are multiple ME angles. This is due to the fact that the power measurement from the Yokogawa power analyzer varied during operation, hence the evaluated measurements are not precise enough to determine the exact ME angle. However, it is deemed that the ME angle is located in the range of the green points. Furthermore, it can be seen in the attachment, 'EEI_Angle_Sweep.xlsx', for the EEI angle sweep measurements that the variation of the input power around the ME angle is only a few Watts, thus the exact location is not crucial. It can be seen that both the ME angles and the MTPA angles occur at a larger angle as the speed and torque increase. The MTPA angle moves from 125° for EEI 4 to 137.5° for EEI 1. It should be noted that the result that the MTPA angle for EEI 1 occurs at 137.5° seems unlikely since the maximum theoretical MTPA angle is 135° and should in fact be below this value when considering the torque equation. The larger current measurement at 137.5° could be due inaccurate power measurements. The angle for the MTPA angle increases with the torque since the reluctance torque varies with the current squared, meaning that the reluctance torque will contribute more to the torque compared to the PM torque. The ME angle for EEI 1, which is high speed and torque occurs at 142.5° whereas the ME angle for EEI 4 occurs between 130° to 137.5°. According to Equation (2.4) the core losses vary with the frequency squared, hence the core losses are larger for EEI 1 compared to EEI 4. The increasing MTPA angle and larger core losses at higher speed results in the ME angle to be at a higher angle for EEI 1 than EEI 4.

Due to the fact that the true EEI 1 operating condition of 12.7 Nm and 3000 rpm cannot be reached, the remainder of the experiments only consider EEI 2, 3 and 4. The power measurements used to calculate the efficiencies in Figure 6.6 will be used to evaluate if the MEA finds the optimum angle during operation of the FASynRM for the remainder of the experiments in this chapter.

6.4 Input Power Measurements

As described earlier the input power can be determined by Equation (5.3) and calculated in dSpace. Here, the real voltage sent to the machine is determined by the command voltage and the voltage error found in Section 4.5. The calculation of the input power from dSpace and the input power measured by the yokogawa power analyzer is shown in Figure 6.7.

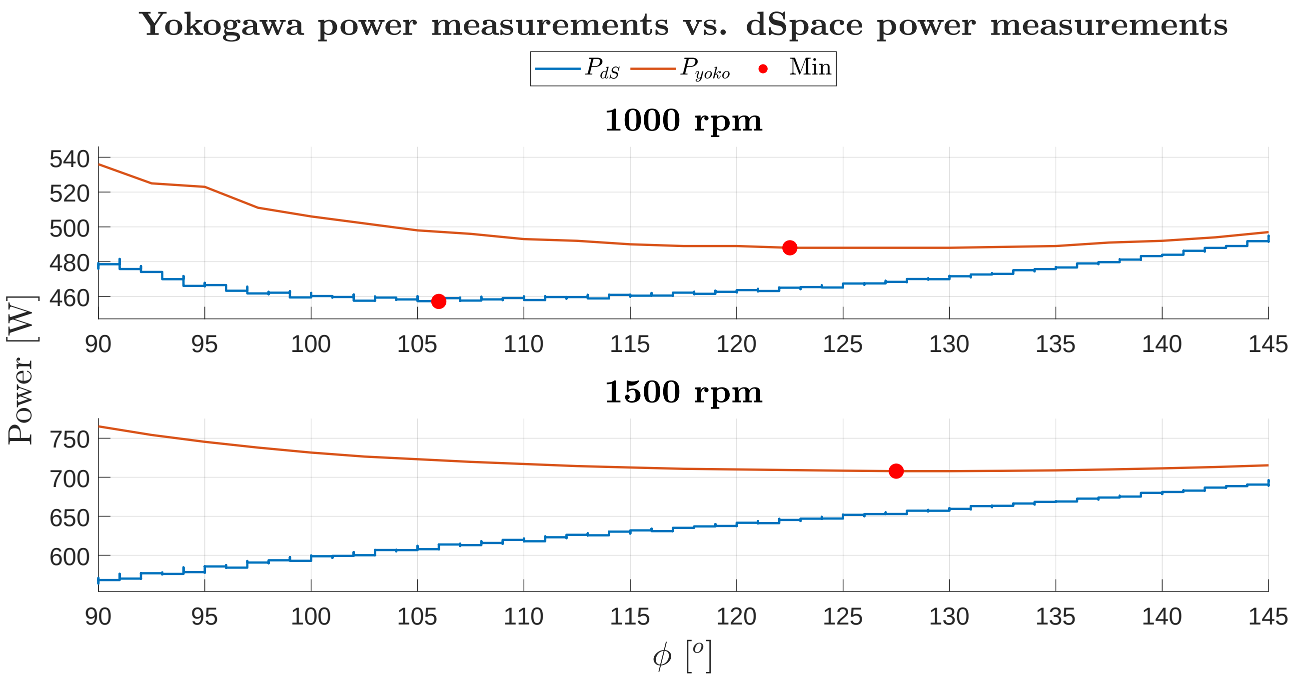

Figure 6.7. The measured power from the Yokogawa power analyzer and the calculated input power from dSpace at 1000 and 1500 rpm and 4 Nm.

It can be seen from Figure 6.7 that the input power measured by the Yokogawa power analyzer is shaped as a parabola, when the current vector angle is varied. However, for neither the 1000 nor the 1500 rpm case, the calculated input power from dSpace matches with the real input power. At 1000 rpm the ME angle from dSpace is located at 106° while it is located at 122.5° when measured by the Yokogawa power analyzer. At 1500 rpm, the calculated power from dSpace is seen to rise during the entire angle sweep. As such, the calculated input power from dSpace is deemed unreliable as both the shape and magnitude does not correspond with measured input power.

Since the calculated power measurements from dSpace cannot be used, the power measurements from the Yokogawa power analyzer investigated in Section 6.3 will be used to validate the MEA. The measurements are comprised into a 1D LUT with the measured d-axis current as input for each of the EEI operating conditions. As the d-axis current is measured real-time the LUT can be regarded as an online measurement and will therefore be used to validate if the MEA can find the optimum angle during online operation.

6.5 MEA Validation

The MEA described in Section 5.3 is implemented in dSpace. As the idea of the algorithm is to find the optimum angle for the current vector when the machine is operating in steady state the update rate of the MEA should fit with the time it takes for the system to reach steady-state. When the angle of the current changes it results in a transient in the speed since the current vector amplitude must change accordingly to provide the correct torque. As seen in Figure 6.6 the ME angle lies between 130° and 145°, thus these two angles are chosen to define the initial angle interval and the inner angle is chosen to be 137.5°. A steady-state power measurement is needed for all three angles and therefore, the speed response during a step change from 130° to 137.5° and a step change from 137.5° to 145°, has been tested and the results can be seen in Figure 6.8.

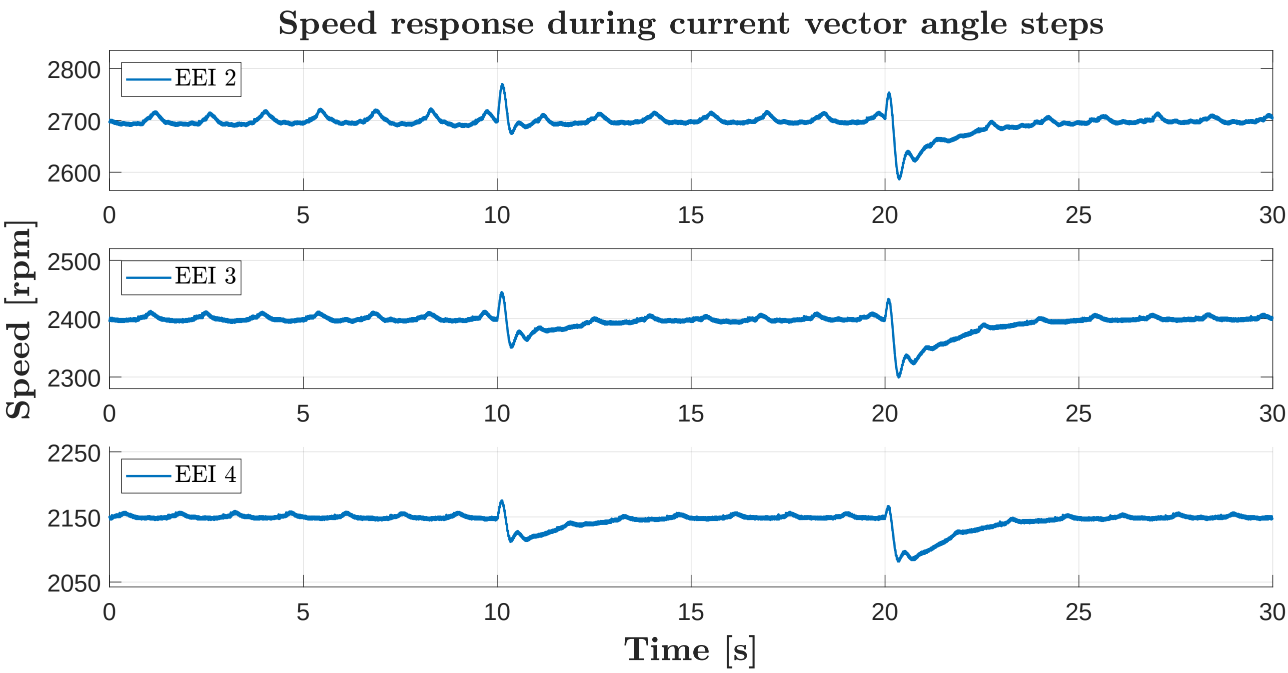

Figure 6.8. Settling time of the FASynRM when it is subjected to a step in the current vector angle. The angle is changed from 130° to 137.5° at 10 s and from 137.5° to 145° at 20 s.

As can be seen in Figure 6.8 there is a transient in the speed when the current vector angle is changed at both 10 and 20 seconds. As the speed decreases during the step at 20 seconds it must mean that the current vector amplitude is too small for the corresponding angle and torque, thus causing the machine to decelerate. This matches well with the MTPA angle for these EEI operating conditions earlier shown in Figure 6.6 occurring in the range of $125° - 135°$. As this is the smallest possible current vector magnitude for these operating conditions the amplitude of the current vector will have to increase when the current vector angle changes to 145° at 20 seconds. It takes approximately 5 seconds for the speed to settle completely for the three speeds shown in the figure. The settling time of the speed could be reduced by tuning the speed and current controller, however the slow controllers are necessary to ensure a stable system as earlier described in Section 6.3. This results in the settling time of the speed to be relatively slow. Since it takes 5 seconds for the speed to settle the frequency of the MEA is set to be 0.2 Hz, hence the angle of the current vector will be updated every 5 seconds.

EEI 2 - 2700 rpm, 9.5 Nm

The MEA is tested with the input power LUT for the four different EEI cases where the angle has been varied. This power measurement is sent to the MEA where the quadratic interpolation to determine the optimum angle is made. The stop criterion for these tests is $\delta = 0.1$ W. This value is quite small when considering that the resolution of the power measurements is 1 W. However, the convergence capability of the algorithm deteriorates the smaller the stop criterion is. So to test the convergence capability a small stop criterion is chosen. The MEA has been tested on EEI 2 and the results can be seen in Figure 6.9.

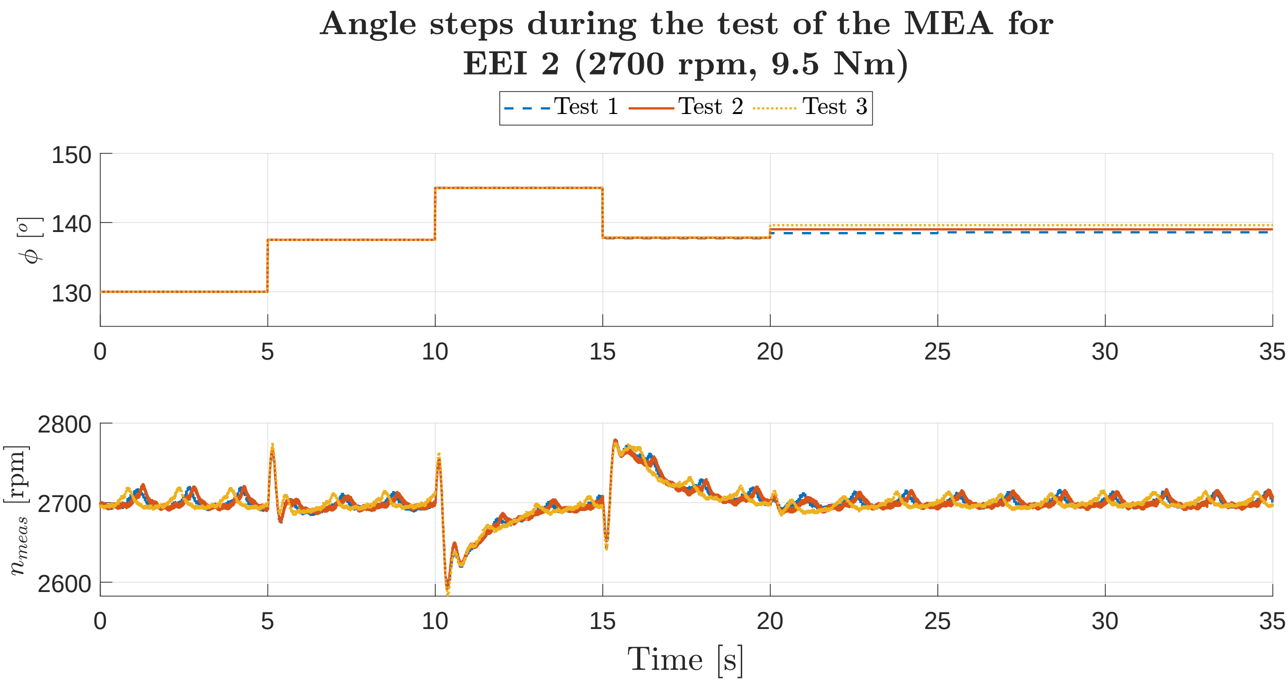

Figure 6.9. Results for the test of the MEA for EEI 2 where the input power LUT with the measured d-axis current has been used as an input. The output angle from the MEA for the three repeated tests is shown.

In Figure 6.9 the results for the test of the MEA on EEI 2 using the input power LUT can be seen. It can be seen that the current vector angle settles after 20 seconds i.e. 4 iterations and the final angle of the three tests are seen in Table 6.1.

EEI 2	Test 1	Test 2	Test 3	ME Range
Angle	138.6°	139°	139.6°	[137.5°; 142.5°]

Table 6.1. Final current vector angle for the MEA when the LUT for EEI 2 is used for all three tests. The ME range was marked by the green dots in Figure 6.6

In Table 6.1 it can be seen that the final angle for all tests are within the ME range, hence the algorithm finds the optimum angle when the input power LUT is used for EEI 2. It can be seen in Figure 6.9 that the speed reaches steady state before the angle is changed again after each iteration. Hence the period of the MEA fits with the settling time for the system with the used controllers.

EEI 3 - 2400 rpm, 6.6 Nm

The results for the test of the MEA when the machine is operated at EEI 3 can be seen in Figure 6.10.

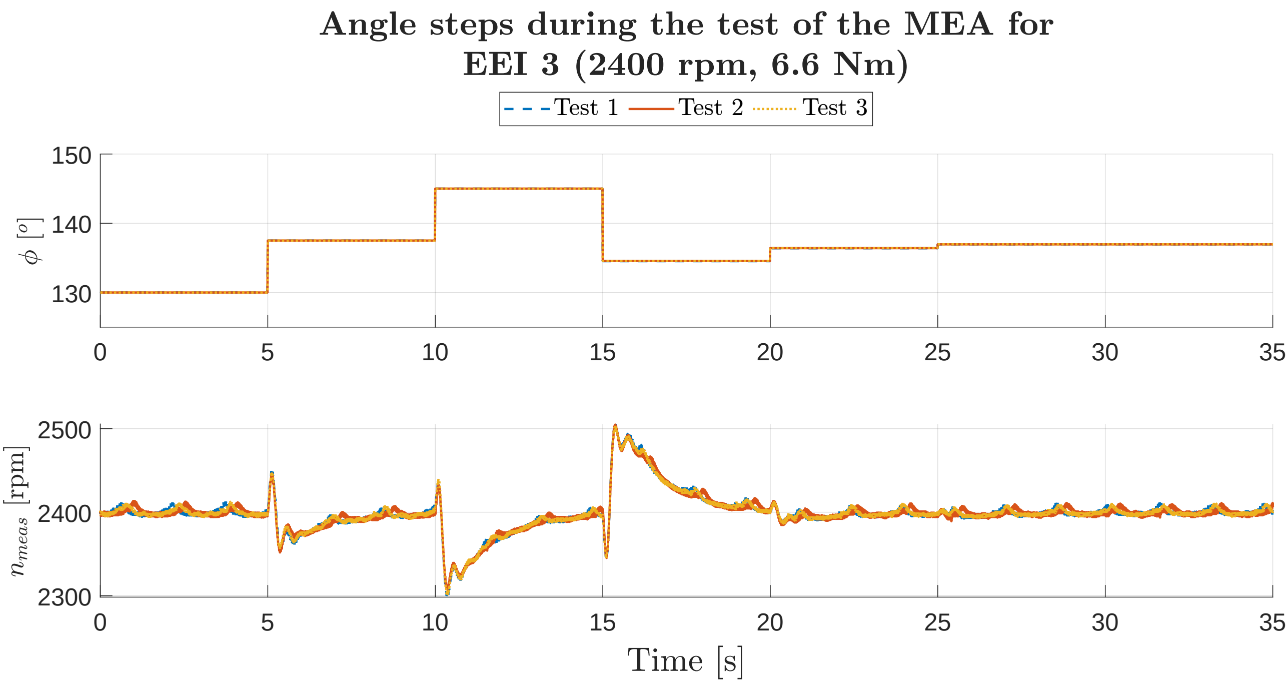

Figure 6.10. Results for the test of the MEA for EEI 3 where the input power LUT with the measured d-axis current has been used as an input. The output angle from the MEA for the three repeated tests is shown.

It can be seen in Figure 6.10 that the algorithm for EEI 3 stops changing the angle after 25 seconds corresponding to 5 iterations. The final angle of the three tests are seen in Table 6.2.

EEI 3	Test 1	Test 2	Test 3	ME Range
Angle	136.9°	137°	137°	[135°; 137.5°]

Table 6.2. Final current vector angle for the MEA when the LUT for EEI 3 is used for all three tests. The ME range was marked by the green dots in Figure 6.6

It can be seen in Table 6.2 that the algorithm stops within the ME range for all tests. But it is already within the range after 20 seconds corresponding to iteration 4. Here the angle for all three tests is around 136.4°. The last iteration does not change the efficiency according to the input power LUT so in principle it is redundant. If the stop condition of $\delta = 0.1$ W was increased the algorithm might have stopped at iteration 4.

EEI 4 - 2150 rpm, 4.2 Nm

The results for the test of the MEA when the machine is operated at EEI 4 can be seen in Figure 6.11.

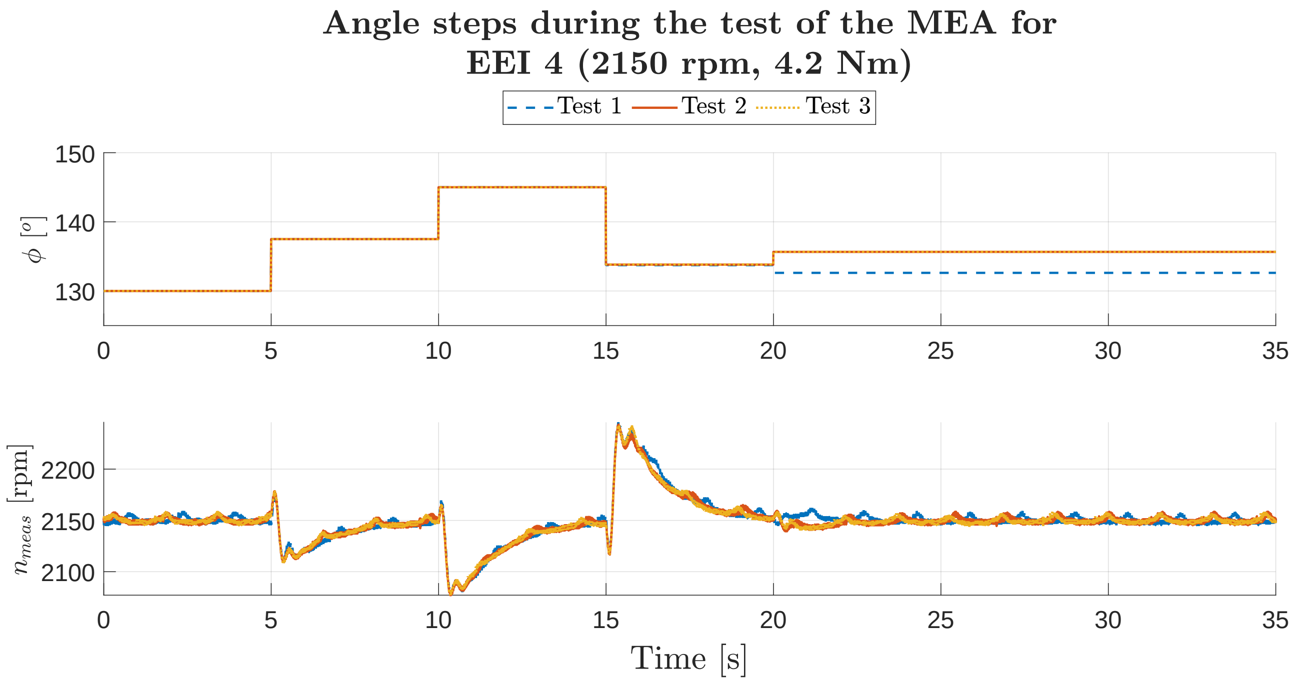

Figure 6.11. Results for the test of the MEA for EEI 4 where the input power LUT with the measured d-axis current has been used as an input. The output angle from the MEA for the three repeated tests is shown.

In Figure 6.11 it can be seen that the algorithm stops changing the angle after iteration 4 corresponding to 20 seconds. The final angle for all tests can be seen in Table 6.3.

EEI 4	Test 1	Test 2	Test 3	ME Range
Angle	132.2°	135.7°	135.7°	[130°; 135.7°]

Table 6.3. Final current vector angle for the MEA when the LUT for EEI 4 is used for all three tests. The ME range was marked by the green dots in Figure 6.6

It can be seen in Table 6.3 that the MEA stops within the range of the ME angle for all tests. However, the behaviour of the algorithm is not the same for all three tests. The last iteration results in a different angle for test 1 compared to test 2 and 3. The deviation for this test could be due to the i_d measurements for this specific test being different than the two others. However, the algorithm still behaves as expected for all three test since the final angle is within the ME range for all tests.

The results described above confirms that the MEA converges to the true ME angle during operation. Having validated the MEA, it can now be investigated if the MEA can also converge to the true ME angle by using an estimated power loss profile.

6.6 Power Loss Estimation Profile

It was shown in Section 6.5 that the MEA was able to converge to the true ME angle for all the EEI operating conditions by using an input power LUT for each of the EEI operating conditions. This method works well but it is impractical to create LUTs for a wide range of speed and torque combinations, hence a straightforward approach requiring only few measurements is desirable. As described earlier in Section 5.2 the input power can be reduced by minimizing the losses in the machine with Equation (5.5). It is therefore necessary to determine a function for $P_{\text{core}}(I_{\text{s,pk}}(\phi))$, which should be usable for multiple combinations of speeds and torques and only require few tests. A way to measure the core losses is to conduct experiments where the output power is measured by the torque transducer and the copper losses are determined by the measured current and these are subtracted from the input power measured by the Yokogawa power analyzer as described in Section 5.2. To determine a core loss profile the input power is measured where the output torque is varied for three different speeds which are 2000, 2500 and 3000 rpm. The measured input power for 2500 rpm for various torques where the current vector angle has been varied are shown in Figure 6.12 and the results for the other speeds can be seen in the attached Excel file, 'Coreloss_Measurements.xlsx'

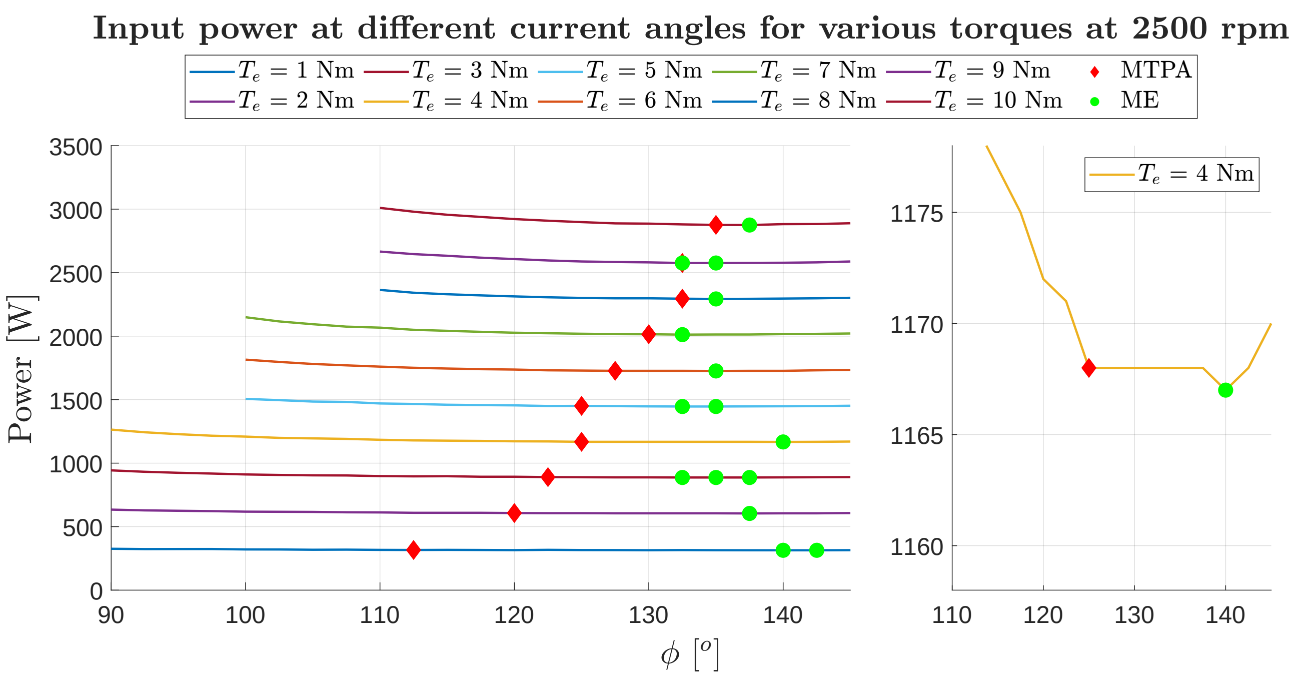

Figure 6.12. Input power as a function of current vector angle for various torques at 2500 rpm. The red diamonds indicate the MTPA angles and the green circles indicate the ME angles for the different torque lines. The right graph shows a zoomed view of the 4 Nm torque line to showcase the small variation in power around the ME angle. The resolution is 2.5° and 1 W for the angle and power, respectively.

It can be seen in Figure 6.12 that the MTPA angle marked with red dots increase with increasing torque. This is as expected since the current increases with increasing torque and the reluctance torque, which varies with the current squared carries more and more weight compared to the PM torque hence the copper losses are smallest when the current vector angle approaches 135°. For the ME angles the optimum angle is between 132.5° and 142.5° and always larger than the MTPA angle, except at 9 Nm. As the load torque increases the difference between the MTPA and the ME angle decreases. The reason for this is due to the copper and core losses and their weight relative to the total amount of losses. At 1 Nm and 2500 rpm, the copper losses are low compared to the core losses, due to the small current vector amplitude but high speed. Therefore, even though the MTPA angle already occurs at 112.5° the ME angle is at 140° – 142.5° because the copper losses do not contribute much to the overall losses. The ME angle is then mostly determined by the core losses, which are reduced by flux-weakening, requiring a numerically large negative d-axis current, explaining the large ME angle. As the torque increases, the copper losses weigh more in the overall losses and the MTPA and ME angle will be drawn towards each other. In Figure 6.12 there are several ME angles for one torque curve as seen for 3 Nm. This is because the measurement obtained from the Yokogawa power analyzer was varying with 2-3 W each second making it difficult to manually read the precise value from the power analyzer. Furthermore, the power only varied with a few watts around the ME angle. This can be seen in 'Coreloss_Measurements.xlsx', where the ME and MTPA angle has been marked with green and red, respectively. It can also be seen in the right plot of Figure 6.12 that the power is constant from 125° to 137.5° and then it reduces with 1 W at 140° making this the ME optimum angle. A more precise ME angle could have been determined if the system disturbance issue was solved and a higher power measurement resolution was used, however it is deemed that the real ME angle is close to the obtained angles seen in the figure and the power around the ME angle did not change significantly.

By using the measured input power, the output power from the torque transducer and the calculated copper losses, the core losses are estimated. These can also be seen in 'Coreloss_Measurements.xlsx'. It is desired to find a relation between the current and the core losses to determine a function for $P_{\text{core}}(I_{\text{s,pk}}(\phi))$ mentioned in Section 5.2. It is investigated how the core losses vary with the d- and q-axis currents respectively. The core loss as a function of the d- and q-axis current for different speeds and torques where the current vector angle has been varied are shown in Figure 6.13.

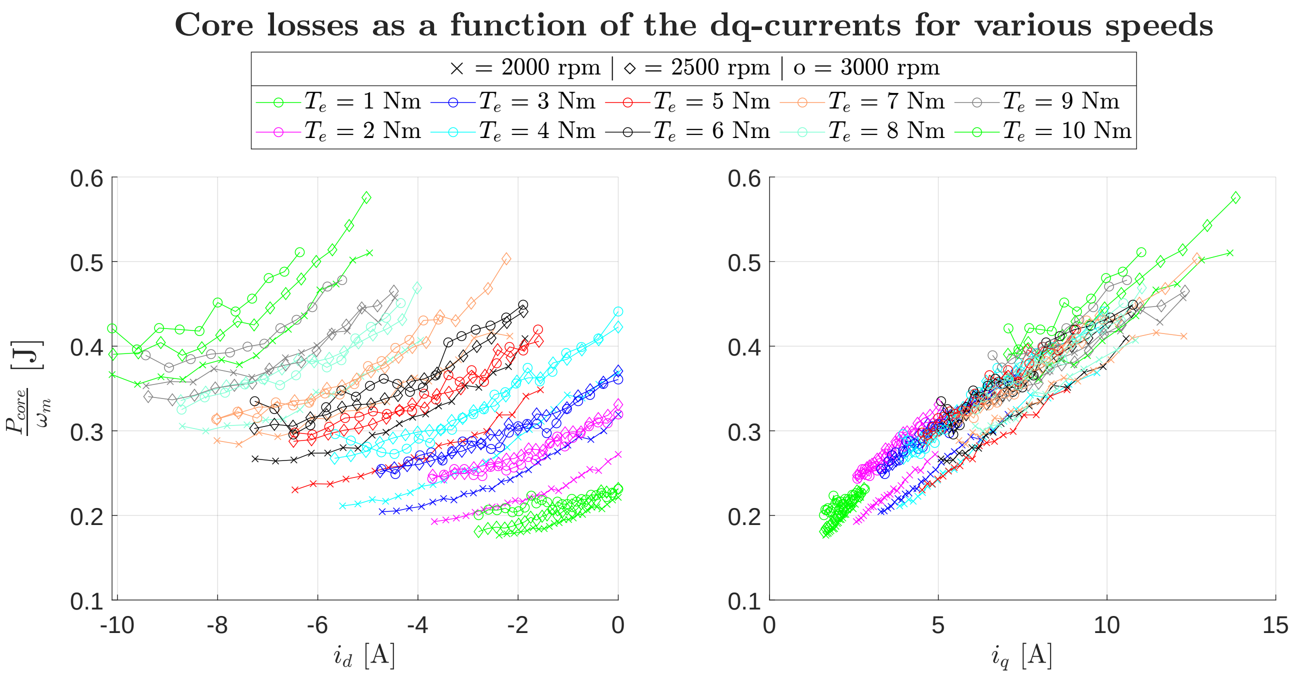

Figure 6.13. Core losses as a function of the d- and q-axis currents for various speeds. The core losses have been divided by the speed so the core loss profiles are speed independent

The results shown in Figure 6.13 are obtained by sweeping the current vector angle for various output torques represented by different colors. These tests have been done at 2000, 2500 and 3000 rpm, shown by the three different symbols in the figure. The current vector angle is swept with a resolution of 2.5° in an interval earlier shown in Figure 6.12 for the different torque curves. As it can be seen in

Figure 6.13 the core losses and the corresponding d-axis current increase with the torque. This makes it impossible to have a unified core loss function that can estimate the losses without knowing the torque. However, the results in the right figure suggests that the core losses are linearly dependent on the q-axis current when the current vector angle is varied and this relationship is independent of the torque. A further investigation can be seen in Figure 6.14 where the core loss profile for 2000, 2500 and 3000 rpm has been separated and a linear regression line has been fitted.

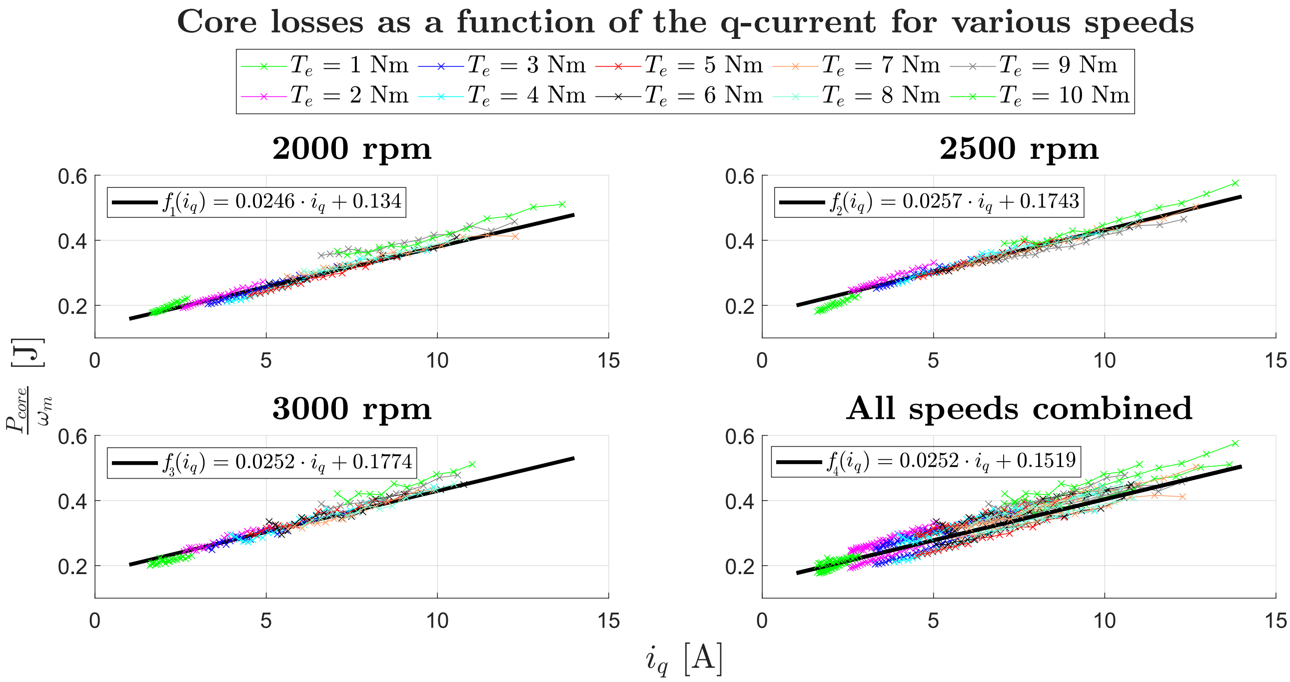

Figure 6.14. Plot of the core losses divided by the speed vs. i_q-current, for 2000, 2500 and 3000 rpm and all speeds in the same plot. A linear regression line has been fitted for each speed and for all speeds combined. The function equation for each regression line is also shown.

In Figure 6.14 it can be seen that a linear regression line can be fitted and the data follows these regression lines to a reasonable degree. A regression line has been fitted for each speed, since it is desired to evaluate if a core loss profile can be adequately determined based on one speed only. This would be advantageous since fewer experiments would have to be conducted in order to find the core loss profile and ultimately the ME angle. For 2000 rpm it can be seen that the b-value which describes the intersection with the y-axis is different from the other speeds. Furthermore, the curves for 9 and 10 Nm are larger than the other torque curves for 2000 rpm. However, the slope of the 9 and 10 Nm curves are deemed to be the same as the other torque curves. From the function expression for 2000, 2500 and 3000 rpm it can be seen that the slope of the regression lines are approximately the same for all speeds, but the intersection with the y-axis differs. The power loss function with the linear regression function added is given by Equation (6.1).

$$P_{\text{loss}}(I_{\text{pk}}) = \frac{3}{2} \cdot R_{\text{s}} \cdot I_{\text{pk}}^2 + (a \cdot I_{\text{pk}} \cdot \sin(\phi) + b) \cdot \omega_{\text{m}} \tag{6.1}$$

where a is the slope of the regression lines and b is the intersection with the y-axis found in Figure 6.14. From Equation (6.1) it can be seen that angle of the optimum point for the loss function is not affected by the b-value of the regression functions. The b-value only affects the value for the estimated power, i.e. a higher b-value gives an overall larger estimation of the core losses. Hence, the optimum angle stays the same regardless of the b-value.

In Figure 6.14 a unified function for all speeds has also been found. It can be seen that the slope is the same as the one from the 3000 rpm, but the intersection with the y-axis is different from the rest, however its influence on the optimum angle is the same argument as in the above stated paragraph. In the following section the four different core loss profiles will be tested to see if there is a difference in the estimated optimum angle when the MEA is used.

6.7 MEA Testing with Power Loss Estimation Profile

The MEA is now tested on the power loss estimation profile described by Equation (6.1), where the four functions for the different core loss profiles are given in Table 6.4.

Function	Speed (rpm)
$f_1 = 0.0246 \cdot I_{\mathrm{s,pk}} \cdot \sin(\phi) + 0.134$	2000
$f_2 = 0.0257 \cdot I_{\mathrm{s,pk}} \cdot \sin(\phi) + 0.1743$	2500
$f_3 = 0.0252 \cdot I_{\mathrm{s,pk}} \cdot \sin(\phi) + 0.1774$	3000
$f_4 = 0.0252 \cdot I_{\mathrm{s,pk}} \cdot \sin(\phi) + 0.1519$	Combined

Table 6.4. The core loss profiles found by linear regression in Figure 6.14.

Table 6.4 shows the core loss profiles for three different speeds and one for all speeds combined. The stop criterion for the MEA is evaluated based on the oscillations in the estimated power loss in steady-state shown in Figure 6.15.

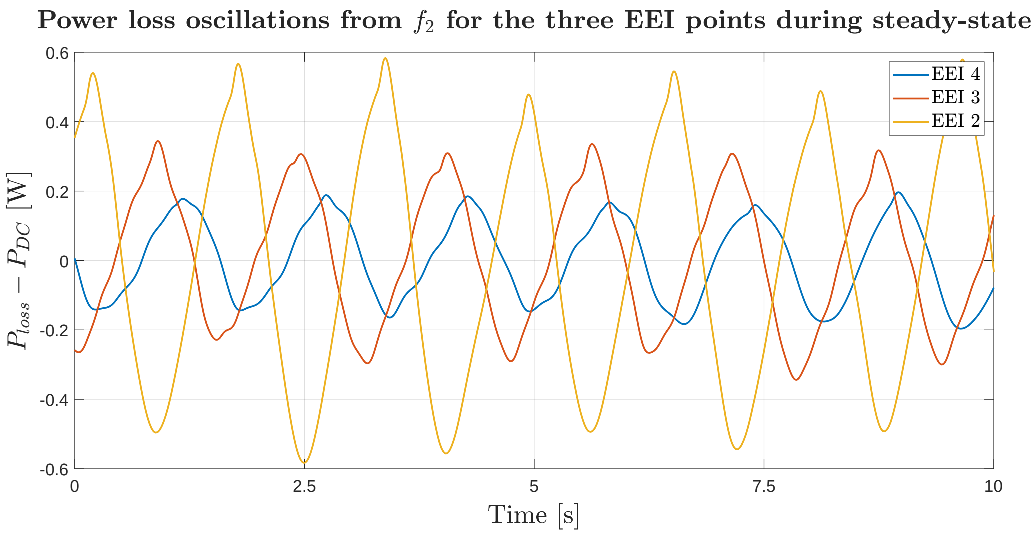

Figure 6.15. The oscillations in the estimated power loss from f_2 during steady-state. The DC-bias for the three EEI functions has been subtracted to easily compare the peak-to-peak oscillations for all three operating points.

From Figure 6.15 it can be seen that the oscillation in the estimated power loss during steady-state varies for the three operating points. The estimated power loss is based on f_2 as this function has the largest slope, thus resulting in the largest power loss oscillation, when the current vector amplitude varies. The current vector amplitude oscillates with a period of 1.5 s due to the speed oscillation earlier described in Section 6.5. The peak-to-peak values are approximately 1.2, 0.6 and 0.4 W for EEI 2, 3 and 4, respectively. To avoid that the MEA reacts to this variation in the estimated power loss the stop criterion, δ, is set to 1.5, 0.8 and 0.6 W for EEI 2, 3 and 4, respectively.

EEI 2 - 2700 rpm and 9.5 Nm

The experiments have been conducted five times for each function presented in Table 6.4 where the machine operates in EEI case 2 and the results of the tests can be seen in Figure 6.16.

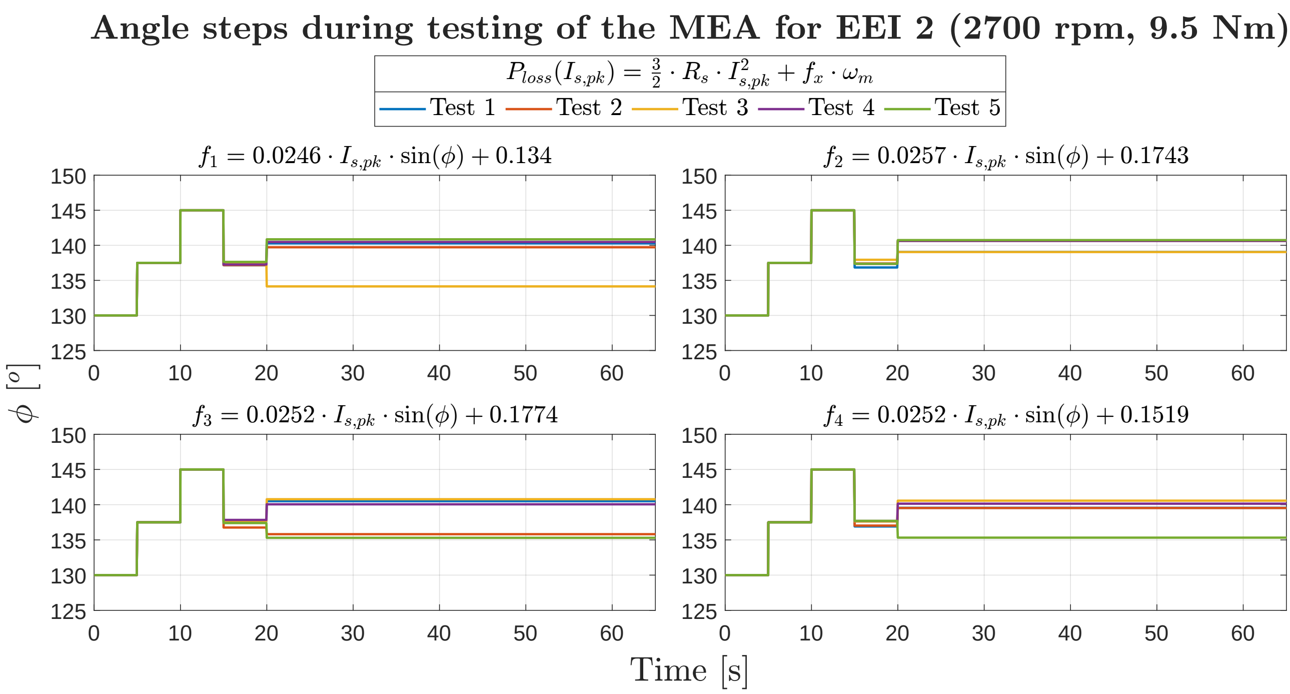

Figure 6.16. Results showing how the algorithm finds the optimum current vector angle for EEI 2 operating condition. The power loss function is shown in the top as well as one plot for each function that was found in Figure 6.14.

EEI 2		Test 1	Test 2	Test 3	Test 4	Test 5	ME range
f_1	MEA angle [°]	140.28	139.7	134.1	140.5	140.9	[137.5 ; 142.5]
	MEA power [W]	2952	2952	2954	2952	2952	2952
f_2	MEA angle [°]	139.05	140.6	139	140.6	140.7	[137.5 ; 142.5]
	MEA power [W]	2952	2952	2952	2952	2952	2952
f_3	MEA angle [°]	140.50	135.8	140.8	140.1	135.3	[137.5 ; 142.5]
	MEA power [W]	2952	2954	2952	2952	2954	2952
f_4	MEA angle [°]	139.56	139.5	140.6	140.2	135.3	[137.5 ; 142.5]
	MEA power [W]	2952	2952	2952	2952	2954	2952

Table 6.5. Converged MEA angles for the five tests during testing of core loss function 1-4 for EEI 2. The MEA power is the power measurement corresponding to the MEA angle read from the LUT measured from the Yokogawa power analyzer. The last column shows the range of the MEA angle measured by the Yokogawa power analyzer and the power at this angle.

Figure 6.16 shows the results for EEI case 2 and Table 6.5 shows the converged MEA angles. The stop criterion for this case is $\delta = 1.5$ W. For core loss function f_1 given in the top left plot it can be seen that the algorithm stops changing the angle after 20 seconds, i.e. 4 iterations. It can be seen that the algorithm stops inside the range of the optimum angle four out of five times. For test 3 it can be seen that the final angle value is 134.1°, corresponding to an input power of 2954 W. The difference in power for this test is 2 W relative to the ME angle. It can be seen that the algorithm where f_2 is used, outputs an angle that is within the ME range for all tests. For f_3 two of the tests are outside the range and ends at an angle around 135° which gives an input power of around 2954 W. For function f_4, which is the unified function for all speeds and torques, the final angle determined by the algorithm is inside the ME range four out of five times. For test 5 it is outside the range at 135° as before. Since it is the power loss function that is to be minimized, it will be investigated how it varies, when the current vector angle is changed. The estimated power loss for function f_1 can be seen in Figure 6.17.

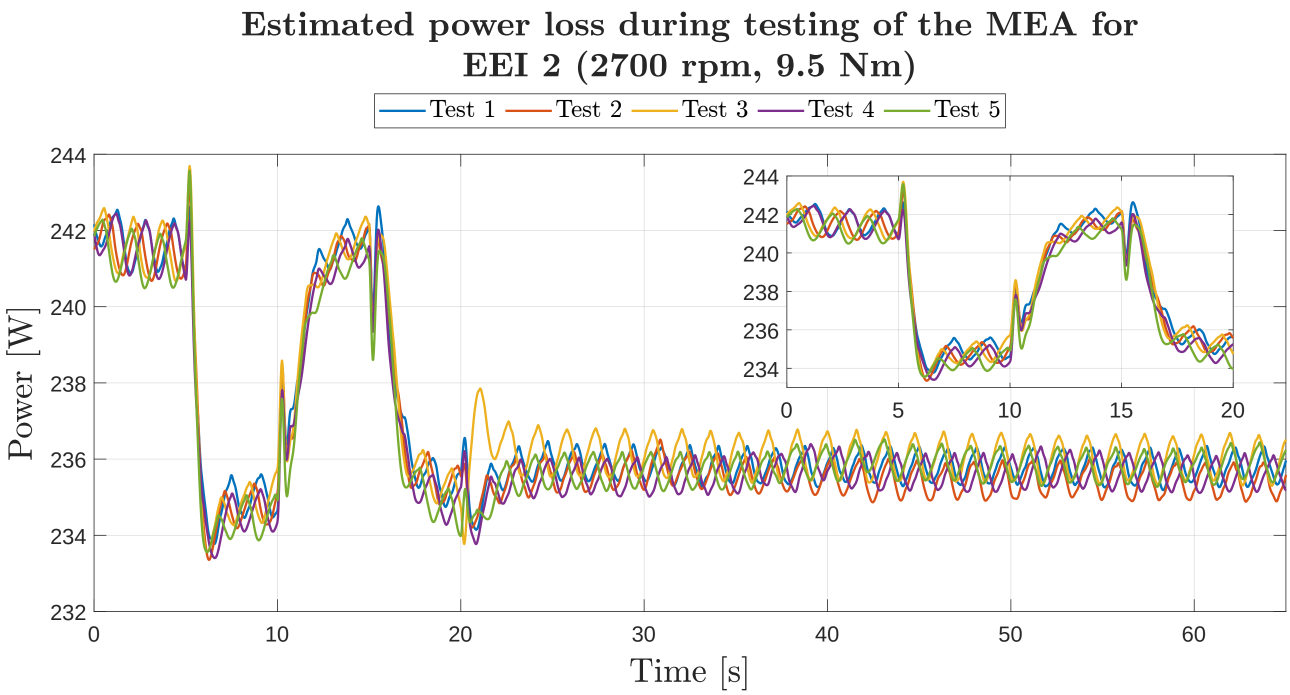

Figure 6.17. Estimated power loss during testing of the MEA for EEI 2. The figure in the top right corner shows the estimated power loss for the first 20 seconds. Only the estimated power loss from f_1 is shown.

In Figure 6.17 it can be seen that power behaves in approximately the same way for all tests. It can be seen that the estimated power loss starts high at 5 seconds, decreases at 10 seconds and increases again at 15 seconds. From these measurements the MEA is able to determine that the optimum angle lies in the range of 137.5° – 142.5° for most of the tests.

EEI 3 - 2400 rpm and 6.6 Nm

The results for the experiments with the EEI case 3 and the four different core loss functions can be seen in Figure 6.18 and Table 6.6.

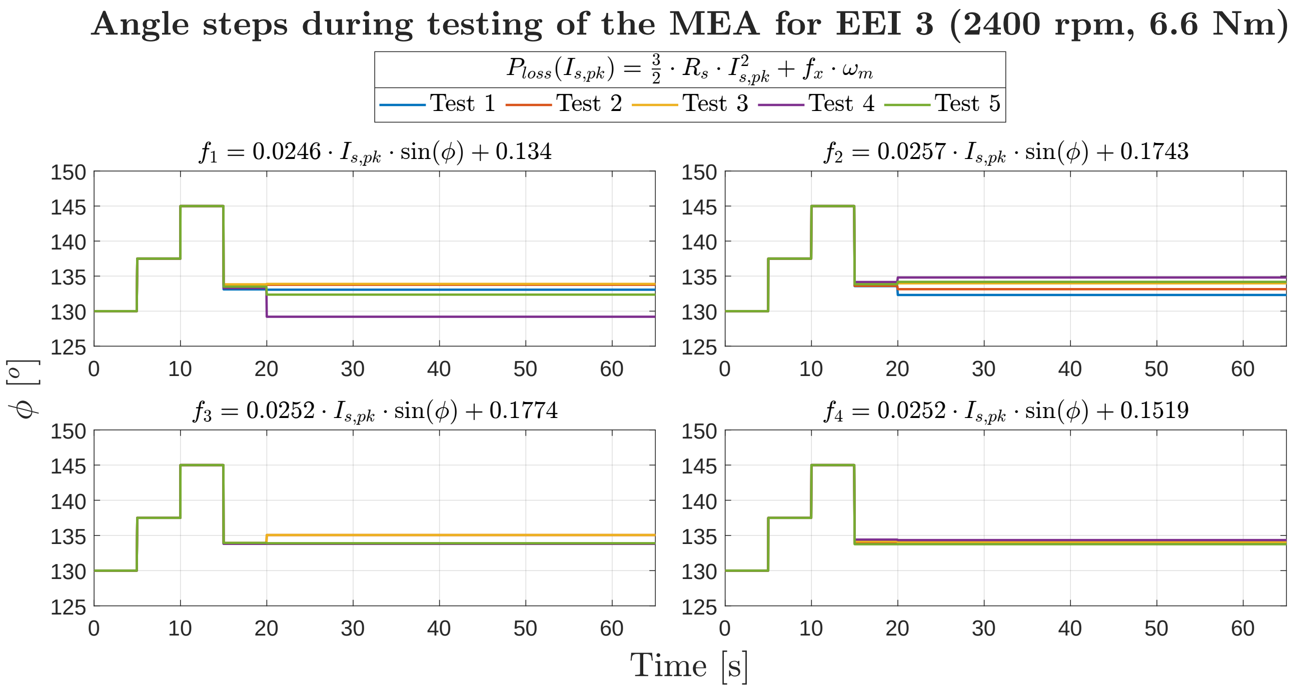

Figure 6.18. Results showing how the algorithm finds the optimum current vector angle for EEI 3 operating condition. The power loss function is shown in the top as well as one plot for each function that was found in Figure 6.14.

EEI 3		Test 1	Test 2	Test 3	Test 4	Test 5	ME range
f_1	MEA angle [°]	133.06	133.8	133.9	129.2	132.4	[135 ; 137.5]
	MEA power [W]	1831	1830	1830	1831	1831	1830
f_2	MEA angle [°]	132.31	133.1	134	134.8	134.2	[135 ; 137.5]
	MEA power [W]	1831	1831	1830	1830	1830	1830
f_3	MEA angle [°]	133.8	135.1	135.1	133.8	133.9	[135 ; 137.5]
	MEA power [W]	1830	1830	1830	1830	1830	1830
f_4	MEA angle [°]	134.1	133.9	134.0	134.3	133.8	[135 ; 137.5]
	MEA power [W]	1830	1830	1830	1830	1830	1830

Table 6.6. Converged MEA angles for the five tests during testing of core loss function 1-4 for EEI 3. The MEA power is the power measurement corresponding to the MEA angle read from the LUT measured from the Yokogawa power analyzer. The last column shows the range of the MEA angle measured by the Yokogawa power analyzer and the power at this angle.

Figure 6.18 and Table 6.6 show the results for operating case EEI 3 where each of the four core loss functions have been tested 5 times. It can be seen that all the tests for f_1, f_2 and f_4 are outside of the ME range. In fact, only test 2 and 3 for core loss function 3 converges to an angle within the measured ME range. However, the input power is approximately 1831 W for the converged angle furthest away from the ME range, which is seen at test 4 for core loss function 1, where the angle is 129°. This is only 1 W more than the 1830 W at the optimum current vector angle. Even though 18 of the 20 tests failed, due to the converged MEA angle being outside the ME range, the input power for most cases is still equal to that inside the ME range since the used resolution is 2.5° and 1 W, for the angle and power, respectively. So the MEA is still able to provide a satisfactory result, due to the small difference in the input power for the converged angles.

The variation in the estimated power loss, when the current vector angle changes, can be seen in Figure 6.19.

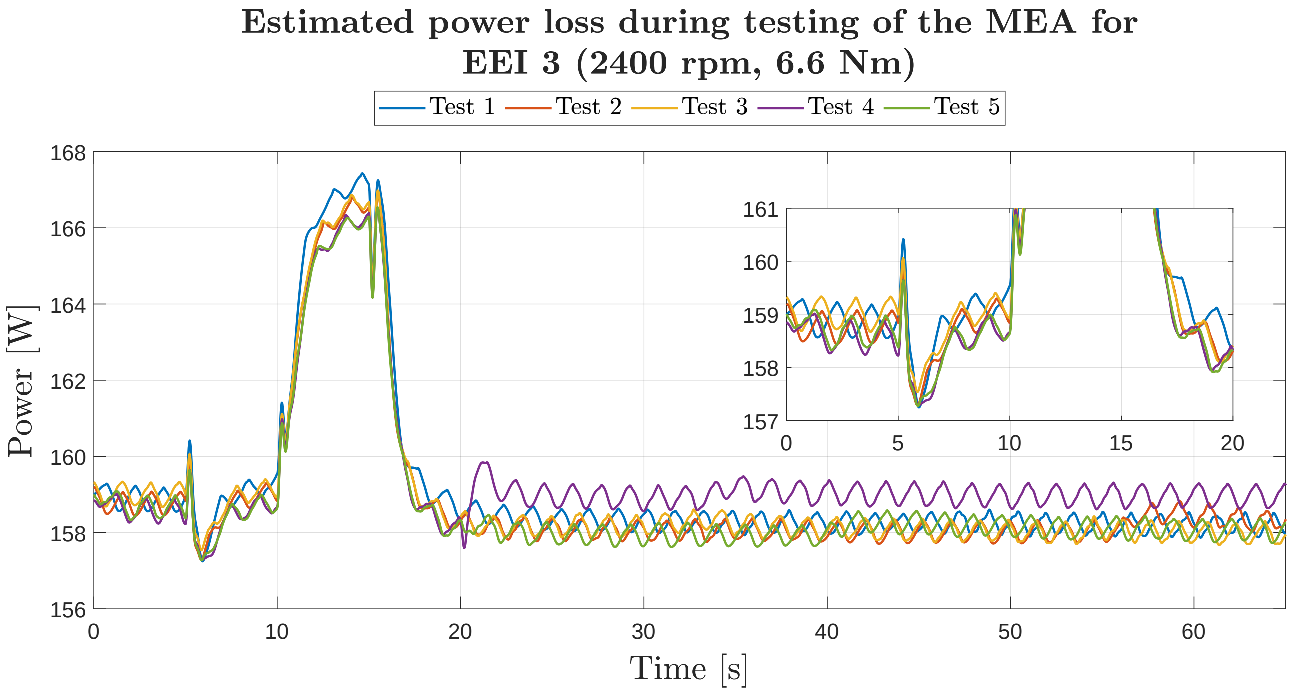

Figure 6.19. Estimated power loss during testing of the MEA for EEI 3. The figure in the top right corner shows the estimated power loss for the first 20 seconds. Only the estimated power loss from f_1 is shown.

In Figure 6.19 it can again be seen that the power behaves in approximately the same way for all tests for f_1. However, it can be seen in the zoomed view that the power measured at 5 seconds and 10 seconds is approximately equal. This could potentially make it difficult for the MEA to estimate where the optimum lies since the power measurements at the three distinct angles ideally should vary like a parabola, where the power loss for the inner angle should be lower than the power at the lower and upper angle of the interval. From Figure 6.18 it was seen that the estimated optimum angle was outside the range of the ME angles. This could be due to the fact that the power measured at 5 seconds and 10 seconds were approximately equal. If the initial angle interval was increased the estimated angle might be closer to the real optimum.

EEI 4 - 2150 rpm and 4.2 Nm

The results for when the machine is operating at EEI 4 where the MEA uses the four core loss functions can be seen in Figure 6.20 and Table 6.7.

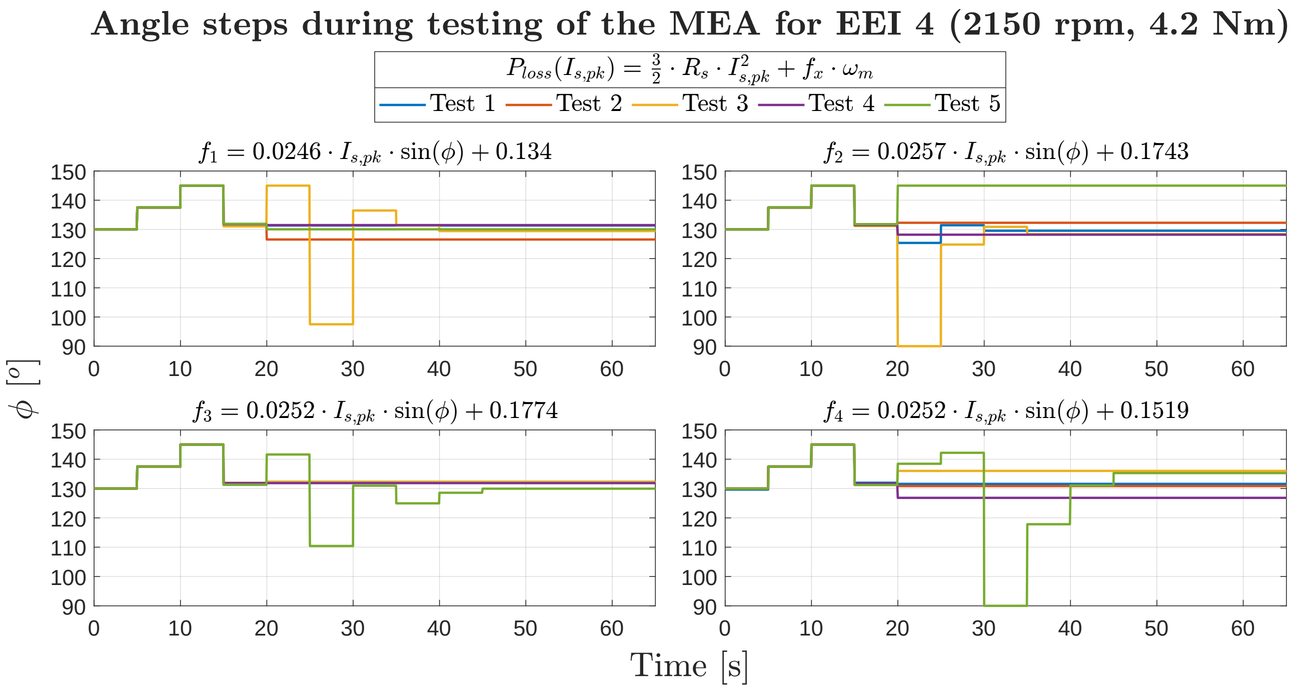

Figure 6.20. Results showing how the algorithm finds the optimum current vector angle for EEI 4 operating condition. The power loss function is shown in the top as well as one plot for each function that was found in Figure 6.14.

EEI 4		Test 1	Test 2	Test 3	Test 4	Test 5	ME range
f_1	MEA angle [°]	131.3	126.5	129.4	131.5	130.0	[130 ; 137.5]
	MEA power [W]	1054	1055	1054	1054	1054	1054
f_1	MEA angle [°]	129.6	132.3	128.4	128.2	145	[130 ; 137.5]
	MEA power [W]	1054	1054	1055	1055	1060	1054
f_3	MEA angle [°]	132.3	132	132.3	131.9	129.9	[130 ; 137.5]
	MEA power [W]	1054	1054	1054	1054	1054	1054
f_4	MEA angle [°]	131.6	130.8	136.0	126.8	135.3	[130 ; 137.5]
	MEA power [W]	1054	1054	1054	1055	1054	1054

Table 6.7. Converged MEA angles for the five tests during testing of core loss function 1-4 for EEI 4. The MEA power is the power measurement corresponding to the MEA angle read from the LUT measured from the Yokogawa power analyzer. The last column shows the range of the MEA angle measured by the Yokogawa power analyzer and the power at this angle.

In Figure 6.20 and Table 6.7 it can be seen that the MEA stops at an angle within the ME range, three out of five times for f_1. The test that is furthest away from the ME range is test number 2. The final angle for this one 126.5°, which corresponds to an input power of 1055 W. The input power at the ME angle is 1054 W, which means that the power difference is 1 W. For f_2 it can be seen that one of the tests is inside the ME range and four are outside. Three of them stop at approximately 129° where the input power is around the optimum point of 1054 W. For test 5 it can be seen that the MEA stops at 145°. The input power at this angle is 1060 W, which is 6 W above the optimum input power. For f_3 it can be seen that the converged angle for all the tests is approximately inside the ME range, hence the MEA with this function is able to find the ME angle. For f_4 four of the tests are inside the interval, but one of them is outside. The outlying angle is approximately 127°, which gives an input power of 1055 W, which is 1 W away from the optimum.

It can be seen that for the majority of tests it takes around 20 seconds, i.e. 4 iterations to reach the final estimated angle. But at least one of the tests for each function takes more iterations than the rest, which is up to nine iterations. A common thing for the tests with more iterations is that one of the estimated angles falls outside of the initial angle interval. The initial angle interval is defined to be from 130° to 145° with 137.5° as the inner angle. The ME range for EEI 4 is from 130° to 137.5° which means that the two initial power measurements are already within the ME range where the power does not change significantly. This could have the effect that the algorithm has a hard time estimating the optimum angle.

To investigate why the algorithm behaves in a different way, for one of the tests, the estimated power loss can be seen in Figure 6.21.

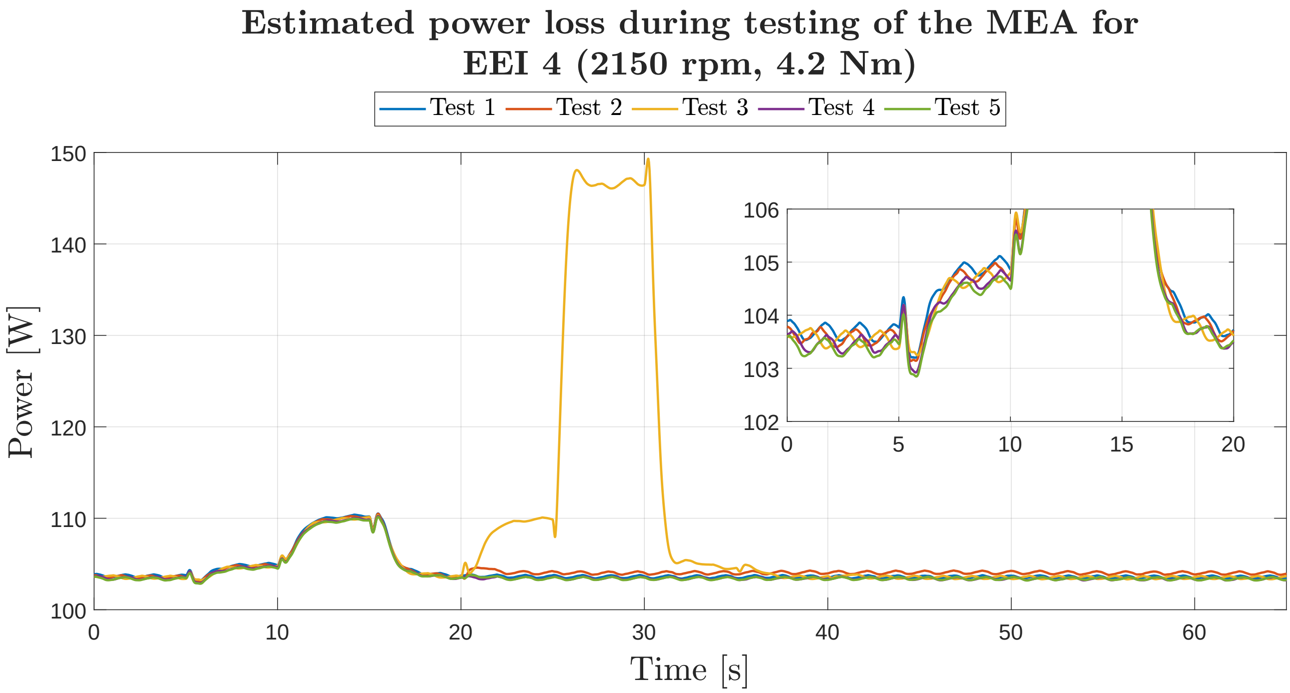

Figure 6.21. Estimated power loss during testing of the MEA for EEI 4. The figure in the top right corner shows the estimated power loss for the first 20 seconds. Only the estimated power loss from f_1 is shown.

In Figure 6.21 it can be seen that for test 3 for f_1 the power varies a lot compared to the other tests. The reason for this might be that the power increases when the angle changes from 130° to 137.5 at 5 seconds and again from 137.5° to 145° at 10 seconds. This might make it difficult for the MEA to find the optimum angle. The reason for why only one of the tests gives a significantly different result compared to the others could be because the estimated power loss oscillates due to the variation in the speed earlier shown in Figure 6.5. This means that the estimated power loss is not the same at each iteration for all tests. Hence, the influence of the increasing power for the three initial power measurements might be more severe for test 3 making the MEA change the angle to a value outside of the initial angle range. Since the estimated power increases when the angle is changed from 130° to 137.5° and the fact that these two angles are already within the ME range it is desired to see if an increase in the initial angle interval will make the MEA behave in the same way for all tests. This is investigated in the following section.

EEI 4 with larger initial angle interval

It has been chosen to expand the initial angle interval to make sure that the power measurement at the three initial angles are different from each other. The previous initial angle interval for the current vector angle was defined as $[130°; 145°]$ with the inner angle defined as 137.5°. The new initial angle interval is expanded to be $[125°; 145°]$ where 135° is the inner angle of the interval. The MEA with the new initial angle interval has been tested for EEI 4 and the results can be seen in Figure 6.22.

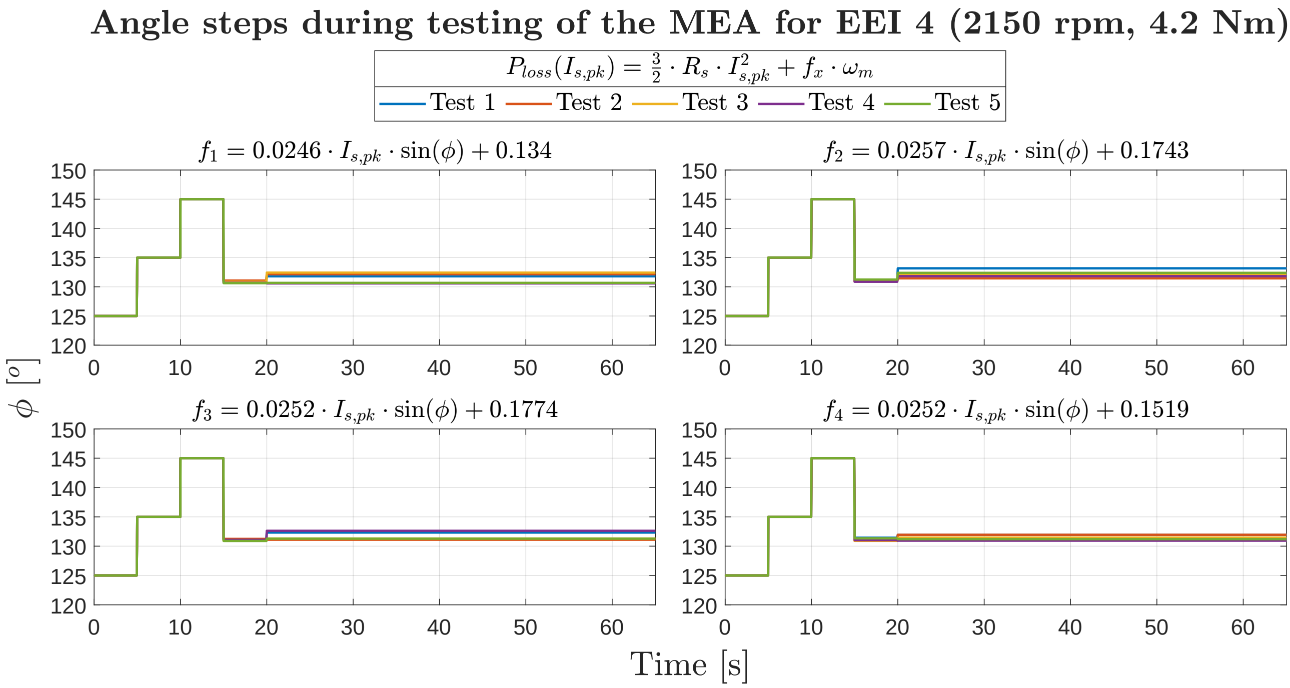

Figure 6.22. Results showing how the algorithm finds the optimum current vector angle for EEI 4 operating condition with a larger initial angle interval. The power loss function is shown in the top as well as one plot for each function that was found in Figure 6.14.

EEI 4 New angle interval		Test 1	Test 2	Test 3	Test 4	Test 5	ME range
f_1	MEA angle [°]	131.8	132.2	132.4	130.6	130.7	[130 ; 137.5]
	MEA power [W]	1054	1054	1054	1054	1054	1054
f_2	MEA angle [°]	133.2	131.5	132.1	131.8	132.4	[130 ; 137.5]
	MEA power [W]	1054	1054	1054	1054	1054	1054
f_3	MEA angle [°]	132.3	131.1	131.3	132.6	131.3	[130 ; 137.5]
	MEA power [W]	1054	1054	1054	1054	1054	1054
f_4	MEA angle [°]	131.9	131.9	131.5	130.9	131.2	[130 ; 137.5]
	MEA power [W]	1054	1054	1054	1054	1054	1054

Table 6.8. Converged MEA angles for the five tests during testing of core loss function 1-4 for EEI 4 for the expanded initial angle interval. The MEA power is the power measurement corresponding to the MEA angle read from the LUT measured from the Yokogawa power analyzer. The last column shows the range of the MEA angle measured by the Yokogawa power analyzer and the power at this angle.

From Figure 6.22 it can be seen that the final angle is found after 20 seconds which corresponds to 4 iterations for all tests and all power loss functions. From Table 6.8 it can be seen that all of the different tests for each different function is within the ME angle range. When comparing Figure 6.22 and 6.20 it can be seen that none of the tests for the new initial angle interval behaves strangely. They all behave in approximately the same way. This indicates that the power measurements for the three initial angles constituting the initial angle interval have to be noticeably different in order for the MEA to have a satisfactory behaviour all the time. The power loss determined from the power loss function during the tests with an increased initial angle interval for EEI 4 can be seen in Figure 6.23.

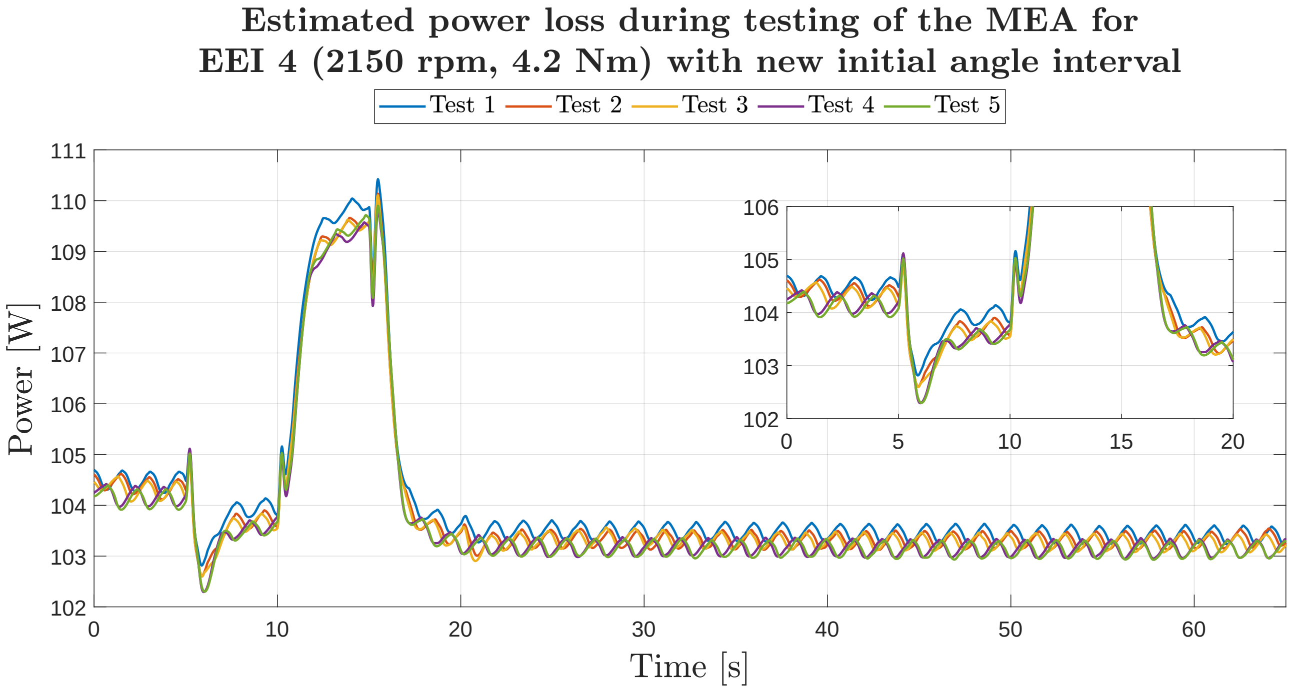

Figure 6.23. Estimated power loss during testing of the MEA for EEI 4, where the first two angles have been changed to 125° and 135°. The figure in the top right corner shows the estimated power loss for the first 20 seconds. Only the estimated power loss from f_1 is shown.

In Figure 6.23 it can be seen that the estimated power loss at 5 seconds has a larger value compared to the value at 10 seconds. This was not the case for the experiments shown in Figure 6.21 and this is expected to be the reason that the MEA now behaves in approximately the same way for all tests and functions. It is therefore deemed necessary to have an initial angle interval that guarantees that the power measured at the inner angle is lower than the power measured at the lower and upper angle of the interval.

Chapter 7

Discussion

Chapter 6 presented the results for several experiments that aimed to find the ME angle of the FASynRM when operating with the EEI operating conditions. One of the experiments intended to find the ME angle by using the active power equation. This approach has the advantage that it can be performed online without many preliminary offline measurements. Only the voltage errors from the inverter will have to be measured offline and comprised into a LUT. Thus, with Equation (5.3) it should be possible to measure the input power by the use of the dSpace command voltages, the voltage error LUT and current measurements. However, it was found in Section 6.4 that the active input power calculated in dSpace was inconsistent with the actual power measuered by the Yokogawa power analyzer. As the current measurements in dSpace matched with the ones seen from the Yokogawa power analyzer the error possibly stems from the estimated voltages. Voltage measurements could also have been used but since the voltages generated by the inverter are PWM signals, some calculations will have to be performed real-time to extract the fundamental component, which is used in the active power equation. This approach completely eliminates any preliminary offline measurements but necessitates both current and voltages measurements alongside the added computation power for the fundamental voltage component.

Another set of experiments were conducted in Section 6.3 where the Yokogawa power analyzer was used to develop 1D LUTs for the different EEI operating conditions. Using LUTs for each of the EEI operating conditions showed compelling results, as the MEA was able to find the ME angle for all the tests in Section 6.5. However, in case the FASynRM is to operate under other operating conditions the LUT approach falls short, as LUTs will have to be produced for all possible torque and speed combinations. This approach is very cumbersome and requires many offline measurements before the FASynRM is able to operate in a wide range of operating conditions.

In Section 6.6 a power loss profile was determined. To determine this power loss profile experiments were conducted, where the FASynRM was operated at a constant speed of 2000, 2500 and 3000 rpm. During the tests for each speed the load torque was varied from 1 to 10 Nm and for each torque the current vector angle was swept. The core losses were determined from the input power measurement, the transducer output power measurement and the calculated copper losses as the current vector angle was varied. From the results presented in 6.14 it was found that the core losses had a linear relation with the q-axis current and a linear regression function was found for each specific speed. A fourth function was determined where the results for all the speeds was combined. It was found that the slopes for each of the determined functions were approximately equal, but the intersection with the y-axis varied slightly. However, it was argued that the intersection with the y-axis only influenced the estimated value of the power loss and did not affect the ME angle estimation. Since the slope of all the functions was approximately equal, this indicates that the core loss profile was independent of the speed and also the torque as different torque curves had the same slope.

In Section 6.7 the four different power loss estimation functions were tested. Generally, it was found that the final angle output from the MEA for the majority of the tests was close to the ME range for all the determined functions. This indicates that the core loss profiles that were found can be used to find the ME angle. However, it was also found that the initial angle interval had an influence on how successful the MEA was to locate the ME angle. This can be seen when comparing the results in Table 6.7 with Table 6.8 where the initial angle interval was expanded from [130°;145°] to [125°;145°].

With the expanded interval the MEA was successful in determining a final angle that was within the ME range for all tests. This indicates that a power loss estimation profile based on the copper losses and the core loss profile can be used to obtain maximum efficiency control. Since all the four functions worked well it is only necessary to test for one speed. Additionally, for this project 10 different torques were tested where the current vector angle was varied but as the different torque profiles overlapped each other the number of different torque lines could also possibly be reduced to create the same core loss profile However, a proper initial angle interval must be used.

It was evident in the MEA testing with both the input power LUTs in Section 6.5 and the power loss estimation profile in Section 6.7 that the converge time of the MEA was rather slow, i.e minimum 20 seconds. Even though the MEA was able to find the ME angle after down to four iterations, the slow frequency of the MEA of 0.2 Hz, meant that the FASynRM was operating at a non-optimal current vector angle for some time. However, the slow update rate of the MEA was due to the slow controllers in the FOC scheme that were deemed necessary because of a disturbance in the speed seen in Figure 6.5. In case the disturbance can be attenuated or removed, faster controllers might be attainable, thus allowing for a higher frequency of the MEA. This issue might not be present in other setups as the speed oscillation was deemed to be because of the dSpace Controlbox used in the laboratory. Regarding the EEI operating conditions it can also be argued that it is more important to obtain the true ME angle even if the system is slow, than a faster less precise MEA angle, as the Grundfos TPE pump likely operates under the four distinct EEI operating conditions for a prolonged amount of time.

In Figure 6.6 it can be seen that the MTPA and ME points are not equal, hence there is a difference in the efficiency of the motor if the MTPA or ME angle is used. Furthermore, it can be seen that the ME angle range does not change significantly for the different EEI operating conditions. An easier way to control the FASynRM would be to have a Constant Angle (CA) of the current vector, which could reduce computational effort. However, it requires some experiments at the desired operating conditions to indicate which angle would provide the best compromise to maximize the efficiency across all operating conditions.
The differences in efficiency for the different EEI cases for the ME, MTPA and CA points can be compared. The angle of the CA control has been chosen to be 137.5° since this angle is within in the ME angle range for EEI 2, 3 and 4. Additionally, this angle is chosen since EEI 3 and 4 carry a larger weight in the EEI value. The power consumption and the efficiencies for the different EEI points can be seen in Table 7.1.

	EEI case #	P_{in} (W)	P_{out} (W)	η (%)	P_{avg} (W)	EEI value	kWh/year	Diff (kWh)
ME	1	4,289	3,911	91.2	1,804.4	0.3657	15,817	-
	2	2,952	2,688	91.07				
	3	1,830	1,665	90.99				
	4	1,054	952.5	90.37				
MTPA	1	4,294	3,911	91.09	1,806.23	0.3661	15,833	16
	2	2,954	2,688	91				
	3	1,831	1,665	90.94				
	4	1,056	952.5	90.2				
CA (137.5°)	1	4,294	3,911	91.09	1,804.7	0.3658	15,820	3
	2	2,952	2,688	91.07				
	3	1,830	1,665	90.99				
	4	1,054	952.5	90.37				

Table 7.1. Efficiency and input power for the different EEI cases where the angle for ME, MTPA and a constant angle has been chosen. It should be noted that the EEI 1 operating conditions of 12.7 Nm and 3,000 rpm could not be reached and instead 12.4 Nm was used. P_{avg} and the EEI value are calculated from Equation (1.1) and Equation (1.2), respectively. The kWh consumption of the pump is taken as the kWh consumption per year from the P_{avg}. The last column shows the difference in kWH relative to the ME control for the other control techniques.

From Table 7.1 it can be seen that the difference in input power between the ME and MTPA when comparing each EEI case is 2 W for EEI 4, 1 W for EEI 3, 2 W for EEI 2 and 5 W for EEI 1. For CA the only difference in input power is for EEI 1 where the difference is 5 W. Because of this small difference in input power the efficiencies of the different cases for each control method are practically equal. This also means that the the EEI value is around 0.366 for ME, MTPA and CA. The kWh consumption per year has been calculated from the P_{avg} and the difference can be seen to be 16 kWh between ME and MTPA and 3 kWh between ME and CA. Hence, by using ME instead of MTPA or CA, 16 and 3 kWh can be saved per year, respectively.

A final note regarding the results obtained in Chapter 6, is that the true rotor d-axis might not have been found after all. The results earlier shown in Figure 6.4 show that the three torque lines, compensated by the angle offset lie, on top of each other, however they do not look completely linear and the slope seems to be increasing, as the current vector amplitude increases. This could indicate that the current vector is not placed at 90° but in the first quadrant of the rotor dq-reference frame. Additionally, the slope of the lines are $0.154 \cdot \frac{3 \cdot N_{\text{pp}}}{2}$, where they should be $0.140 \cdot \frac{3 \cdot N_{\text{pp}}}{2}$ to match with the PM flux linkage of 0.140 Wb. This mismatch, could be caused by the non-linearities in the inverter, as the command voltages sent to the inverter are used to determine the rotor d-axis. These are assumed to be equal to the BEMF of the FASynRM, since the current in the system is controlled to be zero, however there might be some voltage drops across the transistors in the inverter meaning that the command voltages cannot be substituted with the BEMF used in the rotor d-axis calculation. The misalignment with the true rotor d-axis could also be the cause for the faster saturation of the q-axis inductance shown in Figure 4.2, since the q-axis marked by the chalk mark will also be misaligned with the low reluctance path of the rotor. Despite this, the results from all the experiments in Chapter 6 are still all valid, since the misalignment with the rotor d-axis will only cause all the results for the MTPA and ME angles to shift. As it looks like the current vector is placed in the first quadrant of the rotor dq-reference frame, the true rotor d-axis is leading the defined rotor d-axis meaning that the angles found for the MTPA and ME points are too large. This will also make more sense with regards to the MTPA angle, as it was found to be at 135° or above for EEI 1 and 2. However, due to the PM torque explained in Section 2.2 and the cross-saturation in the d- and q-axis inductances[11], the MTPA point should not be located at 135° for the FASynRM, but at some angle lower than this.

Chapter 8

Conclusion

In Chapter 3 the following problem statement was presented and will be answered through the following paragraphs.

"How can online maximum efficiency control be achieved for a FASynRM and is the implementation of maximum efficiency control worthwhile compared to other control techniques when considering the EEI?"

To maximize the efficiency of the FASynRM, this thesis has developed an MEA, which employed quadratic interpolation for various power functions in the system. The first approach was with the active power equation, having the advantages of online execution and minimal preliminary offline measurements. For this method the command voltage sent to the inverter could be used in real-time with a voltage error compensation LUT along with the current measurements, to calculate the input power. Unfortunately, it was found that the calculated input power from the active power equation did not match with the measured input power from the Yokogawa power analyzer. In case voltage measurements on the input side of the motor were attainable, the necessity for preliminary offline measurements could be completely eliminated. Although, it came at the cost of additional computational power to extract the fundamental voltage component from the PWM voltage signal provided by the inverter. This method was not tested.

The second approach consisted of measuring the input power with the Yokogawa power analyzer and develop input power LUTs which could be used to determine the ME angle, when the FASynRM was operating under the EEI operating conditions. Here, the MEA was capable of locating the ME angle for all tests and operating conditions. However, developing LUTs only works for the experimentally tested operating conditions and cannot be extended to other combinations of load torques and speeds making this approach very limited and inconvenient since a lot of experiments are needed.

The last approach aimed to develop a power loss estimation profile that could be determined by a few sets of experiments and would work for a wide range of operating conditions. For this profile, the copper losses were calculated in real-time and the core losses were found for load torques from 1 to 10 Nm at 2000, 2500 and 3000 rpm. A linear regression line was fitted onto the core losses as a function of the q-axis current, for the three different speeds as well as one for all three speeds combined. The trend lines for all four cases were very similar indicating that the core losses could in fact be determined based on a set of experiments for only one speed and different torques. This was validated when the MEA was tested with the four functions in conjunction with the online copper loss estimation. Here, the MEA showed good converge for all four functions for all the EEI operating conditions, provided that the power measurements at the three angles in the initial angle interval were noticeably different from each other. This approach seems like the most promising of the three ways to measure the power to be minimized, as it only requires few experiments to measure the core losses at one speed and at a variety of load torques.

Based on Table 7.1 it was seen that the annual energy savings when using ME control relative to MTPA control was 16 kWh, and 3 kWh when using ME control instead of applying a constant angle. These savings are very low, when considering the additional effort to implement ME control. The MTPA control can be realised online without any offline experiments other than resistance measurements.

The CA control requires the user to measure the input power for all the desired operating conditions in order to evaluate the most optimal angle for all conditions. In case the FASynRM is only to operate under the four EEI operating conditions, this means only four sets of experiments. The power loss estimation profile enables the FASynRM to operate with the most optimal angle across a wide range of operating conditions, but requires a set of experiments at a fixed speed and various load torques.
Both MTPA and ME require additional implementation effort as an algorithm will have to be used, in order to find the optimum angle. The CA control on the other hand is very easy to implement, as the angle is fixed for all operating conditions. The work needed to implement the three different control strategies can be seen in Table 8.1.

	MTPA	**ME**	**CA**
Number of power tests	0	$<$10	One per operating condition
Implementation effort	High	High	Low

Table 8.1. Work needed for MTPA, ME and CA control.

Based on Table 8.1 it is up to the user to choose which control method is the best, based on the number of different operating conditions and implementation effort for the specific use case, as the annual energy consumptions are basically equal.

Chapter 9

Future Work

High-Frequency Signal Injection

This thesis relied on determining the location of the rotor d-axis by the means of BEMF measurements. This method relies on rotating a machine connected to the FASynRM, which is impractical in real applications. High-frequency signal injection could be used instead, which applies a large DC current to lock the rotor position and then injects a high-frequency AC signal to locate the rotor d-axis.

Active Input Power with Voltage Measurements

It was shown that the active power equation was not able to calculate the true input power when the inverter voltage commands and voltage error LUTs were used. A second approach would be to measure the PWM voltages sent by the inverter to the FASynRM and then perform fourier analysis to determine the fundamental component. This would enable an online ME control that eliminates any necessity for offline measurements. However, in order to extract the fundamental component, the PWM voltages will have to be measured for one fundamental period before they can be estimated. This will delay the power measurements by one fundamental period, but since the machine operates in steady-state the input power should be constant, provided the current vector remains the same.

Bibliography

[1] Qian Wu. Moulding technology based ferrite assisted synchronous reluctance machine, 2018. ISSN 24461636.

[2] Frederik S. Valeur, Gintares Zubavicius, and Peter K. Magnussen. Investigation of step skewed ferrite assisted synchronous reluctance machine. AAU Student Projects, 2020.

[3] James D. Widmer, Richard Martin, and Mohammed Kimiabeigi. Electric vehicle traction motors without rare earth magnets. Sustainable Materials and Technologies, 3:7–13, 2015. ISSN 2214-9937. doi: https://doi.org/10.1016/j.susmat.2015.02.001. URL `https://www.sciencedirect.com/science/article/pii/S2214993715000032`.

[4] Dong Wang. Course material from modern electrical drives at aau, 2018. Available on request.

[5] Ladislav Knebl, Cestmir Ondrusek, and Jiri Kurfürst. Ferrite assisted synchronous reluctance motor design, manufacturing and material influence on motor characteristics. IEEE, pages 1–6, 2018.

[6] Sebastian Lang, Gerhard Ludwig, Peter Pelz, and Bernd Stoffel. General methodologies of determining the energy-efficiency-index of pump units in the frame of the extended product approach. 2013.

[7] Andreas Krings. Iron Losses in Electrical Machines - Influence of Material Properties, Manufacturing Processes, and Inverter Operation. TRITA-EE. Doctoral thesis, 2014. ISBN 9789175950990.

[8] W. G. Hurley and W. H. Wölfle. High frequency effects in the windings. In Transformers and Inductors for Power Electronics, page 11. John Wiley and Sons, Ltd, Chichester, UK, 2013. ISBN 1119950570.

[9] Stephen D. Umans. Fitzgerald & Kingsley's Electric Machinery. McGraw-Hill Education, 2014. ISBN 97812592546666.

[10] Junggi Lee, Kwanghee Nam, Seoho Choi, and Soonwoo Kwon. Loss-minimizing control of pmsm with the use of polynomial approximations. IEEE Transactions on Power Electronics, 24(4): 1071–1082, 2009. doi: 10.1109/TPEL.2008.2010518.

[11] Anantaram Varatharajan, Sérgio Cruz, Hazem Hadla, and Fernando Briz. Predictive torque control of synrm drives with online mtpa trajectory tracking and inductances estimation. In 2017 IEEE International Electric Machines and Drives Conference (IEMDC), pages 1–7, 2017. doi: 10.1109/IEMDC.2017.8002104.

[12] Grundfos. Grundfos tpe pump datasheet. URL `https://product-selection.grundfos.com/products/tp-tpe/tpe-series-1000-tpe2/tpe-65-2502-99113898?tab=variant-curves&pumpsystemid=1554528461`.

[13] Kristian B. Pedersen, Gansheng Huang, and Frederik B. Severinsen. Comparative study of bemf based observers for pmsm sensorless drives. AAU Student Projects, 2021.

Appendix A

MEA Matlab script

The script used to run the MEA in Simulink and dSpace:

```
function [angle,x_est,xl,xi,xu,y_est,yl,yi,yu] = fcn(P_in,Phi2,Phi3,Start_angle,Count,Vec_in,Delta)

% First measurement point is at 130 degrees
x_est_in = Vec_in(1);
xl_in = Vec_in(2);
xi_in = Vec_in(3);
xu_in = Vec_in(4);
y_est_in = Vec_in(5);
yl_in = Vec_in(6);
yi_in = Vec_in(7);
yu_in = Vec_in(8);

if Count == 1 % Initial sampling at 130 degrees
    xl = Start_angle;
    yl = P_in;
    angle = Phi2; % 137.5 degrees (xi) Middle angle
    xi = angle;
    yi = 0;
    % Undefined variables
    x_est = 0;
    xu = 0;
    y_est = 0;
    yu = 0;
elseif Count == 2 % Sampling at 137.5 degrees
    yi = P_in;
    yl = yl_in;
    angle = Phi3; % 145 degrees (xu) Upper angle
    xu = angle;
    xi = xi_in;
    xl = xl_in;
    % Undefined variables
    x_est = 0;
    y_est = 0;
    yu = 0;
elseif Count == 3 % Sampling at 145 degrees
    yu = P_in;
    a2 = 1/(xu_in-xi_in)*((yu-yl_in)/(xu_in-xl_in)-(yi_in-yl_in)/(xi_in-xl_in));
    a1 = (yi_in-yl_in)/(xi_in-xl_in)-a2*(xl_in+xi_in);
%     a0 = yl-a1*xl-a2*xl^2;
    x_est = -1/(2*a2)*a1;
    angle = x_est;
    xl = xl_in;
    xi = xi_in;
    xu = xu_in;
    yl = yl_in;
    yi = yi_in;
    % Undefined variables
    y_est = 0;
elseif Count == 4 % Compute the estimated optimum angle
    y_est = P_in;
```

```
    if xi_in < x_est_in
       if yi_in < y_est
           xl = xl_in;
           xu = x_est_in;
           xi = xi_in;
           yl = yl_in;
           yu = y_est;
           yi = yi_in;
           a2 = 1/(xu-xi)*((yu-yl)/(xu-xl)-(yi-yl)/(xi-xl));
           a1 = (yi-yl)/(xi-xl)-a2*(xl+xi);
           x_est = -1/(2*a2)*a1;
           angle = x_est;
       else
           xl = xi_in;
           xu = xu_in;
           xi = x_est_in;
           yl = yi_in;
           yu = yu_in;
           yi = y_est;
           a2 = 1/(xu-xi)*((yu-yl)/(xu-xl)-(yi-yl)/(xi-xl));
           a1 = (yi-yl)/(xi-xl)-a2*(xl+xi);
           x_est = -1/(2*a2)*a1;
           angle = x_est;
       end
    else
        if yi_in < y_est
            xl = x_est_in;
            xu = xu_in;
            xi = xi_in;
            yl = y_est;
            yu = yu_in;
            yi = yi_in;
            a2 = 1/(xu-xi)*((yu-yl)/(xu-xl)-(yi-yl)/(xi-xl));
            a1 = (yi-yl)/(xi-xl)-a2*(xl+xi);
            x_est = -1/(2*a2)*a1;
            angle = x_est;
        else
            xl = xl_in;
            xu = xi_in;
            xi = x_est_in;
            yl = yl_in;
            yu = yi_in;
            yi = y_est;
            a2 = 1/(xu-xi)*((yu-yl)/(xu-xl)-(yi-yl)/(xi-xl));
            a1 = (yi-yl)/(xi-xl)-a2*(xl+xi);
            x_est = -1/(2*a2)*a1;
            angle = x_est;
        end
    end
elseif Count > 4 % Compare the estimated optimum angle with the previous value
    y_est = P_in;
    if abs(y_est-y_est_in) < Delta % Optimum angle is found
        angle = x_est_in;
        x_est = x_est_in;
        xl = xl_in;
        xi = xi_in;
        xu = xu_in;
        yl = yl_in;
```

```
        yi = yi_in;
        yu = yu_in;
    else % Optimum angle is not found
        if xi_in < x_est_in
           if yi_in < y_est
               xl = xl_in;
               xu = x_est_in;
               xi = xi_in;
               yl = yl_in;
               yu = y_est;
               yi = yi_in;
               a2 = 1/(xu-xi)*((yu-yl)/(xu-xl)-(yi-yl)/(xi-xl));
               a1 = (yi-yl)/(xi-xl)-a2*(xl+xi);
               x_est = -1/(2*a2)*a1;
               angle = x_est;
           else
               xl = xi_in;
               xu = xu_in;
               xi = x_est_in;
               yl = yi_in;
               yu = yu_in;
               yi = y_est;
               a2 = 1/(xu-xi)*((yu-yl)/(xu-xl)-(yi-yl)/(xi-xl));
               a1 = (yi-yl)/(xi-xl)-a2*(xl+xi);
               x_est = -1/(2*a2)*a1;
               angle = x_est;
           end
        else
            if yi_in < y_est
                xl = x_est_in;
                xu = xu_in;
                xi = xi_in;
                yl = y_est;
                yu = yu_in;
                yi = yi_in;
                a2 = 1/(xu-xi)*((yu-yl)/(xu-xl)-(yi-yl)/(xi-xl));
                a1 = (yi-yl)/(xi-xl)-a2*(xl+xi);
                x_est = -1/(2*a2)*a1;
                angle = x_est;
            else
                xl = xl_in;
                xu = xi_in;
                xi = x_est_in;
                yl = yl_in;
                yu = yi_in;
                yi = y_est;
                a2 = 1/(xu-xi)*((yu-yl)/(xu-xl)-(yi-yl)/(xi-xl));
                a1 = (yi-yl)/(xi-xl)-a2*(xl+xi);
                x_est = -1/(2*a2)*a1;
                angle = x_est;
            end
        end
    end
else % MEA is OFF
    angle = Start_angle;
    xl = 0;
    xu = 0;
    xi = 0;
```

```
    yl = 0;
    yu = 0;
    yi = 0;
    x_est = 0;
    y_est = 0;
end

% Limit the output angle of the MEA
if angle > 145
    angle = 145;
elseif angle < 110
    angle = 110;
else

end
```